Gamma-ray astronomy at high energies

C. M. Hoffman and C. Sinnis

Los Alamos National Laboratory, Los Alamos, New Mexico 87545

P. Fleury

LPNHE-Ecole Polytechnique, IN2P3-CNRS, Paris, France

M. Punch

PCC-Collège de France, IN2P3-CNRS, Paris, France

Progress in high-energy gamma-ray astronomy has depended upon the development of sophisticated detectors and analysis techniques. Observations in this decade using space-based and ground-based detectors have observed gamma-ray emission from a variety of sources. For the first time a consistent picture of the γ-ray sky has emerged. This article describes the detection techniques in γ-ray astronomy, the nature of the astrophysical objects studied, and the present state of the observations. Several possible new directions in the field are also described. [S0034-6861(99)00304-9]

CONTENTS

I. Preface 898
II. Introduction 898
A. Background 898
B. Definition of terms 898
III. Motivation for the Study of High-Energy Gamma-Ray Astronomy 899
A. Introduction 899
B. Probe of acceleration mechanisms 899
C. Cosmic-ray origins 900
D. Study of exotic objects 900
1. Active galaxies 901
a. The unified model of active galaxies. 901
b. Particle acceleration in AGNs. 902
2. Pulsars 903
3. X-ray binaries 903
4. Primordial black holes 903
5. Gamma-ray bursts 904
6. Other phenomena 905
E. Study of photon propagation—cosmological implications 905
F. Study of nuclear and particle physics at high energies 906
IV. The Techniques of High-Energy Gamma-Ray Astronomy 906
A. Introduction 906
B. Satellite-based detectors 907
C. Earth-based detectors 908
1. Properties of extensive air showers 908
2. Air Čerenkov detectors 910
a. Detection of Čerenkov radiation from extensive air showers 910
b. Rejection of cosmic-ray background. 910
c. Trigger and readout electronics 912
d. Energy estimation and spectral measurement 913
e. Effect of observatory altitude and large-zenith-angle observations 913
3. Extensive air-shower particle detector arrays 914
4. Air fluorescence detectors 916
D. Estimating the background 916
V. Early Observations 916
A. Satellites 916
B. Early ground-based results 916
1. Cygnus X-3 917
2. Hercules X-1 917
3. The Crab 917
VI. Observations in the 1990s 917
A. CGRO–EGRET 918
1. Diffuse emission 918
2. Galactic sources 918
a. Pulsars 918
b. Unidentified sources 919
3. Extragalactic sources 919
4. Gamma-ray bursts 919
B. Air Čerenkov 919
1. The Crab 919
2. PSR1706-44 920
3. Vela 920
4. Active galactic nuclei 921
a. Markarian 421 921
b. Markarian 501 922
c. 1ES 2344+514 922
d. Implications of the VHE detection of AGNs 922
e. Intergalactic absorption of γ rays 924
5. Other objects 925
C. Extensive air-shower particle detector arrays 925
1. Introduction 925
2. Point-source searches 926
3. All-sky surveys 926
4. Searches for UHE emission from gamma-ray bursts 926
5. Searches for primordial black holes 926
6. Diffuse emission 927
D. Discussion 927
VII. Future Prospects 927
A. Satellite-based detectors 927
1. AMS 928
2. GLAST 928
B. Improvements in atmospheric Čerenkov telescopes 929
1. Better angular and time resolution 929
2. Detecting more Čerenkov photons 929
3. Use of several imaging telescopes 930
4. Other strategies: Solar plants 930
5. Major future projects 930
C. Improvements in extensive air-shower particle detector arrays 931
1. Higher altitude 931

2. Increased sampling of the extensive air shower 931
VIII. Outlook and Conclusions 932
Acknowledgments 932

I. PREFACE

High-energy γ-ray astronomy is a relatively new field. Despite impressive progress, it is only now becoming part of mainstream astronomy. This may be attributed to the fact that most of the scientists working in high-energy γ-ray astronomy have backgrounds in nuclear or particle physics rather than astronomy. In addition, many of the important results of the field have appeared in the *Proceedings of the International Cosmic Ray Conference* or in physics journals, where they are not likely to be read by astronomers.

Consequently review articles have played a particularly important role in high-energy γ-ray astronomy, both to inform the astronomical community as to the status of the field and to place the results in a broader astronomical context. A number of reviews of high-energy γ-ray astronomy have been written over the past decade. The most widely read are two articles that appeared in 1988 (Weekes, 1988; Nagle *et al.*, 1988) and a later review that concentrated on techniques rather than results (Cronin *et al.*, 1993). A recent review article by Ong (1998) contains a complete list of recent observations. An article by Fichtel and Trombka (1997) concentrates on the energy regime below 20 GeV. In addition, some topics in high-energy γ-ray astronomy are discussed by Longair (1994a).

In the 1980s, observations in high-energy γ-ray astronomy appeared to show the existence of a number of strong astrophysical sources of photons above 1 TeV. Some of these observations, if correct, would have required new physics, either a new kind of high-energy photon interaction or the existence of a new type of long-lived neutral particle. This brought the field to the attention of a wide scientific audience. Within high-energy γ-ray astronomy, there is now a consensus that most of these early observations were erroneous. However, many outside of the field do not know why this is so, nor do they realize that consistent, exciting observations are now being made. This article will concentrate on how the consensus view of the field emerged from the early contradictory results, survey the present state of the field, and discuss how it points towards future progress. In addition, we shall discuss how the observations relate to the underlying astrophysical processes.

II. INTRODUCTION

A. Background

Astronomy is an observational science, rather than an experimental science in which repeatable experiments are prepared and performed. Astronomers observe the universe using instruments on earth, on balloons, and on spacecraft. From these observations and an understanding of known physical processes, they attempt to understand the physical universe.

Historically, observations have driven the science. Time and time again astronomers have made observations that have profoundly altered our picture of the universe. Progress in astronomy has often been the direct result of the development of a new observational technique, either the study of a previously unexplored wavelength region of the electromagnetic spectrum or a great enhancement in sensitivity compared with earlier observations. The development of new techniques in high-energy γ-ray astronomy holds the promise of similar progress.

High-energy γ-ray astronomy resulted from two distinct fields of study. In the early 1970s, space-based detectors extended the field of x-ray astronomy upwards in energy and observed a number of discrete sources of 100-MeV photons. The study of cosmic photons above $\sim$1 TeV (10^{12} eV) was pursued by physicists with ground-based instruments, which were an outgrowth of cosmic-ray studies. Here, however, the development of new detection techniques did not immediately reveal new sources or phenomena. It was only recently, after the development of second- and third-generation telescopes, that the ground-based observations began to contribute to our understanding of the cosmos.

While the techniques of space-based and ground-based γ-ray astronomy are distinct, the science addressed by them overlaps considerably. In addition, detectors are being developed to bring the energies studied on earth and in space closer together. Thus this article will review the status of observations using both techniques, although it will concentrate on the ground-based observations.

B. Definition of terms

The two types of high-energy γ-ray detectors are satellite-based telescopes that convert the photon and track the resulting electron-positron pair to determine the photon direction, and ground-based instruments that detect the extensive air showers produced when high-energy photons interact with the earth's atmosphere. Instruments that detect the Čerenkov light produced in extensive air showers are called atmospheric Čerenkov detectors. Air fluorescence detectors are sensitive to the light emitted when nitrogen molecules, excited by ionizing particles in an air shower, de-excite. Scintillation counter arrays that detect the (primarily charged) air-shower particles that survive to ground level have traditionally been called "extensive air-shower" (EAS) detectors or EAS arrays. However, both air Čerenkov and air fluorescence detectors also detect extensive air showers, and they may consist of arrays of detectors. To avoid this ambiguity, we shall use the term "air-shower particle detector arrays" to describe the counter arrays.

The term "γ ray" is generally used to denote electromagnetic photons with energies above several hundred thousand electron volts (eV). Photons with energies

TABLE I. Gamma-ray astronomy nomenclature.

Energy range (eV)	Equivalent prefix	Nomenclature	Traditional detection technique
10^7–3×10^7	10–30 MeV	medium	satellite-based Compton telescope
3×10^7–3×10^{10}	30 MeV–30 GeV	high (HE)	satellite-based tracking detector
3×10^{10}–3×10^{13}	30 GeV–30 TeV	very high (VHE)	ground-based atmospheric Čerenkov detector ground-based air-shower particle detector
3×10^{13}–3×10^{16}	30 TeV–30 PeV	ultrahigh (UHE)	ground-based air-shower particle detector
3×10^{16} and up	30 PeV–and up	extremely high (EHE)	ground-based air-shower particle detector ground-based air fluorescence detector

lower than γ rays are called x rays, but above x rays all photons are γ rays. Thus γ rays occupy an extraordinarily broad (in principle, unbounded) range of the electromagnetic spectrum. The term "γ-ray astronomy" is too broad to be descriptive or useful; some subdivision is clearly needed.

Perhaps the most influential attempt at such a subdivision was that suggested by Weekes (1988) in his review article. He proposed a classification scheme based primarily on the range of energies over which a particular detection technique is used. This is a practical scheme that has been widely adopted. However, since the appearance of Weekes' article, the energy range over which a given detection technique has been used has changed somewhat, leading to *de facto* changes in the use of his scheme. Thus we propose to update the nomenclature for γ-ray energy ranges to reflect current usage.

We use the term "high energy" (HE) to include γ rays from 30 MeV–30 GeV. This region is currently explored with satellite-based detectors, such as the EGRET detector aboard the Compton Gamma Ray Observatory (CGRO). Weekes defined the very high energy (VHE) region to cover the range of energies explored by atmospheric Čerenkov detectors. We use VHE to cover the range from 30 GeV–30 TeV, significantly narrower than chosen by Weekes. This reflects the present and planned energy range studied with atmospheric Čerenkov detectors. Accordingly, we define the ultrahigh energy (UHE) region as ranging from 30 TeV–30 PeV (3×10^{16} eV), which more closely describes the range presently studied with air-shower particle detector arrays, and extremely high energy (EHE) as everything above the UHE region. Table I updates the first table in Weekes' article and summarizes the nomenclature we shall use in this article. We shall also see how new detection techniques are being added in several of these energy regimes.

III. MOTIVATION FOR THE STUDY OF HIGH-ENERGY GAMMA-RAY ASTRONOMY

A. Introduction

Until the advent of high-energy accelerators in the early 1950s, experiments at the high-energy frontier were conducted with cosmic rays. The muon, pion, and kaon were all discovered in cosmic-ray experiments. It was only natural that questions about the origin of cosmic rays and how they are accelerated were important to nuclear and particle physicists. Even after most of the experimental work in particle and nuclear physics had moved to terrestrial accelerators, particle-physics research continued with cosmic rays because they could be used to study particle interactions at energies above those available at these accelerators.

The realization that astrophysical sources might produce high-energy γ rays and the discovery of several x-ray sources led to the first efforts in γ-ray astronomy. The study of these sources provides a unique insight into the production of high-energy quanta. As the observed photon spectra are nonthermal, they allow us to study acceleration mechanisms in sources such as supernova remnants and active galactic nuclei. Extragalactic sources serve as beacons that allow us to probe the intervening intergalactic medium and thus may give us clues to the early universe. The production of VHE γ rays may serve as a "marker" for Fermi acceleration of charged particles and provide a means of determining the origin of the cosmic rays, since they propagate undeviated by intergalactic or interstellar magnetic fields.

In this section we describe the major science areas addressed by high-energy γ-ray astronomy.

B. Probe of acceleration mechanisms

Twenty-five years after the discovery of cosmic rays, Enrico Fermi devised the first plausible mechanism to

explain their acceleration. Fermi postulated that plasma clouds in the interstellar medium might act as magnetic mirrors and reflect charged cosmic rays (Fermi, 1949). If the cloud is moving toward a cosmic ray, the cosmic ray will gain energy, while if the cloud is moving away, the cosmic ray will lose energy. There tend to be more collisions between particles and clouds that are moving toward each other, leading to a net energy gain to the cosmic ray (Longair, 1994b). This process is known as second-order Fermi acceleration. Fermi noted that this is a very slow process and, in competition with various energy-loss processes, may not be able to account for the observed high-energy cosmic rays.

The next advance came when this idea was applied to a shock front. In the rest frame of the shock, material both upstream and downstream of the shock moves toward the shock. A charged particle trapped between the upstream and downstream regions will gain energy every time it crosses the shock front, as it is always reflected by an approaching wall. This process is known as first-order Fermi acceleration (Bell, 1978; Blanford and Ostriker, 1978). Legage and Cesarsky (1983) applied this model to the shock front produced by a supernova explosion and estimated that this mechanism could accelerate protons up to $\sim 10\,\mathrm{TeV}$. While particles with gyroradii larger than the radius of the shock will escape the acceleration region, the maximum attainable energy is determined by the lifetime of the shock. In fact, it is predominantly determined by the lifetime of the blast phase of the shock (Legage and Cesarsky, 1983). Shocks are believed to be common in the universe; they may form where matter accretes onto a compact object, such as in an x-ray binary system or an active galaxy.

Electromagnetic mechanisms may also be responsible for the acceleration of cosmic rays. The rotation of a magnetized neutron star with a period P (sec) can give rise to strong electric fields that can accelerate particles with charge Z to $\sim 3\times Z/P^2$ TeV (Goldreich and Julian, 1969; Cheng *et al.*, 1986). Accretion disks may be another environment that can create strong electric fields. Matter in accretion disks is usually in the form of highly conductive plasma. Since gravity dictates the particle trajectories, the inner part of the disk rotates at a different speed than the outer part. This differential rotation of a conducting disk forms an electric generator—a unipolar inductor. The accretion disk around a neutron star could give rise to particles with energies up to $10^{17}\,\mathrm{eV}$ (Chanmugam and Brecher, 1985).

Energetic protons and electrons in the vicinity of astrophysical objects will produce high-energy photons. The electrons generate low-energy photons through synchrotron radiation in magnetic fields. These photons can be boosted to TeV energies by inverse Compton scattering with other high-energy electrons. Protons and nuclei undergo strong interactions with surrounding matter, producing high-energy pions; neutral pions decay into photons. If there is less than ~ 1 radiation length of matter surrounding the acceleration region, the γ rays can escape. Thus observations of VHE γ rays can elucidate the nature of cosmic-particle accelerators.

C. Cosmic-ray origins

The first hints that cosmic rays existed came in the late 1800s when it was observed that gold-leaf electroscopes slowly discharged, and no explanation could be found. Faraday postulated the existence of ionizing radiation that penetrated the electroscope. By the early 1900s natural radioactivity had been discovered, and this was believed to be the origin of the ionizing radiation. In 1910, Victor Hess (1913) made a series of balloon flights and determined that the ionization rate (the rate of ions produced per unit volume) increased with altitude above $\sim 2\,\mathrm{km}$. Hess was awarded the Nobel Prize for determining the cosmic origin of the radiation. In 1938 Pierre Auger found that the radiation reaching the ground was correlated over large distances (up to 300 m) and short time scales (1 μs; Auger, 1939). He had discovered extensive air showers. Now, more than 100 years after the first observations, we know that the earth is bombarded by an isotropic flux of high-energy nuclei. The energy spectrum of the cosmic rays has been measured up to $\sim 10^{20}\,\mathrm{eV}$, some information on the relative abundance of the elements is known below $\sim 10\,\mathrm{TeV}$ and above $\sim 10^{17}\,\mathrm{eV}$, and the age of the cosmic rays (10 million years) has been measured. However, there is still no universally accepted theory of their origin. The search for the origin of cosmic rays is one of the major motivations for the study of γ-ray astronomy.

Our galaxy is pervaded by a magnetic field of strength ~ 1 microgauss (μG). The bending radius of a charged particle in a magnetic field is $R = 0.01\times(p/zB)$, where the momentum p is in TeV, the magnetic field is in μG, the charge z is given in units of the electron charge, and the radius R is in parsecs. Thus protons with energies up to $10^{18}\,\mathrm{eV}$ coming from galactic sources $\sim 10\,\mathrm{kpc}$ away have lost all directional information before reaching the earth. Since γ rays do not bend in the galactic magnetic field, they can trace the sources of the cosmic rays.

D. Study of exotic objects

Two types of objects that have been conclusively detected in the TeV energy band, pulsars and active galaxies, contain compact objects—neutron stars and black holes, respectively. Until the late 1980s, it was thought that x-ray binary systems (composed of a neutron star or black hole and a main-sequence star) were prolific sources of TeV and PeV γ rays. While recent observations have not confirmed these claims, they may yet turn out to be sources of TeV photons. X-ray binaries share many characteristics with active galaxies, albeit on a smaller scale.

In addition, there are speculative objects, such as primordial black holes and cosmic strings, that may produce TeV photons. While these objects have not been observed in any wavelength band and may not even exist, the TeV band is an ideal place to search for them.

FIG. 1. An artist's conception of the unified model of a radio-loud active galactic nucleus (AGN). For some viewing angles, the thick torus obscures the inner regions of the AGN and is responsible for the infrared emission. The jets are composed of relativistic particles and are responsible for both the radio emission (synchrotron radiation) and the high-energy γ radiation (from GeV to multi-TeV). The dark blobs are the high-velocity clouds, responsible for the broad emission lines, and the light blobs are the slower clouds responsible for the narrow line emission. From Urry and Padovani, 1995. This picture is reproduced with permission from the Astronomical Society of the Pacific.

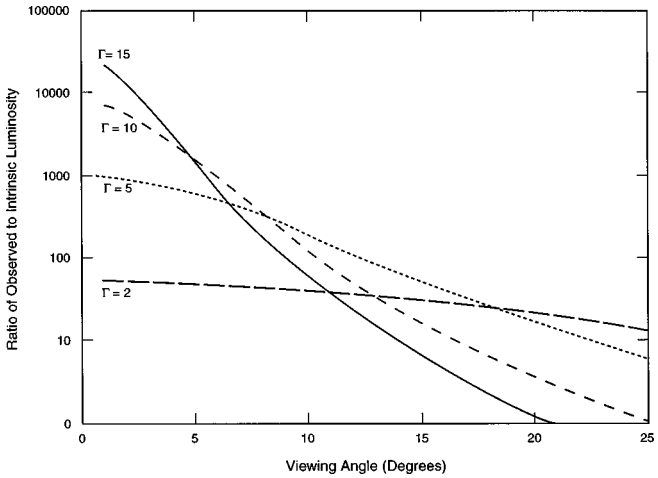

FIG. 2. The ratio of observed to intrinsic luminosity for a jetlike source with an E^{-1} integral energy spectrum as a function of viewing angle.

1. Active galaxies

a. The unified model of active galaxies

A problem encountered in studying active galaxies is the proliferation of classes and subclasses of active galactic nuclei (AGN)—quasars, Seyfert galaxies (types I and II), radio-quiet or radio-loud galaxies, Fanaroff-Riley galaxies (types I and II), narrow line, broad line, no lines, highly polarized lines, flat spectrum, steep spectrum, optically violent variables, BL Lacs, etc. These classes are based on observational properties, both optical and radio, rather than the nature of the underlying objects. In the last two decades, a unified theory of the various classes has emerged that enjoys wide acceptance within the community (Begelman *et al.*, 1984). Here we shall briefly present this unified model of AGN and discuss the properties that are relevant to TeV γ-ray astronomy.

Figure 1 illustrates the unified AGN model. In this model, the central engine of an AGN contains a supermassive black hole $M \sim 10^7 - 10^{10} M_\odot$. (The Schwarzschild radius of a $10^{10} M_\odot$ black hole is 0.001 pc.) There is a thin accretion disk around the hole, surrounded by a thick torus lying in the equatorial plane of the hole. In addition, radio-loud AGNs have well-collimated jets perpendicular to the accretion disk. Of less interest to us are the clouds around the black hole (Begelman *et al.*, 1984; Padovani, 1997), which are responsible for the observed emission lines. In this model, the central engine is powered by accretion—the change in gravitational potential energy of infalling matter. This is a very efficient process, which may convert 10% of the rest mass of the accreted matter into radiation (Shapiro and Teukolsky, 1983; Frank *et al.*, 1992).

Active galaxies emit radiation over the entire electromagnetic spectrum from radio waves to TeV γ rays. Thermal emission emanates from the accretion disk (infrared to x rays) and the torus (infrared). The nonthermal emission (radio and γ ray) comes from the jets.

Starting with this basic model, it is possible to understand most of the different AGN classifications as consequences of different viewing angles with respect to the rotation axis. There are two effects of viewing angle on the observations: simple shadowing effects of the torus (at large viewing angles, the torus obscures certain emission regions from view) and the Doppler boosting of a relativistic jet viewed at a small angle.

Superluminal motion (apparent motion that is greater than the speed of light) is a consequence of relativistic flow viewed at small angles (Rees, 1966). Superluminal motion has been observed in many AGNs. The relativistic beaming also causes the apparent luminosity to increase dramatically and allows high-energy photons to escape from regions with high radiation fields. The Doppler factor is defined as

$$D = \{\gamma[1 - \beta \cos(\theta)]\}^{-1} \simeq 2\gamma(1 - \theta^2\gamma^2), \tag{1}$$

where $\beta = v/c$, $\gamma = 1/\sqrt{(1-\beta^2)}$, and θ is the viewing angle from the jet axis; the approximation is valid for $\theta^2\gamma^2 \ll 1$. The observed luminosity $\mathcal{L}_{\rm obs}$ is related to the intrinsic luminosity $\mathcal{L}_{\rm int}$ (Padovani, 1997) by

$$\mathcal{L}_{\rm obs} = D^{2+\alpha} \mathcal{L}_{\rm int}, \tag{2}$$

where α is the integral spectral index of the source (typically 1). Figure 2 shows the multiplication in observed luminosity for a jetlike source due to this effect. In order to observe TeV γ rays from an AGN, the viewing axis must be within $\sim 10^\circ$ of the jet axis.

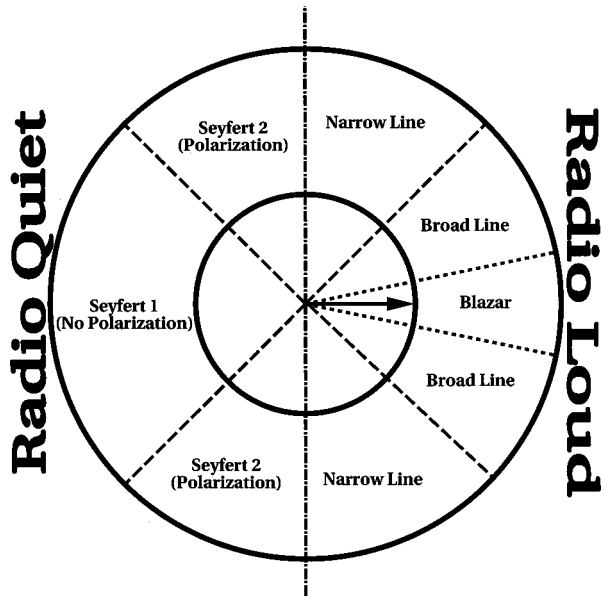

FIG. 3. Schematic diagram of the unified model of active galactic nuclei. The right half represents a radio-loud AGN; the arrow corresponds to the jet axis. The left-hand side represents a radio-quiet AGN (Seyfert galaxy). Note that no jet is present; however, there is still a preferred direction defined by the rotation axis. Possible observer positions are on the outer ring.

These considerations lead to relationships between viewing angle (with respect to the jet direction) and observed properties of radio-loud AGNs, as summarized in Fig. 3. In a radio-loud AGN viewed at a large angle, the torus obscures the clouds that are close to the black hole. Only the distant clouds (which are moving slowly) are unobscured, so narrow emission lines are observed. The Doppler factor is small, so no TeV emission is observed. At smaller angles, the high-velocity clouds become visible, leading to the observation of broad emission lines. At very small angles, the Doppler factor becomes large and TeV emission is observed.

The time scale of the variability of emission also depends upon the viewing angle. As the line of sight gets closer to the jet axis, the relativistic beaming becomes greater (causing a Doppler contraction of the time scale) and the apparent size of the emission region becomes smaller. Therefore the variability time scale decreases as the viewing angle decreases. Active galactic nuclei viewed at small angles should be identified with blazars. This relatively new term includes BL Lacs and optically violent variables. While fewer than $\sim 1\%$ of all AGN are blazars, all of the 50 MeV–GeV extragalactic sources and both of the extragalactic TeV sources are blazars.

BL Lacs deserve special mention. The distinguishing feature of their emission spectrum is the faintness or absence of emission lines. At present this is not understood. It may be that the intensity of the emission lines is small compared to the core-dominated emission (as the observer is looking down the jet axis) and hence unobservable. BL Lacs are the only class of AGNs that have been observed to emit VHE photons. (In the GeV regime the majority of observed blazars are optically violent variables.) Whether this is a result of the poor statistics or something fundamental is not known.

The much more numerous (90% of all AGNs) radio-quiet AGNs are known as Seyfert galaxies and show no evidence of high-energy γ radiation (Lin *et al.*, 1993). Here again, viewing angle is important. When the angle between the observer and the rotation axis is greater than $\sim 45^\circ$ one is viewing a larger fraction of light reflected from the surrounding torus and the reflected light tends to be polarized. This accounts for the apparent difference between Seyfert 1 and Seyfert 2 galaxies (Antonucci and Miller, 1985). It is clear that the difference between radio-quiet and radio-loud AGNs is not simply a matter of viewing angle. One possible explanation is that large accretion rates may quench the formation of jets, leading to radio-quiet AGNs (Begelman *et al.*, 1984).

b. Particle acceleration in AGNs

While there is general agreement that the TeV photons are created in the jets of AGNs, there is still uncertainty as to the mechanism responsible for the high-energy emission. There are two basic models: the inverse Compton models (Levinson and Blandford, 1991) and the proton-initiated cascade (PIC) models (Protheroe *et al.*, 1992; Mannheim, 1993).

The inverse Compton model has several variants: synchrotron self-Compton, external Compton, and inhomogeneous models. In the basic model, electrons are accelerated in the jets and they upscatter photons, via inverse Compton scattering, to high energies. The various models place the photon source and the acceleration site at different locations along the jet. In the Synchroton Self-Compton model (Maraschi *et al.*, 1992), the electrons are themselves the source of the photons (via synchrotron radiation). In the external Compton model, the source of the photons is outside of the jet (Dermer and Schlickeiser, 1993; Sikora *et al.*, 1994) and does not come from synchrotron radiation. In the inhomogeneous models, emission at different energies originates in different regions of the jet. In any of these models, energy-loss mechanisms (inverse Compton scattering and synchrotron radiation) limit the maximum γ-ray energy to $\sim 10\,\mathrm{TeV}$ (Protheroe *et al.*, 1992; Kirk *et al.*, 1997).

In the hadronic models, protons are shock accelerated to ultrahigh energies, $10^{10}\,\mathrm{GeV}$. The protons interact with ambient photons ($p\,\gamma \rightarrow \Delta$), producing neutral pions that decay and initiate an electromagnetic cascade. As with the Compton models, the photons can come from an external source (E-PIC) or from the synchrotron emission from the high-energy electrons generated in the cascade (S-PIC).

There is a range of observations that confront these models. Since electrons are lighter than protons, they are accelerated and cooled more rapidly. Therefore rapid flaring activity tends to favor electron models (Henri, 1999). Flaring on time scales less than 10–15 minutes is difficult to reproduce in proton models. This

same rapid cooling makes it more difficult to accelerate electrons to very high energies. The maximum attainable energy depends on the magnetic-field strength. However, γ-ray energies above 10–20 TeV favor proton models. In all models, TeV emission favors acceleration sites well beyond the torus. TeV γ rays produced below the torus would be absorbed by the intense infrared radiation field arising from the torus. Finally, correlations between the optical to x-ray emission range and the GeV to TeV emission range favor the homogeneous models. Further high-energy observations, especially of flaring states in conjunction with x-ray and optical observations, are critical in improving our understanding of these objects.

2. Pulsars

Pulsars are rapidly rotating neutron stars with periods between a few milliseconds and a few seconds, and strong magnetic fields ($\sim 10^{12}$ G). Neutron stars have a maximum mass of $\sim 3 M_{\odot}$ and a radius of ~ 10 km (Shapiro and Teukolsky, 1983). They are the densest stable form of matter known.

The spinning magnetic fields generate electric fields strong enough to remove electrons from the surface of the neutron star. These electrons (and positrons created by pair production in the high magnetic fields) are anchored to the magnetic field lines and arrange themselves in the magnetosphere such that $\mathbf{E}\cdot\mathbf{B}=0$. At the radius where these field lines are traveling at the speed of light (known as the light cylinder), the pulsar wind region begins. This region terminates with a shock, beyond which lies the nebular region.

The condition $\mathbf{E}\cdot\mathbf{B}=0$ prohibits particle acceleration. Acceleration can occur only in regions devoid of plasma (where $\mathbf{E}\cdot\mathbf{B}\neq 0$). These ''vacuum gaps'' are thought to form near the magnetic poles and near the light cylinder. Pulsed emission from the radio wavelengths to GeV γ rays is thought to originate from these regions.

To date, TeV γ rays have been detected only from a class of pulsars known as plerions, and only unpulsed TeV emission has been observed. A plerion is a supernova remnant with a filled morphology. Figure 4 is a schematic view of the environment around a plerion. Electrons and positrons escape from the magnetosphere along the open field lines and enter the pulsar wind region. This region terminates in a shock that accelerates the electrons and positrons. After they are accelerated to high energies, they escape the shock front and enter the nebula. The high-energy electrons emit synchrotron radiation as they spiral around the magnetic field lines in the nebula. They then upscatter these photons to TeV energies via inverse Compton scattering. This model is known as the synchrotron self-Compton (SSC) model (deJager and Harding, 1992).

3. X-ray binaries

X-ray binaries are systems composed of a neutron star and a main-sequence star in a tight orbit around each other. Matter drawn from the companion star forms an accretion disk around the neutron star. This matter spirals inward (transferring angular momentum outward through viscous forces) under the influence of gravity until the magnetic forces dominate. At this point, the matter flows along the field lines and accretes onto the magnetic poles of the neutron star. This leads to the formation of ''hotspots'' at the poles of the neutron star, with $T \approx 10$–15 keV. If the magnetic and rotation axes are not aligned, an x-ray pulse is observed as the magnetic pole sweeps past the observer.

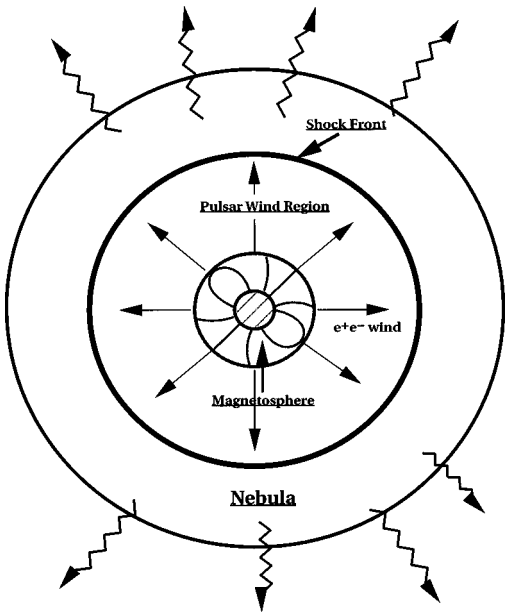

FIG. 4. Schematic diagram of a plerion (a pulsar with a filled remnant) and its environment. The light cylinder is the circle just outside the magnetosphere. The remnant (nebula) is filled with an electron-positron plasma, supplied by the pulsar.

Some galactic x-ray binary systems are observed to have relativistic jets, similar to the radio-loud AGN. Thus one might expect to observe TeV emission in these sources. In fact, in the early 1980s there were many reports of TeV–PeV γ-ray signals from x-ray binary systems (Cygnus X-3, Hercules X-1, etc.). However, these detections have not been confirmed by more modern detectors, as we discuss below.

4. Primordial black holes

In the 1970s, Stephen Hawking (1975) showed that black holes are not truly black. They radiate a nearly thermal spectrum, where the effective temperature is related to the radius of curvature of the event horizon: $T = (10^{13}/M)$ GeV, where M is the mass in grams. As with any gravitationally bound system, the specific heat of a black hole is negative. The more energy it loses, the hotter it gets. The luminosity of a blackbody is proportional to the fourth power of the temperature, and the surface area of the event horizon is proportional to the square of the temperature ($r = 2M \propto 1/T$). Therefore the luminosity of a black hole increases with the square of the temperature $[\mathcal{L} = (c^3/G)^2 K\hbar/M^2 \text{ ergs sec}^{-1}]$ (Thorne *et al.*, 1986). Here K is related to the number of

TABLE II. Black-hole emission parameters.

Mass (grams)	Temperature	Luminosity (ergs $\sec^{-1}$)	Lifetime (years)
10^{22}	1 eV	5×10^{2}	2×10^{32}
10^{17}	100 keV	5×10^{12}	2×10^{17}
10^{12}	10 GeV	6×10^{23}	15
10^{10}	1 TeV	8×10^{27}	380 (seconds)
10^{8}	100 TeV	8×10^{31}	4×10^{-4} (seconds)

available states (elementary particles) for the radiation, which increases with the temperature of the black hole. This runaway process leads to the complete evaporation of the black hole, with a rather spectacular end (infinite luminosity). To put this discussion in perspective, we give several examples of black-hole radiation in Table II.

A detector of TeV γ rays is well suited to search for the evaporation of a black hole. At lower energies the luminosity is low, the background is high, and there is no unique time signature. At higher energies too little total energy is released. These calculations assume that no photosphere forms around the evaporating hole. However, recent work (Heckler, 1997) indicates that a photosphere does form, in which case the flux of TeV γ rays is dramatically reduced.

The black holes of interest here have very small masses (holes with a mass of $\sim10^{14}$ grams at the Big Bang would be evaporating now), and it is natural to ask how they would form in our universe. The most appealing process is the density fluctuations in the early universe. The COBE experiment has measured the density fluctuations in the early universe on very large length (mass) scales—of order 100 Mpc (10^{55} grams; Smoot, 1992). The measured value of the fluctuations $\delta\rho/\rho$ are too small to create observable numbers of primordial black holes. However, to rule out primordial black holes, one would have to extrapolate the COBE results over 40 orders of magnitude in mass scale. Thus it remains an open question whether primordial black holes were formed in the early universe.

5. Gamma-ray bursts

Gamma-ray bursts (GRBs) are perhaps the outstanding puzzle of modern astrophysics. First observed in the 1960s by scientists searching for nuclear tests over the Soviet Union (Klebesadel *et al.*, 1973), these objects still elicit fierce debate. Observationally, gamma-ray bursts are short-duration (1 ms to tens of seconds) bursts of x rays that come from apparently random locations in the sky. Before the launch of the BATSE detector on board the Compton Gamma Ray Observatory (CGRO), there was seemingly strong evidence that GRBs were caused by some events on galactic neutron stars. The apparent detection of cyclotron splitting in a very strong magnetic field (Fenimore *et al.*, 1988; Murakami *et al.*, 1988) naturally led to such an explanation. At that time only a handful of GRBs had been detected.

Two distributions of GRB locations are of prime interest: (1) the distribution in galactic coordinates and (2) the radial distribution from the earth. If galactic neutron stars are the sources of GRBs, one would expect the distribution of GRBs to be similar to the distribution of galactic matter—a thin disk. In fact, after the detection of over 1,000 bursts by BATSE, the distribution is clearly isotropic. The radial distribution, plotted as the intensity distribution of the observed bursts, shows an underabundance of low-fluence bursts—an indication that we are seeing to the edge of the source distribution. The actual manner in which this distribution falls off at low fluence is consistent with a cosmological origin for gamma-ray bursts.

Current models fall into two categories: cosmological models and galactic halo models. Naturally if the sources of GRBs are cosmological, they must be much more energetic than if they are associated with an extended galactic halo. In fact, the energy required for a cosmological GRB is roughly equivalent to that released in a supernova. The favored cosmological model is a relativistically expanding fireball (perhaps the aftermath of the merger of a binary neutron star system) (Cavallo and Rees, 1978; Meszaros and Rees, 1993). Galactic halo models rely on a population of old neutron stars that inhabit an extended halo surrounding our galaxy. This population may have formed from high-velocity neutron stars, neutron stars that were kicked out of binary systems when they were formed in supernovae explosions. It is estimated that roughly half of all neutron stars are formed with sufficient velocity to escape the galaxy.

EGRET, the high-energy gamma-ray detector aboard the CGRO, has observed emission from several bursts. These observations have placed severe constraints on the ''compactness'' parameter of GRB models. The time scale of the bursts places upper limits on the source size (the light travel time across the source). The observed luminosity places limits on the energy of the photons that can escape the source. In order for high-energy photons to escape from an intense source (especially true for cosmological models), the source must be moving towards us at an extremely high velocity (such as in AGN jets).

Recently, a new gamma-ray burst detector, Beppo-Sax, was launched. Beppo-Sax has three x-ray detectors on board—an all-sky burst monitor, a wide-field camera (with an angular resolution of 3 arc min), and a narrow-field camera (with an angular resolution of 50 arc sec). The ability of the wide-field camera to localize the burst

position has led to the discovery of a soft x-ray afterglow that may last for days after the initial burst. The precise localization of the bursts has also enabled powerful x-ray, optical, and radio telescopes to search for emission from gamma-ray bursts.

As of this writing, several optical and radio counterparts to GRBs have been observed (Kulkarni *et al.*, 1997; Sahu *et al.*, 1997; van Paradijs *et al.*, 1997). The optical counterparts have a visual magnitude of $<\sim 20$ and a decay time of ~ 1 day. The radio counterparts have a similar decay time. The optical spectrum of GRB970508 had an absorption line that has been used to place limits on the distance to the GRB, $0.8<z<2.3$ (Metzger *et al.*, 1997). The radio and optical observations are consistent with the fireball model and point to a cosmological origin to GRBs (Reichart, 1997).

6. Other phenomena

While cosmologists tend to favor a universe whose density is exactly equal to the critical density (ρ_c), so that the universe is exactly closed, the measured amount of luminous matter in the universe is only roughly 1% of ρ_c. In addition, nucleosynthesis in the early universe and the observed abundances of helium and lithium require that the density of baryonic matter in the universe be $\leqslant 0.2\Omega_0$. Thus, if $\rho=\rho_c$, most of the matter must be nonbaryonic dark matter. If this dark matter is composed of stable massive (TeV) super-symmetric particles, then ground-based gamma-ray telescopes might be able to detect them. One of the more promising methods is to search for annihilation lines. Massive dark matter should concentrate in the galactic disk and at the galactic center (along with the other matter). Under these conditions, the neutralino (a neutral supersymmetric particle) pair annihilation line $\chi\chi\rightarrow\gamma\gamma$ may be detectable over the background (Urban *et al.*, 1992). Recent calculations (Bergström *et al.*, 1997; Bergström and Ullio, 1997) yield annihilation rates an order of magnitude larger than previous results for Higgsino-like neutralinos. Because the natural width of the neutralino-pair annihilation line is very small ($\Delta E/E\sim 10^{-3}$), good detector energy resolution is important to observe a signal over the cosmic-ray background.

Cosmic strings may also be sources of high-energy γ rays (Hill *et al.*, 1987; MacGibbon and Brandenberger, 1993). Cosmic strings are topological defects that may have formed during phase transitions in the early universe (Kolb and Turner, 1990). Such strings would have masses of $\sim 10^{18}\sigma^2$ grams (where σ is the energy scale of the phase transition measured in GeV) and would stretch across the visible universe. Cusps in cosmic strings emit massive (10^{15}-GeV) particles that would undergo decay and fragmentation processes leading to jets of lower-energy particles (jets similar to those observed in particle accelerator experiments, not like jets associated with AGNs). A problem with attempting to search for TeV γ rays associated with cusp annihilation is the uncertainty in the time scale over which the emission would be visible. One estimate puts the time scale at $\sim 10^{-8}$ sec. Unfortunately this would make such outbursts virtually undetectable to ground-based instruments, as the entire burst would appear as a single energetic event within the time resolution of current detectors.

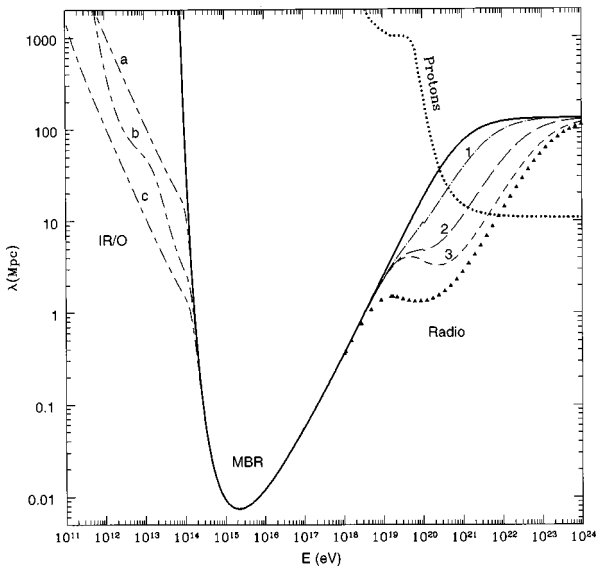

FIG. 5. Mean free path λ for γ rays of energy E, showing absorption by the various extragalactic backgrounds: solid line, effect of the microwave background radiation (MBR); dashed curves (a,b,c), three models of the infrared/optical (IR/O) diffuse background; dashed curves (1,2,3) and triangles, the extragalactic radio background estimates with cutoffs at 5, 2, and 1 MHz, and upper limits assuming the total observed radio background is extragalactic, respectively; dotted line, mean free path for energetic protons. From Coppi and Aharonian, 1997.

E. Study of photon propagation—cosmological implications

The extragalactic diffuse photon background, including infrared and optical photons from stars and dust, the 2.7-K cosmological microwave background radiation, and the diffuse radio noise, sets a limit on the distance from which γ rays can reach us. This is due to the interaction of a γ ray with a photon from this background via $\gamma\gamma\rightarrow e^+e^-$, which is most probable slightly above the reaction threshold, at about $E_{\gamma_1}E_{\gamma_2}=2m_e^2\simeq 0.5\times 10^{12}\,(\mathrm{eV})^2$. Visible light (at ~ 1 eV) and the microwave background radiation (at 10^{-4} eV) absorb TeV and PeV γ rays, respectively. The γ-ray absorption length varies with energy according to the intensity of the photon background at the corresponding wavelength. Figure 5 shows the pair-production mean free path in the current universe as a function of the γ-ray energy. The optical depth for 200-TeV photons is about 1 Mpc, so only γ rays from our galaxy or nearby galaxies can be observed at these energies. The corresponding cutoff for cosmic-ray protons (the cutoff from the reaction $p_{CR}+\gamma\rightarrow N^*$) occurs at much higher energies, as a consequence of the high proton mass and its high exci-

tation energy. Note also that beyond 10^{20} eV, the universe has regained some transparency to γ rays.

The microwave background radiation is by far the most intense source of diffuse photons in the universe. The infrared diffuse intergalactic background is not yet measured, although the density is known to increase rapidly with increasing wavelength. Consequently the optical depth above 10^{11} eV increases quickly with increasing γ-ray energy, as seen in curves a, b, and c in Fig. 5. Distant sources of VHE γ rays are either completely obscured or their energy spectra are distorted. Based on curve a in this figure, the mean free path at 1 TeV would be 1 Gpc or $z=0.3$, while at 10 TeV it would be 100 Mpc or $z=0.03$. For γ rays in the HE regime, the universe is essentially transparent.

The infrared/optical background results from emission from stars at all epochs and from dust in galaxies, which is heated by the stars and reemits at these wavelengths. The strength could provide information on the epoch of star and galaxy formation. MacMinn and Primack (1996) have undertaken a systematic parametrization of diffuse light production by stars from the early universe for various dark matter hypotheses (cold, hot, or cold/hot) and the resulting era of galaxy and star formation (as well as the dynamics of the expansion). Their results imply that a better determination of this background could help distinguish among the hypotheses.

To date, there are only upper limits on the diffuse intergalactic light, except possibly for wavelengths near the microwave background radiation from FIRAS data on the COBE satellite; this determination requires a drastic subtraction of forefront noise from the galaxy (see below). The observation of the absorption of high-energy γ rays would constitute a nearly direct measurement.

Data from the Hubble Space Telescope have indicated high star-burst activity around $z=1$, far later than the epoch of galaxy formation ($z<4$). This late star formation probably results from a high rate of galaxy collisions. According to Stecker and deJager (1998), the formation of infrared light around $z=1$ will impede any direct correlation between the high-energy absorption and the era of galaxy formation. Nevertheless the measurement of the infrared diffuse light remains a major issue.

F. Study of nuclear and particle physics at high energies

High-energy cosmic γ rays and nuclei interact with atoms in the earth's atmosphere, producing large cascades of elementary particles. Ground-based γ-ray telescopes detect particles from these cascades and can study the nature of nuclear and particle interactions at energies above those available at terrestrial accelerators. A nice, although perhaps somewhat dated, review of the connection between cosmic-ray studies and nuclear and particle physics is given in the review article by Gaisser and Yodh (1980).

Claims that UHE γ rays coming from Cygnus X-3 produced anomalous air showers (Samorski and Stamm, 1983a) increased interest in this connection. Among the proposed particle physics explanations of the anomalous showers were new physics leading to an anomalously large neutrino interaction cross section at high energies (Domokos and Nussinov, 1987; Domokos and Kosevi-Domokos, 1988), an increasing total photon cross section at high energies caused by virtual gluons (Drees and Halzen, 1988), and new technicolor-inspired particles (Collins *et al.*, 1989). These claims are no longer generally accepted, as we discuss in Sec. VI.D below.

The search for new phenomena in the interactions of high-energy cosmic particles has motivated many high-energy physicists to enter this field and has enhanced the development of new experimental techniques. This seems fitting, since many of the early seminal discoveries in particle physics came from studies of cosmic-ray interactions.

IV. THE TECHNIQUES OF HIGH-ENERGY GAMMA-RAY ASTRONOMY

A. Introduction

Three important facts govern the techniques that are used in high-energy γ-ray astronomy.

(a) The earth's atmosphere is opaque to high-energy photons. At sea level, the atmosphere is 1030 g/cm^2 thick, which corresponds to 28 radiation lengths; this implies that the probability that a high-energy photon incident from the zenith will reach ground level without interacting electromagnetically is $\sim 3\times 10^{-10}$. Even at mountain altitudes, where the atmosphere is considerably thinner, the probability that a photon will survive to ground level is negligibly small. Thus only a detector above the earth's atmosphere, in a balloon or a satellite, can detect primary cosmic γ rays.

(b) The fluxes of high-energy γ rays from astrophysical sources are quite low and decrease rapidly with increasing energy. For example, Vela, the strongest γ-ray source in the sky, has a flux above 100 MeV of 1.3×10^{-5} photons/cm^2/s, and a differential flux that falls as $E^{-1.89}$ (Hermsen *et al.*, 1981). This implies that above some energy, a detector in a satellite will be too small to detect enough photons to be useful. A $\sim$1000-cm^2 detector in a satellite would detect approximately one photon/minute from Vela above 100 MeV, and one photon every two hours above 10 GeV. The pursuit of γ-ray astronomy at TeV energies must be done with much larger instruments than can currently be launched on a satellite. Thus VHE and UHE astronomers use earth-based detectors.

(c) The flux of high-energy charged cosmic rays is much larger than the γ-ray flux. These charged particles are bent in the interstellar magnetic fields so that they form an essentially isotropic background. The cosmic-ray proton flux has been measured from 100 GeV to $\sim$400 TeV to be

$$dN/dE=(9.2\pm 2.4)\times 10^{-2}E^{-2.76}\,\mathrm{m^{-2}s^{-1}sr^{-1}TeV^{-1}}, \quad (3)$$

where E is expressed in units of TeV (Burnett *et al.*, 1990). The all-particle cosmic-ray flux is about a factor of 3 higher in this region. Rejection of the large cosmic-ray background is extremely important in high-energy γ-ray astronomy.

B. Satellite-based detectors

Satellite-based instruments detect the primary photon using techniques that have been developed in experiments at accelerators. The photon direction is determined with tracking detectors following conversion of the photon into an electron-positron pair; the photon energy is usually measured in a total-absorption calorimeter. A charged-particle veto counter discriminates against the large background produced by incident charged cosmic rays.

Good angular resolution is important for identifying point sources of photons and for minimizing the effects of diffuse backgrounds. The angular resolution can be no better than the angle between the incoming photon and the outgoing electron-positron pair. There are two contributions to this angle, the intrinsic angular difference in the pair-production process and the multiple Coulomb scattering angle in the converter. The typical rms angle between an incident photon of energy E and a secondary electron (or positron) in pair production is

$$\theta_{\rm rms}^{pp} \approx (m_e c^2/E)\ln(E/m_e c^2), \tag{4}$$

while the typical rms angle in multiple scattering is

$$\theta_{\rm rms}^{ms} \approx (20/p\beta)(L/L_R)^{1/2}, \tag{5}$$

where p is the electron or positron momentum in MeV/c, β is the particle's velocity in units of c, L is the particle's path length in the converter, and L_R is the radiation length of the converter material. Generally, $\theta_{\rm rms}^{ms} > \theta_{\rm rms}^{pp}$, so the resolution can be reduced by using thinner converters. One is then faced with a trade-off between wanting a large number of thin converters to increase the overall conversion efficiency while preserving good angular resolution, and needing to limit the number of detector channels. Note that Eqs. (4) and (5) imply that the angular resolution should improve with increasing energy for a given detector configuration, until the resolution of the tracking detectors becomes important.

A photon produces an electromagnetic cascade that develops in the calorimeter; the calorimeter measures the integrated path length of the charged particles in the cascade, which is proportional to the energy of the primary photon. The energy resolution generally improves with increasing energy until leakage of shower particles out of the calorimeter becomes important. Common calorimeter materials include sodium iodide, cesium iodide, and lead glass. Good energy resolution is needed to determine the energy spectrum of a source, often an important clue to the acceleration mechanism.

Another important parameter of a detector is its effective area, which is defined as the physical area of the detector convoluted with the γ-ray detection efficiency.

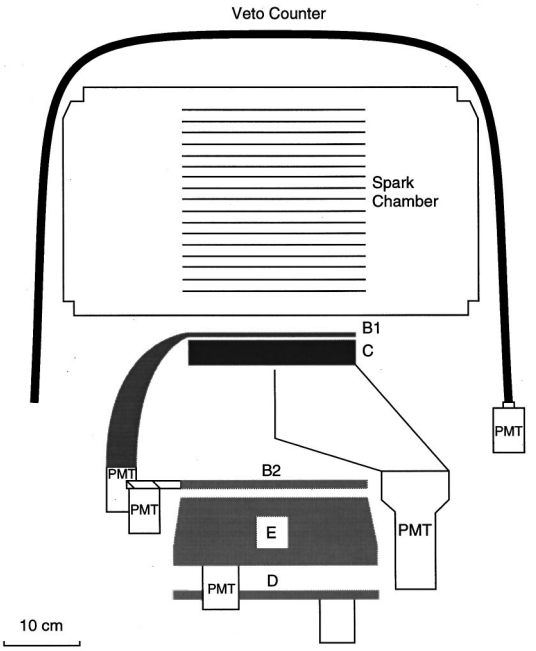

FIG. 6. Sectional view of COS-B, a gamma-ray-detecting satellite launched in 1975. B1, B2, and D are scintillation counters, C is a Čerenkov counter, and E is a CsI calorimeter.

If a detector is exposed to a photon flux $\phi(E)$ photons/m^2/s from a point source for a period of time T and records N events, the effective area $A_{\rm eff}$ is defined as

$$A_{\rm eff}(E) = \frac{N}{\phi(E)T}. \tag{6}$$

Two gamma-ray satellites were launched in the 1970s: SAS-2 in 1972 (Derdeyn *et al.*, 1972) and COS-B in 1975 (Bignami *et al.*, 1975). Figure 6 shows a sectional view of the COS-B gamma detector. Photons converted in thin $(0.042\,L_R)$ tungsten plates within wire spark-chamber modules, which recorded the direction of the resulting electron-positron pair. Scintillation and threshold Čerenkov counters provided a trigger; the Čerenkov counter discriminated against particles traveling upward through the instrument. The electromagnetic energy was measured in a CsI calorimeter; weight limitations restricted the calorimeter thickness to $4.7\,L_R$. The upper part of the telescope was surrounded by an anticoincidence counter to assure that only electrically neutral particles triggered the instrument. Table III summarizes

TABLE III. COS-B characteristics.

Photon energy	Energy resolution (FWHM)	Angular resolution (FWHM)	Effective area
70 MeV	50%	7.2°	12 cm^2
150 MeV	45%	4.5°	37 cm^2
300 MeV	50%	3.2°	52 cm^2
1 GeV	67%	2.4°	48 cm^2

TABLE IV. EGRET characteristics.

Photon energy	Energy resolution (FWHM)	Angular resolution (FWHM)	Effective area
100 MeV	26%	5.5°	930 cm^2
500 MeV	20%	2.0°	1570 cm^2
1 GeV	19%	1.2°	1300 cm^2
10 GeV	26%	0.4°	690 cm^2

some of the characteristics of COS-B (Scarsi *et al.*, 1981).

The COS-B energy resolution improves with increasing energies until shower leakage becomes important, at which point it degrades rapidly. At low energies, the effective area rises with increasing energy because the photon conversion probability rises. The effective area reaches a maximum at roughly 400 MeV and then decreases because of the increasing probability that a charged shower particle will escape from the spark chambers and fire the anticoincidence counter. COS-B achieved a typical source sensitivity of 10^{-6} photons/cm^2/s above 100 MeV.

The most sensitive high-energy γ-ray telescope to date is the EGRET instrument aboard the Compton Gamma-Ray Observatory (CGRO; Thompson *et al.*, 1993). CGRO was launched on April 5, 1991, after a long delay due to the explosion of the *Challenger* space shuttle. EGRET, shown in Fig. 7, is similar to the earlier COS-B detector, although it is much larger. The performance of EGRET is outlined in Table IV.

EGRET has a multilayered spark chamber with tantalum photon-conversion foils followed by a spark chamber with widely spaced plates to measure the electron-pair direction. The photon energy is measured in a NaI(Tl) calorimeter 8 radiation lengths thick. A scintillation-counter time-of-flight system assures that the triggering particle is traveling downward towards the calorimeter, and an anticoincidence counter eliminates charged-particle triggers. The performance of EGRET was thoroughly tested and calibrated with beams of photons from the SLAC and Bates electron accelerators and with protons from the AGS at Brookhaven National Laboratory (Thompson *et al.*, 1993). The minimum integral photon flux above 100 MeV detectable by EGRET is $\sim 5\times10^{-8}$ photons/cm^2/s in a two-week run, a large improvement over COS-B.

C. Earth-based detectors

Gamma rays striking the earth's atmosphere interact with air molecules high in the atmosphere. Earth-based γ-ray astronomy telescopes detect the products of these interactions.

1. Properties of extensive air showers

The total cross section for photon-proton collisions has been measured for center-of-mass energies up to 200 GeV (Aid *et al.*, 1995), which is equivalent to a 20-TeV photon colliding with a proton at rest. Although an extrapolation is necessary to describe the initial interactions of higher-energy photons, the physics of the interactions is believed to be well known. The predominant interactions are electromagnetic; the cross sections for the production of hadrons and muon pairs are several orders of magnitude smaller than that for electron-pair production. In the electromagnetic shower, photons produce electron-positron pairs, and electrons and positrons produce photons via bremsstrahlung. The resulting electromagnetic cascade grows nearly exponentially as it propagates through the atmosphere; the primary energy is divided among more and more particles until the mean energy of the electrons and positrons approaches the critical energy ϵ_0 ($\approx$80 MeV in air). At this point the ionization energy-loss mechanism, which does not produce additional shower particles, becomes more important than bremsstrahlung. Thus energy is lost from the shower and the number of particles in the shower decreases as the shower continues to propagate.

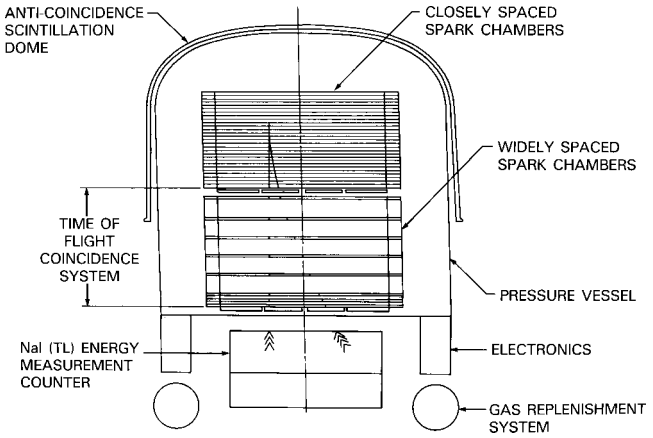

FIG. 7. Schematic view of EGRET, the high-energy gamma-ray detector aboard the Compton Gamma-Ray Observatory.

The longitudinal development (the number of electrons and positrons) of typical photon-induced extensive air showers (EASs) is shown in Fig. 8 for several primary energies; note that after shower maximum, showers become increasingly rich in hard photons. The maximum shower size occurs approximately $\ln(E/\epsilon_o)$ radiation lengths into the atmosphere, generally well above ground for all but the very highest primary energies. Nevertheless, a large number of shower particles may reach the ground, especially at mountain altitudes. In an electromagnetic shower, the particles are ultrarelativistic and the dominant physical processes are sharply peaked forward. Consequently, the cascade arrives at the ground in a thin front only a few meters thick. The lateral extent of a shower is due primarily to multiple Coulomb scattering of the electrons and positrons. The lateral distribution of the electron particle density is described by the so-called NKG function (Nishimura and Kamata, 1952; Greisen, 1956, 1960).

The more plentiful incident high-energy cosmic rays, protons and nuclei, also interact high in the atmosphere,

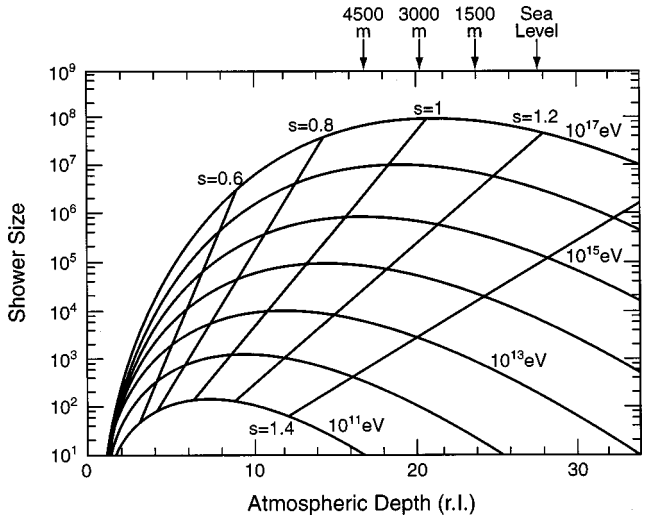

FIG. 8. Longitudinal development of an extensive air shower.

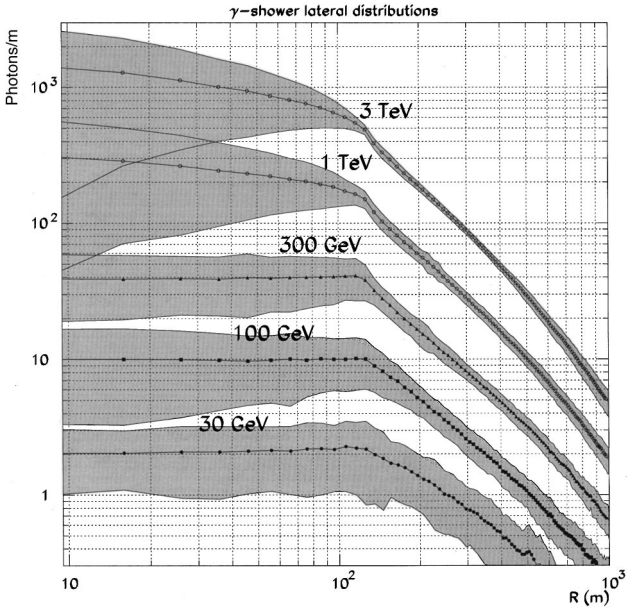

FIG. 9. Density of Čerenkov photons between 300 and 600 nm as a function of distance from the shower impact point (impact parameter R) for various γ-ray energies as seen at 2 km above sea level for vertical showers. At each energy, the mean and spread from a database of 100 showers is shown. The fluctuations are thus for a single 1-m^2 photon counter and can be considerably reduced in more sophisticated detectors, as discussed in the text.

producing extensive air showers; the nuclear collision length is 62 g/cm^2 for protons and less for heavier nuclei. The initial interactions generate a hadronic cascade; these interactions tend to quickly divide the primary energy among a large number of particles, so relatively few hadrons survive to the ground. Some charged pions and other hadrons decay before interacting, producing muons (and neutrinos); the weakly interacting muons generally lose energy only by ionization and so have a relatively high probability of reaching the ground. High-energy neutral pions produced in the hadronic interactions decay rapidly into photons; these photons produce electromagnetic cascades in the same manner as discussed above. Thus the particles reaching the ground in a hadron-induced extensive air shower are mostly electrons, positrons, photons, and muons (plus neutrinos); except for the presence of the muons, a cosmic-ray shower at ground level is not very dissimilar to a γ-ray shower. The muon lateral distribution is considerably wider than that of the electromagnetic particles (Greisen, 1960). There are roughly 20 times more muons in a hadron-initiated EAS than in a photon-initiated EAS of the same energy.

In addition to shower particles, Čerenkov photons are produced in an EAS. Čerenkov light in the atmosphere is produced by charged particles traveling faster than the speed of light in air. This emission is governed by the value of n, the refractive index, which is proportional to the atmospheric density (which decreases exponentially with height, with a scale height of $\sim$8 km). The Čerenkov emission angle is given by $\cos\theta_c=(n\beta)^{-1}$ and the threshold for emission is $E_{th}=m_0c^2/\sqrt{2n-1}$. With increasing energy, the emission angle quickly reaches its maximum value of $\theta_c=\cos^{-1}(1/n)$. At sea level, the threshold energy for Čerenkov emission to occur is 21 MeV for electrons [or 35 MeV at 8 km above sea level (a.s.l.)], 44 GeV for muons, and 39 GeV for protons. The maximum angle of Čerenkov emission is 1.3° at sea level, or 1° at 8 km a.s.l., independent of the mass of the emitting particle.

The maximum of the shower development occurs at a height of between 10 and 7 km a.s.l. for γ rays of energies between 100 GeV and 10 TeV. The median altitude for Čerenkov emission from a 1-TeV γ shower is 8 km (slightly lower for a proton shower on average). Half of the emission occurs within 21 m of the shower axis (70 m for a proton shower; Hillas, 1996). The Čerenkov light from an EAS illuminates a ''light pool'' on the ground, of radius $\sim$130 m (at 2 km a.s.l.), whose extent is determined primarily by the Čerenkov emission angle, as seen in Fig. 9. The average photon density in the light pool for a 1-TeV γ-ray shower is $\sim$200 photons/m^2 (at 2 km a.s.l.) in the visible. The Čerenkov light is a thin front resulting in a pulse of duration 2–3 ns and an angular extent on the sky of $\sim$0.5°. The total distance traveled by all particles above the Čerenkov threshold is directly related to the energy of the primary particle, so the Čerenkov yield gives a measurement of the initial γ-ray energy. Due to the flat distribution in the light pool, a single sample at any point within $\sim$130 m of the impact point gives a good estimate of the primary energy.

The large area of illumination on the ground implies that a single ACT detector anywhere within the light pool can detect the shower, giving an effective detection area of 5×10^4 m^2 at 2 km a.s.l. for vertically incident showers.

An extensive air shower can be detected by observing either the shower particles that reach the ground or the Čerenkov radiation produced in the shower. In both

cases, one uses the properties of the EAS to infer information about the primary particle that initiated it.

2. Air Čerenkov detectors

a. Detection of Čerenkov radiation from extensive air showers

Detectors based on the atmospheric Čerenkov technique consist of one or more mirrors that concentrate the Čerenkov photons onto fast optical detectors. Photomultiplier tubes (PMTs) placed in the focal plane are generally used to detect the Čerenkov photons.

Two problems in using atmospheric Čerenkov telescopes (ACT) are the night-sky background and the large isotropic background from cosmic-ray showers. The energy threshold of an atmospheric Čerenkov telescope is determined by the number of Čerenkov photons needed to observe a signal above the level of the night-sky background. On clear, moonless nights at a dark site at 2 km a.s.l., the night-sky background light between 300 and 600 nm for an acceptance diameter of 1° is

$$\phi_b \sim 0.1 \text{ photons/m}^2\text{/ns/}\phi 1^\circ. \tag{7}$$

At a given primary energy, the detected Čerenkov signal S is proportional to the mirror surface area A, while the night-sky background-noise fluctuations are $\propto \sqrt{A\,\tau\Omega}$, where τ is the integration time and Ω is the solid angle on the sky viewed by the mirror. Thus, for a simple atmospheric Čerenkov telescope,

$$\frac{S}{\sqrt{B}} \propto \sqrt{\frac{A}{\tau\Omega}}. \tag{8}$$

The effects of the night-sky noise can be reduced by increasing the mirror area, decreasing the integration time (to the limit of the Čerenkov pulse length), and decreasing the acceptance solid angle.

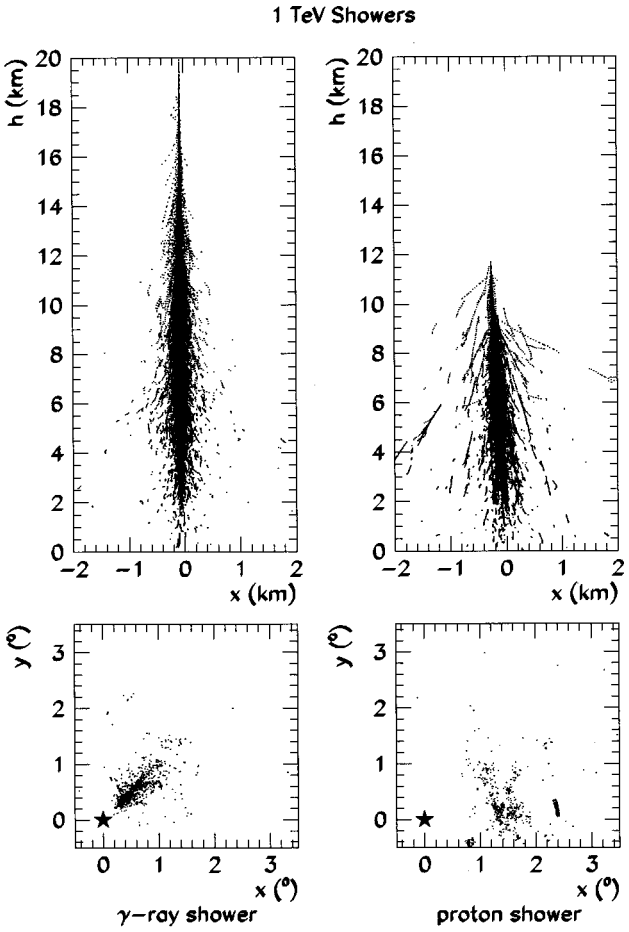

FIG. 10. Development of vertical 1-TeV proton and γ-ray showers in the atmosphere. The upper panels show the positions in the atmosphere of all shower electrons above the Čerenkov threshold; the lower panels show the resulting Čerenkov images in the focal plane of a 10-m reflecting mirror when the showers fall 100 m from the detector. (Note that the center of the focal plane is situated at the bottom left of the bottom panels.)

b. Rejection of cosmic-ray background

The flux of cosmic rays in an acceptance solid angle of 1 msr ($\simeq \varnothing 1^\circ$) is at least four orders of magnitude larger than that from the strongest γ-ray source. Second-generation atmospheric Čerenkov telescopes take advantage of the fact that cosmic-ray showers are more chaotic than γ showers, since their development is governed by a relatively small number of particles in the hadronic core. The larger transverse momentum of hadronic interactions gives a broader lateral distribution. In addition, these interactions also produce many more muons, which can survive to detector level and trigger the air Čerenkov detector. They can also produce Čerenkov photons at large angles to the bulk of the photons from the hadronic shower.

These differences have led to two strategies for the rejection of the cosmic-ray background. First, a measurement of the angular distribution of the Čerenkov photons on the sky for each shower can allow separation between hadronic showers and γ-ray showers. Second, accurate measurement of the shower arrival direction improves the separation between γ-ray showers from point sources and isotropic cosmic-ray showers.

Two detection techniques have been developed utilizing these strategies. In the imaging technique, the angular distribution of the Čerenkov photons on the sky is measured with an array of close-packed photomultiplier tubes in the focal plane of the mirror. The images thus obtained provide both directional and shape information on the shower photons, as can be seen in Fig. 10. The γ shower appears as a glowing rod in the sky seen from a direction close to the end of the rod.

The angular width of the image is a direct measurement of the distribution of Čerenkov-emitting electrons about the shower axis; the image has an rms width of $\sim 0.13^\circ$. The image is circular for a shower falling directly on the detector, becoming more elliptical or cometary in shape with a center of gravity displaced from the source position as the distance from the detector to the shower axis (or "impact parameter" R) increases; the rms length increases from 0.13° to $>0.5^\circ$. Longitu-

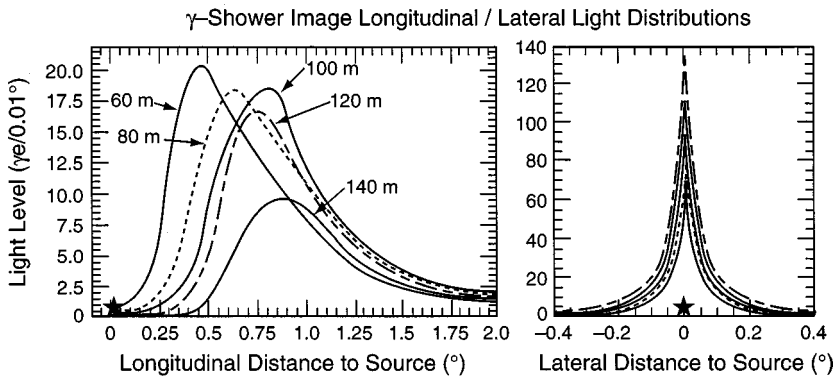

FIG. 11. Projections of the light in average γ-ray images as a function of impact parameter for 500-GeV vertically incident showers as seen by a 10-m dish with standard photomultiplier tubes at 2 km above sea level. The longitudinal (along the axis from the image center to the source) and transverse/lateral distributions are shown for distances to the shower impact point.

dinal and transverse light distributions in the image plane for average showers at 500 GeV are shown in Fig. 11 for various values of impact parameter.

The major axis of the image points toward the source position in the image focal plane through the effect of perspective. This alignment is a measurement of the source position, usually parametrized in terms of the angle α between the major axis of the ellipse and the source position in the image plane [see Fig. 12(a)]. The direction of the image axis is well determined for showers with R greater than a few tens of meters. Alpha values are close to zero for γ rays from a point source, compared to a uniform distribution for the isotropic background [see, for example, Fig. 12(b)]. The shape of the image (parametrized, for example, by the transverse width of the image) provides background rejection, since the cosmic-ray shower images are broader and more chaotic. This analysis uses the fact that the night-sky noise in each photomultiplier tube or pixel (picture element) is small, since the solid angle covered by a PMT is small.

In the second detection technique, wave-front timing, the arrival time of the Čerenkov pulse is measured at a number of mirrors distributed on the ground within the light pool. For γ rays above a few hundred GeV, the Čerenkov photons arrive in a cone with a wide opening angle $(\pi/2-\theta_c)$ centered on the shower axis, as shown in Fig. 13 for a 1-TeV γ ray. The conical shape is the envelope of wave fronts from different altitudes, as shown in the figure. A fit of the arrival times to this cone gives the shower-axis direction and thus the direction of the incident γ ray. Background rejection is provided by correlating the lateral light distribution with the fitted cone. Below 1 TeV, the cone becomes rounded off near the shower core, while at lower energies the conic form becomes more spherical. Thus supplementary measurements of the light pool become necessary at low energies to determine the shower axis. The trigger for such a detector requires that a number of mirrors have signals exceeding a given level in coincidence. While the cosmic-ray rejection power of this technique is not as good as with the imaging technique, the estimate of the primary energy of the γ ray should be better than that of a single imaging detector, as the Čerenkov light pool is sampled at several points on the ground.

Some extensions of these techniques have been explored. For example, the use of several mirrors on the same mount reduces triggers from the night-sky background and from local muons passing near the detector.

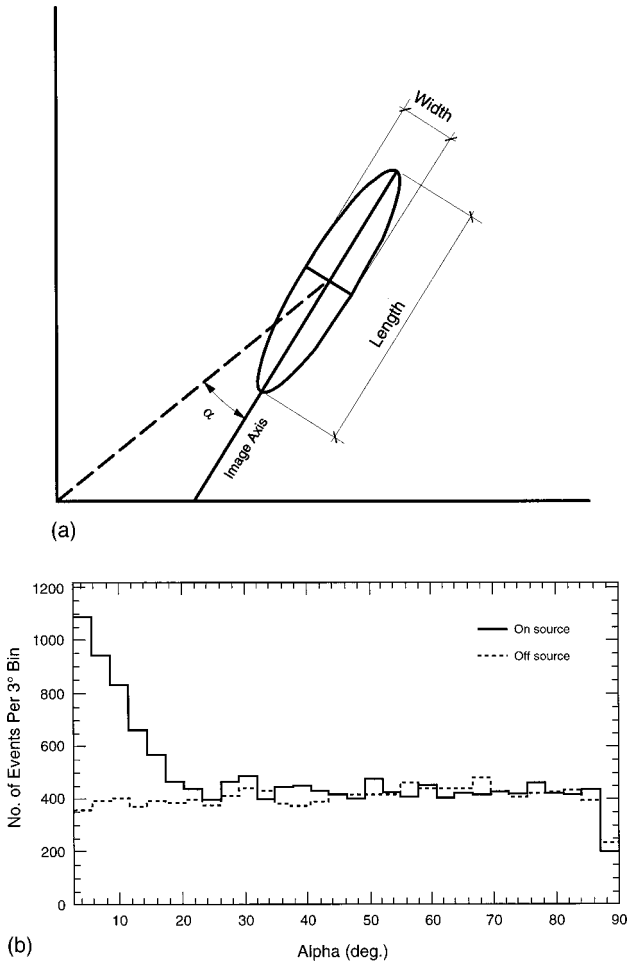

FIG. 12. Imaging parameters used by air Čerenkov telescopes to reject the hadronic cosmic-ray background: (a) Diagram showing the parameters α, width, and length. The ellipse represents the outline of the shower image in the focal plane of the telescope. (b) An α plot of the signal from the Crab Nebula, by the Whipple group using data taken between 1988 and 1989. From Mohanty *et al.*, 1998.

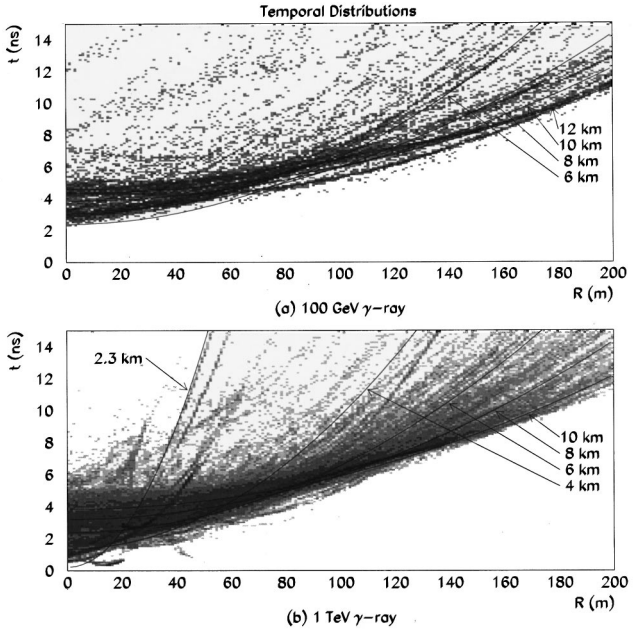

FIG. 13. Arrival-time distribution for Čerenkov photons between 300 and 600 nm as a function of distance from the shower impact point (R) for various γ-ray energies as seen at 2 km above sea level for vertical showers (log contours).

Stereo imaging, the use of a number of imagers, allows the point of origin of each shower, and thus the direction of the primary, to be determined in two dimensions, and completely eliminates problems caused by nearby muons.

The longitudinal development of γ-ray showers of a given energy is well defined with small fluctuations. Consequently the image in the focal plane of an imaging atmospheric Čerenkov telescope has a well-defined longitudinal profile that depends only on the impact parameter and the angular origin of the shower (Fig. 11). In a fine-pixel imaging Čerenkov telescope, this profile can be compared to theoretical γ-ray shower profiles, as a function of the shower energy, impact parameter, and angular origin. In the case of the CAT imaging telescope (Barrau *et al.*, 1998), this gives an angular resolution for individual γ-ray showers of $\sim 0.1°$. For an array of several imaging atmospheric Čerenkov telescopes viewing a shower simultaneously, the angular origin of the shower on the sky of the shower is given by the point of intersection of the shower axes as seen by the telescopes. An angular resolution of $\sim 0.1°$ is achieved with the HEGRA imaging array (Daum *et al.*, 1997; Puhlhofer *et al.*, 1997).

In such second-generation Čerenkov telescopes, the cosmic-ray background can be reduced to a level comparable to, or below, the signal from strong γ-ray sources. Table V lists some of the major atmospheric Čerenkov detectors, all of which use the imaging technique.

c. Trigger and readout electronics

In both the imaging and wave-front timing methods, the trigger uses "majority" logic, requiring a fast coincidence of at least several channels (pixels or dishes) above a given signal level. The time resolution of this coincidence should be in the range of 3–10 ns, depending on the anisochronism of the mirrors, signal jitter, and other uncertainties. Intelligent triggers, which include only those pixels near the brightest part of the image,

TABLE V. Current major atmospheric Čerenkov telescopes.

Group – experiment	Site alt., lat., long. (m,°,°)	Mounts × dishes	Dish area (m^2)	Pixel size (°)	Field of view (°)	Threshold (GeV)
Whipple–10m	Mt. Hopkins, Arizona 2300 32N 111W	1×1	72	0.25	3	250
CAT–Imager	Thémis, France 1650 42N 2E	1×1	17	0.12	3	250
Durham–Mk VI	Narrabri, Australia 250 31S 110W	1×3	42	0.25	4	300
HEGRA–Imagers	La Palma, Canary Islands 2200 28N 18W	5×1	5/8.5	0.25	3.25	500
Telescope Array	Dugway, Utah 1600 40N 113W	3×1	6	0.25	4.5	600
CANGAROO	Woomera, Australia 0 31S 136E	1×1	11	0.19	3	1000
CAO–GT-48	Ukraine, Crimea 1100 45N 34W	2×3	4.5	0.4	3	1000
TACTIC	Mt. Abu, India 1300 25N 73W	1×1	9.5	0.31	3.2	1000
Lebedev–SHALON	Tien Shan, Kazahkstan 3338 43N 77E	1×1	10	0.6	8	1000

have been tested, and a trigger-rate reduction was also obtained by subdividing the camera into overlapping sectors. Even for a relatively low threshold, trigger rates can be 10–50 Hz.

The amplitudes of the photomultiplier signals must be measured by the readout electronics and stored for offline event analysis. This is often done by integrating the output signals during a gate time opened by the trigger, with subsequent encoding by analog-to-digital converters (ADCs). To limit the noise from the night-sky photons, the gate should be short, but fast gates (<10 ns) may introduce electronic noise. An alternative is the use of individual "flash" encoders (F-ADCs) running at a fast sampling rate. The digitized values, stored in a transient memory, are read out at the time of the trigger, giving a sampling of the output of each photomultiplier. The integration can be performed offline. There are very fast F-ADCs running at a GHz, but their cost remains prohibitive. In practice, the effective integration time can be at best ~ 20 ns with 100-MHz F-ADCs. There is still room for technical improvement on this point.

d. Energy estimation and spectral measurement

From Fig. 9 it can be seen that there are large fluctuations (about a factor of 2) in the photon density within the light pool for showers initiated by γ rays of a given energy. This limits the energy resolution of a Čerenkov detector, assuming that the detector is known to be within the light pool. For both the imaging and wavefront timing techniques, the position of the shower axis or center of the light pool is measured typically to within 10–20 m.

Within the light pool, the large fluctuations in the photon density for showers result from two effects: the sampling uncertainty for a single detector and fluctuations in the shower development. Simulations show that the total amount of light reaching ground level varies by only 5%; thus sampling the light pool at several points on the ground can reduce the uncertainty in the determination of the primary energy. In addition, simulations in which the altitude of the first interaction point is fixed (thus reducing the effect of shower fluctuations) show that the photon-density fluctuations are reduced to 30% by this constraint. If the full longitudinal development of the shower is measured as in an imaging detector, the energy resolution for showers coming from a fixed position in the sky can be reduced to 20% with a single sample. With a multitelescope system, such as the HEGRA imaging array, several samples of the light pool are measured at known impact parameters, resulting in an energy resolution of 20% (Daum *et al.*, 1997).

While the atmospheric Čerenkov telescope has the advantage over satellite-borne detectors of a large collection area, one disadvantage lies in the lack of a simple method to determine this collection area and to calibrate the energy response. Such parameters can be directly measured for satellite-borne detectors in particle-beam tests. The atmospheric Čerenkov telescope must rely on extensive Monte Carlo simulations of both γ-ray-induced showers (to determine energy resolution and acceptance) and cosmic-ray protons and heavier nuclei, and local muons (to determine the rejection efficiency for these backgrounds), for a large range of observing angles from the zenith. These simulations have become more robust as they have been refined in parallel with new hadron collision parametrizations from accelerator experiments. Comparisons between different simulations show only minor differences ($<10\%$) in the Čerenkov yield. The remaining uncertainties are the condition of the atmosphere (which can be monitored optically or determined from the zenith-angle dependence of detected events) and the photon collection efficiency of the photomultiplier tubes. For the imaging technique, the Čerenkov light from local muons provides an elegant means of measuring the collection efficiency, as it provides clearly recognizable rings or arcs in the image plane with a well-defined distribution of Čerenkov photons (Vacanti *et al.*, 1994).

e. Effect of observatory altitude and large-zenith-angle observations

The altitude affects the photon density, primarily through the straightforward geometrical expansion of the light pool, which is a cone with an apex at about 12 km a.s.l. With increasing observation altitude, the light-pool area shrinks and the photon density increases accordingly. Thus the Čerenkov signal is enhanced so that the energy threshold is lowered. Conversely, the flux sensitivity is lowered. To a lesser extent, the Čerenkov signal is further enhanced by the lowering of atmospheric absorption, which has an effect of the order of 10–15% per kilometer change in altitude. The night-sky noise increases only slightly with increasing altitude. Altogether, moving an observatory from 2–4 km a.s.l. would lower the energy threshold by about a factor of 2 (with a corresponding loss in flux sensitivity of about 15% due to the decrease in the light-pool area). This is a major advantage, but the cost of running a complex instrument at high altitude must be weighed against other methods of attaining the same objectives.

The changes in zenith angle of the source have small effects on the observations for zenith angles less than about 30°. At larger angles the light pool grows swiftly due simply to the increasing distance of the shower maximum from geometrical effects. The distance to shower maximum is further increased at large zenith angles because an inclined shower encounters more matter at high altitude, and so the maximum occurs higher in the atmosphere. Consequently, the observation of sources at low elevation can be made only at higher energies, but the flux sensitivity is increased in proportion to the light-pool diameter. At 45° the collection area increases by a factor of ≈ 2.5 (and the sensitivity by $\sqrt{2.5}$) and the energy threshold increases by a factor of ≈ 2. Such observations have been carried out with success down to 60° from zenith (McEnery *et al.*, 1998; Tanimori *et al.*, 1998a), allowing the determination of the source spectra to be extended to high energies and lower fluxes. The Crab nebula was observed by the CANGAROO group from Woomera in Australia, at

TABLE VI. Recent major extensive air-shower particle detector arrays.

Group	Location	Array area (m^2)	No. detectors	E_{Peak} (TeV)	μ Det. area (m^2)	Event rate (s^{-1})	Years operational
CASA-MIA	Dugway, Utah 870 g/cm^2 40.2° N, 112.8° W	230400	1089	110	2,500	20	1991–96
CYGNUS	Los Alamos, New Mexico 800 g/cm^2 35.9° N, 106.3° W	86000	204	50	120	5	1986–96
HEGRA EAS-PDA	La Palma, Canary Islands 800 g/cm^2 28.8° N, 17.7° W	41000	257	50	150	12	1992–
Milagrito	Jemez Mts., New Mexico 750 g/cm^2 35.9° N, 106.7° W	1500	225	1	0	300	1997–98
SPASE	South Pole 760 g/cm^2 90° S	10000	24	100		1	1987–92
Tibet	Yangbajing, Tibet	8000	49	8	0	5	1990–93
	600 g/cm^2	44000	221	8	0	230	1995–
	30.1° N, 90.5° E	5000	109	2	0	120	1996–

30° south latitude (Tanimori, 1998b). For this source, at a declination of 22°, such observations from the southern hemisphere are in fact optimal for the high-energy end of the spectrum, as the source remains steadily at low elevation for several consecutive hours.

3. Extensive air-shower particle detector arrays

Extensive air-shower particle detector arrays (EAS-PDAs) are generally used to detect EASs produced by ultrahigh-energy primaries; the fluxes of UHE γ rays are expected to be small, so a detection area in excess of 10^4 m^2 is needed. The cost of a uniformly sensitive detector with this area is prohibitive. However, one can use the fact that a large number of particles reach the ground in a UHE shower; a typical EAS initiated by a 100-TeV photon has roughly 50 000 $e^{\pm}$ and about five times as many γ rays, spread out over an area in excess of 10^4 m^2 at mountain altitudes. Because there are so many particles reaching the ground, an EAS-PDA need sample only a relatively small fraction of these particles. An EAS-PDA generally consists of a number of charged-particle detectors spread over a large area. Typical arrays have from 50 to 1000 scintillation counters, each ~ 1 m^2 in size, spread over an area of $10^4 - 2\times10^5$ m^2; the actual sensitive detector area is less than 1% of the total enclosed area of the array. The performance of the array can be improved by placing lead, roughly one radiation-length thick, above each counter to convert shower photons into charged particles (Linsley *et al.*, 1987; Alexandreas *et al.*, 1992). Table VI lists the recent major extensive air-shower particle detector arrays.

The direction of the primary is reconstructed by measuring the relative times at which the individual counters in the array are struck by the shower front. The angular resolution for ground-based detectors depends upon properties of both the EAS and the detector. To obtain good angular resolution with an EAS-PDA, one must perform a fit to a shower front that is curved by an amount that is a function of position from the shower core (Alexandreas *et al.*, 1992). The typical EAS-PDA angular resolution for a given shower is approximately described by (Ellsworth, 1991)

$$\sigma_\theta = (K\sigma_t)/(N\Delta), \tag{9}$$

where σ_θ is the rms projected angular resolution, the constant $K \approx 1$, N is the number of hit detectors, σ_t is the measured rms timing width in nanoseconds as seen by each detector, and Δ is the separation between neighboring detectors in meters.

The angular resolution for an array can be determined in a number of ways (Merck *et al.*, 1996). The most powerful method uses the measured shape of the shadow of the sun and the moon in the otherwise isotropic flux of charged cosmic rays because it is sensitive to all systematic errors; its major shortcoming is that it determines the angular resolution for cosmic-ray, rather than γ-ray, showers. There is some evidence that the apparent shadow of the sun is markedly displaced by bending in the solar magnetic field for energies around 10 TeV (Amenomori *et al.*, 1996). The earth's magnetic field should displace the apparent shadow of the moon by about one moon diameter at ~ 2 TeV, although the displacement depends upon the location of the moon in the local sky. A method for the measurement of the antimatter content of cosmic rays based on this effect has been discussed (Urban *et al.*, 1992).

Figure 14 shows the angular resolution for the HEGRA EAS-PDA as a function of the number of

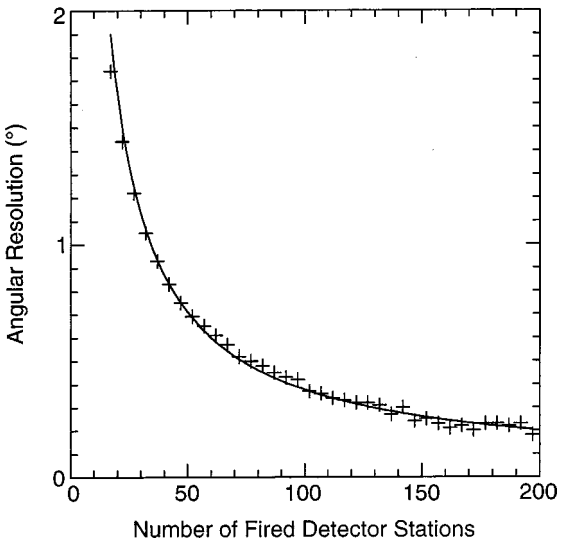

FIG. 14. Angular resolution vs number of counters struck for the High-Energy Gamma-Ray Array (Merck *et al.*, 1996).

struck counters, as determined by dividing an array into two overlapping parts and comparing the angles reconstructed separately from these two arrays (from Merck *et al.*, 1996). The curve is of the form $\sigma_\theta \propto N^{-0.87}$.

The energy threshold of an EAS-PDA depends upon the minimum number of counters that must be struck to allow a shower to be reconstructed, the altitude of the array, and the size and spacing of the counters. While a shower direction can, in principle, be reconstructed with as few as three counters, generally a larger number of counters ($\sim$10) is used to accurately determine the direction. The energy threshold of an array is not a well-defined quantity because the number of shower particles reaching the ground fluctuates greatly from shower to shower for identical primaries; the principal source of these fluctuations is the variation in the altitude and nature of the first interaction. Consequently an array may record some relatively low-energy events because the initial interaction was unusually deep in the atmosphere, and may fail to record some relatively high-energy events because the initial interaction took place unusually high in the atmosphere. In addition, for a given energy primary, the shower size at the ground decreases with increasing angle away from the zenith and also is different for primary photons, protons, and nuclei.

An EAS-PDA does not measure the energy of the primary particularly well. This is not surprising, as all one has to work with is a sparse sample of the number and lateral distribution of particles that have survived to ground level, effectively the leakage out the back of a thick calorimeter. The energy response can be determined with the aid of Monte Carlo simulations of air showers and the array. Figure 15 shows the primary energy distribution for proton-initiated events for the CYGNUS array in Los Alamos. Note that, while the most probable proton energy is around 50 TeV, an appreciable number of 10-TeV proton showers are detected, due to shower fluctuations (Alexandreas *et al.*, 1992). The energy threshold is typically lower for γ-ray

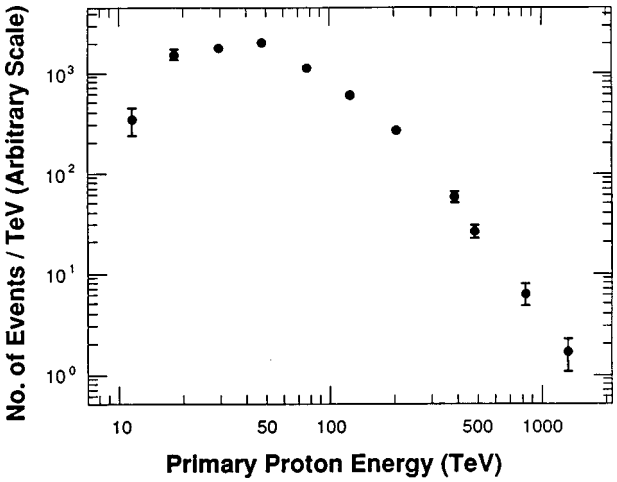

FIG. 15. Energy response for CYGNUS array in Los Alamos.

primaries than for hadron primaries at mountain altitudes, although this is not true when viewing through a large atmospheric overburden such as at large zenith angles (Biller *et al.*, 1994).

The energy response of an array is best described by the effective area, in the same way as is the energy response of a satellite-based detector. For ground-based detectors, the definition of A_{eff} includes the effects of shower fluctuations that affect the probability that an EAS of energy E will trigger the detector. A_{eff} is a function of zenith angle and the primary species. Figure 16 shows the effective area of the CYGNUS array for proton primaries at several zenith angles. Note that A_{eff} is larger than the physical area at high energies, as showers with cores landing outside the array can be detected. Because the energy of the primary is so poorly determined, values of (or limits on) the integral flux above some energy are often given for ground-based measurements. The integral flux can be obtained from the observed (or the upper limit on the) number of events above background and the detector effective area vs primary energy. There is some dependence of the derived integral flux on the assumed spectral shape; this depen-

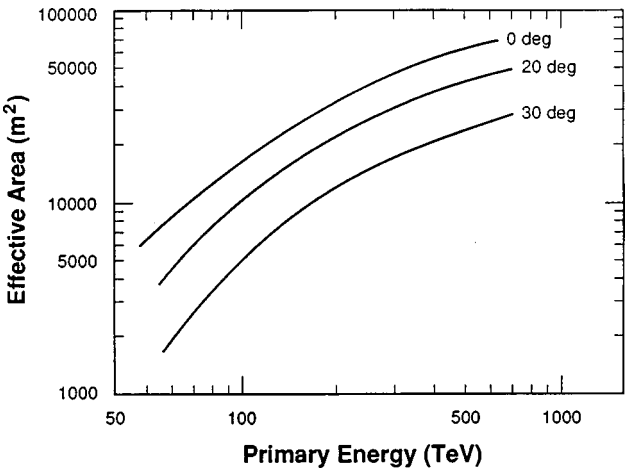

FIG. 16. CYGNUS effective area.

dence can be minimized by giving the integral flux above the median energy of the detector (Gaisser *et al.*, 1989).

4. Air fluorescence detectors

The very low flux of extremely high-energy (EHE) cosmic rays ($\sim 2\,\mathrm{km}^{-2}\,\mathrm{week}^{-1}\,\mathrm{sr}^{-1}$ above 10^{18} eV) necessitates the use of an experimental technique with a huge effective volume at these energies. The beamed nature of the shower particles and the Čerenkov light they emit limit the use of these signatures for EHE cosmic rays. Luckily Nature has provided us with an isotropic source of radiation, allowing very distant air showers to be detected—fluorescence of nitrogen in the atmosphere.

When an ionizing particle traverses the atmosphere it can excite the N_2 molecules. The excited N_2 emits fluorescence photons within about 50 ns of being excited. The photon yield is similar to that of Čerenkov radiation — ~ 5 photons m^{-1} electron^{-1} (Sokolosky, 1989). As with the air Čerenkov detectors, this signal must be detected in the presence of night-sky background photons. As the fluorescence radiation is not beamed, many more shower particles are required to produce an observable number of photons at the detector. Air fluorescence detectors have energy thresholds of order 10^{18} eV and effective apertures of $10–100\,\mathrm{km}^2\,\mathrm{sr}$.

The Fly's Eye detector is currently the only air fluorescence detector in operation. The original detector (1981) consisted of 67 1.5-m-diameter spherical mirrors (Baltrusaitis *et al.*, 1985). Each mirror was viewed by a set of 12–14 photomultipliers. Each PMT viewed a 5.5° hexagonal region of the sky. As the EAS traverses the sky, fluorescence light intercepts different PMTs, forming a track in the detector. The amount of light received in each PMT can be related to the number of electrons in the shower at a specific region of the development of the shower. In 1986 the addition of a second "Eye," located 3.4 km away, allowed stereo reconstruction of each air shower and resulted in much better determination of the trajectory of the shower. Unlike conventional air-shower arrays and air Čerenkov telescopes, this detector has a detailed view of the longitudinal development of the EAS. This information is crucial in determining the atomic weight of the primary cosmic ray. It is in this arena that the Fly's Eye has excelled. While the contribution to γ-ray astronomy has been minimal, the Fly's Eye has made important measurements of the EHE cosmic-ray composition (Bird, 1994).

D. Estimating the background

Signals in ground-based γ-ray astronomy come in the presence of noise from isotropic (hadronic) cosmic rays. In the absence of background rejection, the signal-to-noise ratio is quite poor. For example, the strong signal observed by air Čerenkov detectors from the Crab constitutes an increase in raw counting rate of less than 1%.

With such high background levels, it is imperative to correctly estimate the background rate so that the probability that the observation could be due to a chance fluctuation of the background can be assessed. The background estimate must be made under conditions that can be changing due to changes in local weather, instrumental efficiencies, and detector dead time.

Early air Čerenkov observations alternated periods of looking on source and off source; this technique does not necessarily correctly account for changing conditions. Imaging Čerenkov telescopes allow the signal and background to be separated from a single observation period by measurements of the shape of the Čerenkov image (a plot of α; see Fig. 12).

The background can be estimated with air-shower counter arrays by using the data coming from other parts of the sky with the assumption that γ-ray sources are rare (or weak). Generally, the data are used to characterize the detector response in local coordinates (θ,ϕ) as a function of time; integrating this response over the live time (again obtained from the data) yields the expected background in the region of a point source. This is discussed in greater detail by Alexandreas *et al.* (1993b).

V. EARLY OBSERVATIONS

A. Satellites

Two gamma-ray satellite detectors were launched in the 1970s: SAS-II in 1972 and COS-B in 1975. An electronic failure terminated the SAS-II mission after only seven months of operation. Nevertheless, data from SAS-II showed emission above 100 MeV from the galactic plane, especially in the vicinity of the galactic center (Fichtel *et al.*, 1975), pulsed emission from the Crab and Vela pulsars, detection of Cygnus X-3 (Lamb *et al.*, 1977) and Geminga (although this source was not identified at that time), and observation of diffuse extragalactic emission (Thompson *et al.*, 1976; Fichtel *et al.*, 1978).

The COS-B satellite operated for six and a half years and produced detailed maps of the γ-ray sky, with the prominent feature of the diffuse emission from the galactic plane (Bloemen, 1989). The most important result from COS-B was a catalog of 25 γ-ray sources at energies above 300 MeV (Swanenburg *et al.*, 1981). Some of these "sources" are now believed to be emission from molecular gas clouds (Grenier *et al.*, 1990). Data on the Crab, Vela, and Geminga allowed detailed studies of their γ-ray energy spectra; however, they could not confirm the detection of Cygnus X-3 (Hermsen *et al.*, 1987). The COS-B data established γ-ray astronomy as an exciting field and provided much of the impetus for studies with ground-based instruments.

B. Early ground-based results

Ground-based high-energy γ-ray observations in the 1980s produced many claimed source detections. These are summarized in the review article by Weekes (1988), which presented a "source catalog" containing 13 sources. In this section we briefly review the most widely known results of this period, those involving Cygnus

X-3, Hercules X-1, and the Crab. Later we shall discuss the present view of these results.

1. Cygnus X-3

Cygnus X-3 is an x-ray binary system located about 10 kpc from earth. However, the exact nature of Cygnus X-3 has been difficult to establish, in large part because an optical identification has not been made due to obscuration by galactic dust. The source exhibits a 4.79-h period in its x-ray (but not in its radio) emission, although a complete eclipse is not observed.

Claims of detection of TeV emission from Cygnus X-3 were first made in the mid 1970s and continued through the mid 1980s. Two observations from EAS-PDA were particularly important: the claim of a 4σ steady excess by a group in Kiel, Germany (Samorski and Stamm, 1983b) and a contemporaneous observation at Haverah Park (Lloyd-Evans *et al.*, 1983). These results indicated a very large UHE flux from Cygnus X-3. The Kiel result was particularly striking in that the showers appeared to have a large muon content, indicating new particle physics—either a new uncharged light particle that interacts hadronically or a known neutral particle (photon or neutrino) undergoing new interactions at high energies. Claims of observations of Cygnus X-3 by proton-decay experiments located deep underground helped bring this object (and cosmic-ray physics) to the attention of particle physicists (Marshak *et al.*, 1985).

2. Hercules X-1

Hercules X-1, the second x-ray binary system discovered by the Uhuru satellite (Tananbaum *et al.*, 1972), is not obscured by dust and so is well studied. The 1.24-s x-ray pulsations, discovered by the Uhuru group, are believed to be due to the rotation of the neutron star. The observation of optical and infrared pulsations at frequencies slightly displaced ($\sim 0.1\%$) from the x-ray frequency are understood in terms of x-ray interactions with material in other parts of the binary system (Middleditch *et al.*, 1985).

A number of groups claimed to detect episodic VHE and UHE emission from Hercules X-1 in the 1980s with periodicity at the x-ray period. In 1986, three groups claimed to observe episodic, pulsed emission from Hercules X-1 on different nights at a frequency blue shifted from the x-ray frequency by 0.16%; the observations were made by the Haleakala atmospheric Čerenkov telescope (Resvanis *et al.*, 1988), the Whipple atmospheric Čerenkov telescope (Lamb *et al.*, 1988), and the CYGNUS EAS-PDA (Dingus *et al.*, 1988). The latter two groups claimed that the detected events from Hercules X-1 appeared more like hadron-induced showers than photon-induced showers, the Whipple group on the basis of image characteristics (Reynolds *et al.*, 1991) and the CYGNUS group on the basis of muon content. The situation was reminiscent of the Kiel observation of muon-rich events from Cygnus X-3 and further fueled speculation about new physics at high energies.

3. The Crab

The field of γ-ray astronomy in the GeV-TeV domain was brought to maturity by the detection of emission from the Crab Nebula. This source, a plerion, played an important role in the development of many domains of astronomy, from optical and radio to x ray. Long before the Crab Nebula was observed as a source of VHE photons, Gould (1965) described a model of how it could produce TeV photons. In this model, relativistic electrons from the pulsar undergo synchrotron radiation in the magnetic field of the nebula; the electrons also Compton scatter on the synchrotron photons, boosting the photons to TeV energies. In this model, the flux of VHE photons is a function of the magnetic field in the nebula.

The first detection of VHE emission from the Crab was by Fazio *et al.* (1972), based on 150 hours of on-source data taken during 1969–1972 at Mount Hopkins, Arizona, using a first-generation atmospheric Čerenkov telescope with an energy threshold of 140 GeV. This yielded a flux measurement with a significance of 3σ, $(5.7 \pm 1.8) \times 10^{-11}$ photons $\mathrm{cm}^{-1}\,\mathrm{s}^{-1}$, which was treated as an upper limit.

It was not until over a decade later that the first imaging air Čerenkov detector, a camera with 37 pixels of 0.5° diameter each operated by the Whipple group at Mount Hopkins, saw clear evidence of emission from the Crab. A signal with a 5.6σ statistical significance was found in 34 hours of data taken between 1983 and 1985 (Cawley *et al.*, 1985). With refinements of the data-selection techniques and improvements in electronics, this was enhanced to 9σ from 85 hours of data taken between 1986 and 1988 (Weekes *et al.*, 1989). This detection prompted the move toward higher resolution for the imaging technique. Observations with the present Whipple telescope camera with 109 pixels of 0.25° each in the central region yielded a signal with a significance of 20σ from 30 hours of data taken in 1988–1989 (Vacanti *et al.*, 1991). This result was consistent with the previous detections and indeed with the original 1972 result of Fazio *et al.*

All of these observations were of steady (i.e., unpulsed) emission. A number of groups claimed the detection of pulsed emission from the Crab, either transient or steady. However, the *a priori* significance of these observations is difficult to assess and there were no confirming observations.

VI. OBSERVATIONS IN THE 1990s

At the end of the 1980s, results in high-energy γ-ray astronomy were sparse and often somewhat confusing. The launch of the CGRO satellite was delayed by the Challenger disaster, so there were no satellite-based observations in the 1980s. With the exception of the widely accepted detection of TeV γ rays from the Crab, all other claimed observations of VHE and UHE sources were disputed; in particular, the earlier observations of

emission from Cygnus X-3 and Hercules X-1 were not confirmed despite the advent of detectors with greatly enhanced sensitivity.

The 1990s began inauspiciously when the spark chamber failed on the Gamma-1 telescope aboard the Russian Gamma Observatory, launched in July 1990. Gamma-1 was designed to detect γ rays from 50 MeV–6 GeV, but the spark-chamber failure eliminated the pointing ability of Gamma-1 and severely reduced the capabilities of the mission. Nevertheless, the first seven years of the 1990s brought a remarkably rich view of the γ-ray sky. This was largely due to the new capabilities brought by the EGRET telescope aboard the CGRO. Progress was also made with ground-based UHE detectors (but no detections of sources) and exciting new source detections by air Čerenkov detectors.

A. CGRO–EGRET

The CGRO satellite was launched in 1991 with four telescopes on board. Of particular importance here are the EGRET detector, described above, and the BATSE (Burst and Transient Source Experiment). BATSE consists of NaI timing detectors at each corner of CGRO and was specifically designed to study gamma-ray bursts (GRBs). This will be discussed in Sec. VI.A.4 below. The characteristics of EGRET were discussed in Sec. IV.B.

EGRET has completed all-sky surveys above 100 MeV and has undertaken prolonged observations of specific objects (Thompson *et al.*, 1995; Fichtel, 1966). Highlights of these observations are as follows.

Diffuse γ-ray emission from the galactic plane is the most prominent feature of the γ-ray sky (as previously observed by COS-B). Observations have also been made of emission from the Large and Small Magellanic Clouds, with implications as to the origin of cosmic rays.

Diffuse γ-ray emission is also observed at high galactic latitudes, which is probably of extragalactic origin.

Seven high-energy γ-ray pulsars have been observed.

A new class of objects, high-energy γ-ray blazars, has been identified.

Emission of high-energy γ rays from GRBs has been observed, some at energies above a GeV.

High-energy sources with no counterparts at other wavelengths constitute an intriguing catalog of about 50 ''unidentified'' objects.

A comprehensive review of all of the results from CGRO is beyond the scope of this article; more extensive reviews of EGRET results are available in the literature (Dingus, 1994; Michelson, 1994a; Fichtel, 1996). Below we briefly discuss some of these results, especially those that directly impact ground-based observations.

1. Diffuse emission

Interactions of high-energy cosmic rays with matter are expected to produce γ rays, primarily through the production and decay of neutral pions. Detection of this diffuse γ-ray emission should yield information about the production and propagation of cosmic rays in the Milky Way Galaxy. Diffuse emission within $\sim 10^\circ$ of the plane of our galaxy dominates the γ-ray sky, with the highest intensity coming from near the galactic center. After removal of identified galactic point sources, the diffuse emission shows structure that reflects the main features of the mass distribution in the galaxy. The intensity is generally in agreement with expectations, although the flux above 1 GeV is somewhat larger than expected (Hunter *et al.*, 1997). An updated calculation of the expected galactic diffuse photon spectrum (Mori, 1997) is consistent with earlier calculations and is unable to account for the observed excess of events above 1 GeV. A possible explanation is a harder proton spectrum near the galactic center than in the solar neighborhood.

Diffuse emission has also been observed from the Large Magellanic Cloud, with a flux that is consistent with quasistable equilibrium production by cosmic rays (Sreekumar *et al.*, 1992). The upper limit for diffuse emission from the Small Magellanic Cloud (Sreekumar *et al.*, 1993) demonstrates that cosmic rays are mostly confined to galaxies.

In addition to the diffuse γ-ray flux associated with the Milky Way Galaxy and the Large Magellanic Cloud, EGRET has observed apparently isotropic emission at high galactic latitudes; this is believed to be of extragalactic origin. The differential spectrum above 100 MeV is well fitted by a power law:

$$\Phi(E) = (1.05 \pm 0.04) \times 10^{-8} (E/377\ \text{MeV})^{-2.07 \pm 0.03} \times \text{photons/cm}^2\text{/s/sr/MeV} \quad (10)$$

(Sreekumar *et al.*, 1998). This result is in good agreement with, although considerably more precise than, the earlier measurements made by SAS-2 (Fichtel *et al.*, 1978). The spectrum of the extragalactic emission is consistent with AGNs being the source of this radiation (Stecker and Salamon, 1996).

2. Galactic sources

a. Pulsars

EGRET has detected pulsed high-energy emission from seven pulsars: the Crab, Vela, Geminga, PSR1509-58, PSR1706-44, PSR1055-32, and PSR1951+32. Of these pulsars, only Geminga is not observed in the radio. Geminga was first seen as a steady source by SAS-2 (Fichtel *et al.*, 1976; Thompson *et al.*, 1977). Data from COS-B on the energy spectrum and variability suggested that it might be a Vela-type pulsar (Grenier *et al.*, 1991). The nature of this object has been a great mystery as it was not detected in other wavelengths. In 1992, Halperin and Holt (1992) discovered a 237.0974-ms pulsar period from ROSAT x-ray observations of Geminga. An examination of 1991 EGRET data then revealed pulsed 100-MeV radiation, confirming Geminga as a γ-ray pulsar (Bertsch *et al.*, 1992; Mayer-Hasselwander *et al.*, 1993).

With the exception of the Crab, the pulsar light curves change as a function of wavelength, indicating that different energy photons are emitted from different regions

of the pulsars. Strong unpulsed emission from the Crab above 100 MeV is observed (Ramanamurthy *et al.*, 1995) that is believed to be due to processes in the supernova remnant surrounding the pulsar; the angular resolution of EGRET is not good enough to distinguish possible emission sites within the nebula. There is no strong unpulsed emission from Vela or Geminga. The pulsed energy spectra are relatively hard, with γ-ray emission dominating the observed power, in agreement with the pulsar models; there is also evidence of a spectral cutoff at high energies for Geminga, Vela, and PSR1706-44.

Recent evidence has been published indicating the detection of an outburst of high-energy emission from the massive x-ray binary system Centaurus X-3 by the EGRET telescope (Vestrand, Sreekumar, and Mori, 1997). This is arguably the first evidence for variable GeV emission from an x-ray binary system and would require the sporadic acceleration of particles to GeV energies within such a system.

b. Unidentified sources

Of the 129 high-energy (>100 MeV) γ-ray sources in the second EGRET catalog, more than half are not identified with objects known from observations at other wavelengths. Most of these unidentified objects cluster near the galactic plane, suggesting a galactic origin. Analysis of the data indicates that they cannot be a group of older, low-luminosity pulsars like Geminga (Mukherjee *et al.*, 1995). Some of these sources may be associated with nearby supernova remnants (Sturner and Dermer, 1995; Esposito *et al.*, 1996). Some unidentified source locations overlap SNR locations; γ-ray emission could arise from the decay of neutral pions produced by collisions of shock-accelerated protons with the remnant gas. The fluxes of the possible EGRET sources are consistent with expectations for supernova remnants, provided the remnants transfer most of their kinetic energy to accelerated cosmic rays and the shock is expanding into interstellar gas clouds with densities >1 atom/cm^3 (Drury *et al.*, 1994); however, this hypothesis has not been confirmed by higher-energy observations (see Secs. VI.B.5 and VI.C.2, below).

The bulk of unidentified sources may be related to the molecular clouds belonging to the Gould belt, a 300-pc-radius ring of atomic gas and molecular clouds centered at about 100 pc from the sun. The dense clouds of Aquila Rift and Ophiuchus at positive latitudes, and Orion and Perseus at negative latitudes, belong to this expanding structure; its age (about 50 million years) can be determined from its expansion velocity. A strong correlation of the position of the EGRET sources with the molecular clouds was established by Grenier (1995), who also noted that the blue giant (OB-type) star population also tends to gather in these clouds. A number of giant stars produced in these clouds must have ended their short lives in the last few million years. EGRET may be observing young pulsars generated nearby. To prove the point, radio observations are needed; these are difficult to conduct because of the large EGRET error box. More precise positioning, either from space or from the ground, is needed.

3. Extragalactic sources

Before the launch of CGRO, high-energy γ rays had been observed from only one active galaxy, 3C273, detected by COS-B (Swanenburg *et al.*, 1981). EGRET has observed over 50 AGNs, at redshifts from $z=0.03$ to $z>2$ (von Montigny *et al.*, 1995). The active galaxies observed by EGRET are all blazars, galaxies whose emission is primarily nonthermal and that appear to have jets pointed in our direction. On the other hand, high-energy γ rays have not been detected in many relatively close active galaxies, especially Seyfert galaxies and radio-quiet AGNs (Thompson *et al.*, 1993).

Gamma-ray-emitting blazars represent a new class of objects. The energy being emitted by these objects is extraordinary. Assuming beaming in our direction of one part in a thousand, the typical luminosity is 10^{45} erg/s. There is generally more energy observed in the γ-ray region than in any other wavelength band; the differential energy spectra are well fitted by a power law with an average slope of -2.1. Nearly all of the blazars that have been observed on several occasions exhibit variability in high-energy γ-ray emission on time scales of from months to days; this appears to imply that the high-energy emission region is very small, even with a relativistic correction.

4. Gamma-ray bursts

EGRET has detected six gamma-ray bursts in coincidence with BATSE. Photons above 1 GeV were observed from the ''Superbowl'' burst in 1993 (Sommers *et al.*, 1994) and, even more surprising, delayed photons up to 18 GeV were observed from GRB940217 (Hurley, 1994; see Fig. 17). In addition, the energy spectra for these bright bursts are hard (differential spectral index ~ 2) and show no signs of a high-energy cutoff. The observation of these high-energy photons was not expected in any model.

B. Air Čerenkov

Observations by air Čerenkov telescopes in the 1990s confirmed the earlier detections of VHE emission from the Crab Nebula and discovered a number of additional VHE sources. These are discussed below.

1. The Crab

The detection of VHE γ-ray emission from the Crab Nebula by the Whipple group in the 1980s was subsequently confirmed by a number of other groups. The ASGAT and Thémistocle experiments used the wavefront timing technique (Baillon *et al.*, 1993; Goret *et al.*, 1993; Djannati-Ata, 1995), while the HEGRA and CANGAROO experiments used the imaging technique (Tanimori *et al.*, 1994; Krennrich *et al.*, 1993). There is no convincing evidence for pulsed VHE emission, indicating that the emission emanates from the nebula

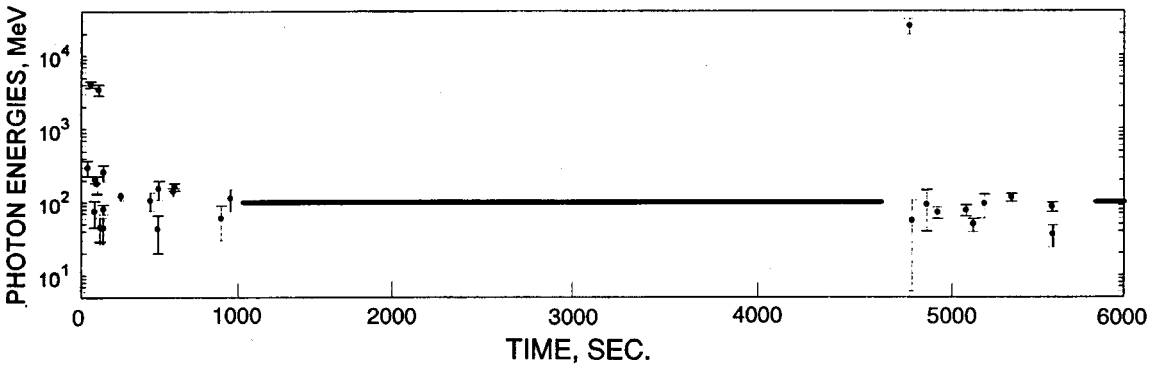

FIG. 17. Energy and time of photons from GRB940217 (EGRET).

rather than the pulsar itself. The observed flux from the Crab has been steady (Carter-Lewis *et al.*, 1998). The spectrum has been measured to 50 TeV by the large-zenith-angle observations of the CANGAROO group (Tanimori *et al.*, 1998a).

The importance of the VHE detection of the Crab, besides its intrinsic interest as a probe of the acceleration mechanisms in the object, is that it has provided a standard candle or test beam for the field. This has allowed the various atmospheric Čerenkov techniques to be compared and data-analysis methods for the rejection of the cosmic-ray background and the localization of a source's position to be refined.

The VHE flux is much higher than expected from an extrapolation of the spectrum given by space-based detectors at lower energies. This can be reconciled using the synchrotron self-Compton (SSC) model (deJager and Harding, 1992), in which the VHE emission is produced by the inverse Compton interaction of high-energy electrons primarily with their own synchrotron emission. This produces a TeV inverse Comptom bump in the spectrum that is a boosted image of the synchrotron bump (~ 10 MeV) seen by the space-based detectors [see Fig. 18(a)]. The fit of the data to the model yields the maximum electron energy in the pulsar magnetosphere ($\sim 2\times 10^{15}$ eV), and the nebular magnetic field (1.6×10^{-4} G; Hillas, 1998). A compilation of the most recent results at VHE energies is shown in Fig. 18(b); the power-law fit shown here is not expected to extend to energies above a few tens of TeV but should reflect the synchrotron cutoff seen at lower energies. There is no strong conflict between the upper limits at UHE energies and the current model.

2. PSR1706-44

PSR1706-44, a supernova remnant, was first detected as a γ-ray source in the COS-B satellite data (Swanenburg *et al.*, 1981). It was identified with the radio pulsar by the detection of the 102-ms pulsations in the EGRET data (Thompson *et al.*, 1992), although the peak in the light curve is displaced from that in the radio. Unlike the Crab, no pulsed signal is seen in either optical or x-ray observations. The pulsar age is estimated from the spin-down rate to be 17 400 years. X-ray observations with the ROSAT satellite indicate an associated x-ray synchrotron nebula (Becker, Brazier, and Trüper, 1995), and a possible association with the shell-type supernova remnant G 343.1–2.3 has been proposed (McAdam, Osborne, and Parkinson, 1993). However, this has been questioned given distance inconsistencies and the lack of interaction between the pulsar and the supernova shell (Frail, Goss, and Whiteoak, 1994).

VHE emission from this source was detected by the CANGAROO group [and confirmed by the Durham group (Chadwick *et al.*, 1998b)] in data from 1992 and 1993 (Kifune *et al.*, 1995), with a steady flux at a level slightly less than that of the Crab (8×10^{-12} photons/cm^2/s above 1 TeV); there is no evidence of pulsed emission. This detection provides a reference source for the southern hemisphere, which can play a role similar to that of the Crab in the northern hemisphere.

3. Vela

The CANGAROO group has also detected continuous emission from the Vela pulsar with a significance of 5–6 σ. Vela (PSR0833-45) is a young ($\sim 10^4$ years), nearby (~ 500 pc) pulsar, which was first detected in the radio band and has also been observed in the optical, x-ray, and γ-ray bands. In the high-energy γ-ray band, it is the brightest discrete object in the sky, with emission that is 100% pulsed with a double-peaked light curve. The spectrum shows a clear break above a few GeV. The pulsar is at the center of the Vela supernova remnant, which has a diameter of 230 light years or 3.3°. The VHE integral γ-ray flux given by the CANGAROO group from data taken from 1993 to 1995 is $2.5\pm 0.5 \pm 0.4\times 10^{-12}$ photons/cm^2/sec above 2.5 ± 1.0 TeV, with all of the emission being unpulsed (with an upper limit to the pulsed component of $2.7\pm 0.5\times 10^{-13}$ photons/cm^2/sec; Yoshikoshi *et al.*, 1997). The VHE emission is displaced by 0.1–0.2° to the southeast from the pulsar, corresponding to a hot spot in the ROSAT x-ray data (Fig. 19) (thought to be the "birthplace" of the pulsar). This point is not along the pulsar rotation axis (which is in the southwest direction) and so is unlikely to result from a pulsar jet. It could be related to shock acceleration at the intersection of the pulsar wind

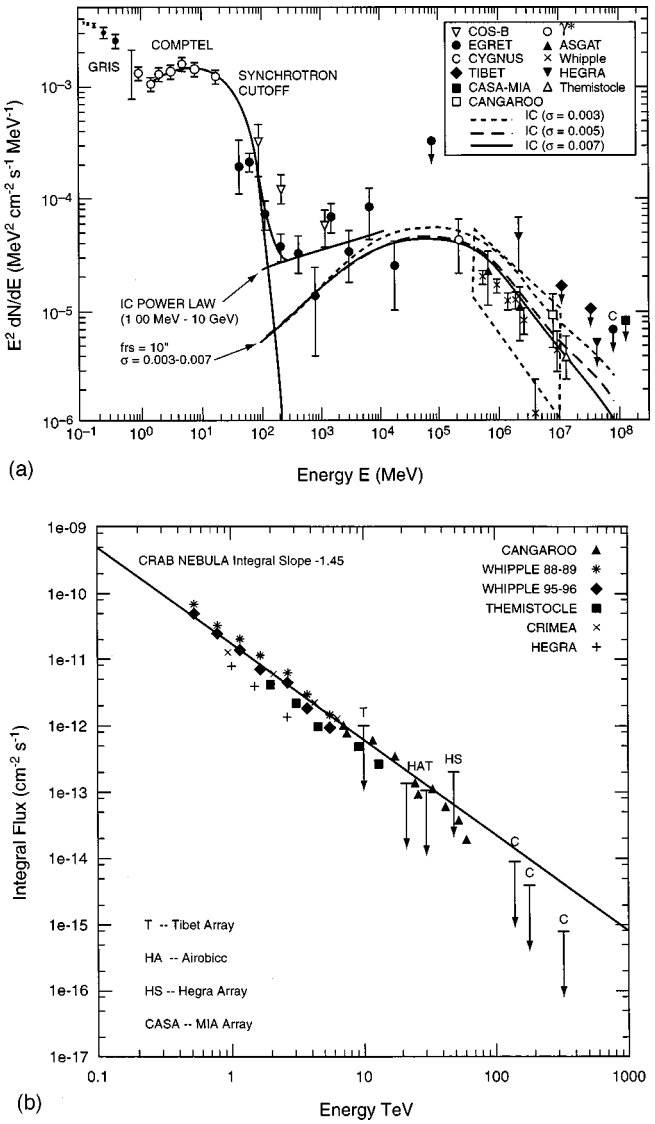

FIG. 18. The observed energy spectrum from the Crab: (a) A comparison of space- and ground-based results and the synchrotron self-Compton model of deJager and Harding (deJager and Harding, 1992); (b) a compilation of recent ground-based results.

with a region of higher matter density. The distance of the emission from the pulsar would put it outside the pulsar light cylinder, so that pulsed emission would not be expected. The displacement of the emission from the pulsar is statistically not highly significant and so remains to be confirmed by detectors with better source location capabilities.

4. Active galactic nuclei

One of the more exciting discoveries of the 1990s has been the observation of TeV emission from extragalactic objects. As of this writing, TeV emission has been detected from three AGNs. Below we discuss the observations of two of these sources (Mrk 421 and Mrk 501) in some detail.

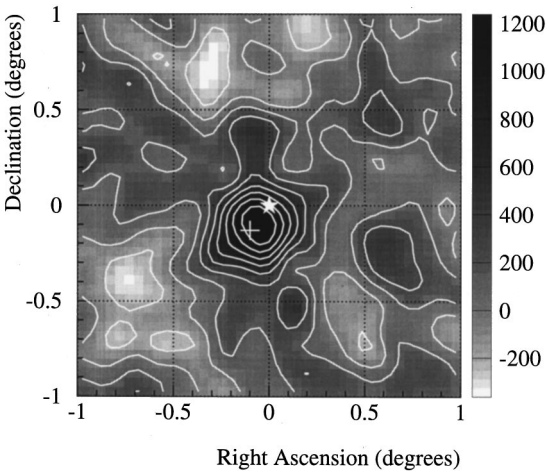

FIG. 19. Map of ROSAT X-ray data from Vela with location of VHE emission from CANGAROO (cross).

a. Markarian 421

The AGN Markarian 421 was first detected (at the 6σ level) by the Whipple group (Punch *et al.*, 1992). Mrk 421 is classified as a BL Lac (a subclass of the blazar family of active galaxies) and is at a redshift of $z = 0.031$. The Whipple group measured a flux of $1.5 \times 10^{-11}/\mathrm{cm}^2/\mathrm{s}$ above 500 GeV (1/3 that of the Crab) during March–June 1992. There was no evidence of variability during this period. This source had been seen by the EGRET detector, though it was the weakest extragalactic object then detected.

The Whipple detection was confirmed (with a significance of 5.8σ) by the HEGRA atmospheric Čerenkov telescope group (Petry *et al.*, 1996) in data taken between December 1994 and May 1995. They measured a flux of $(8 \pm 2^{+6}_{-3}) \times 10^{-12}$ photons/cm^2/s above 1 TeV.

Mrk 421 has been seen by the Whipple group in each subsequent year up to the present (1998). In addition, short-duration flares have been observed. During some flares the flux exceeds that from the Crab (McEnery *et al.*, 1998), as shown in Fig. 20.

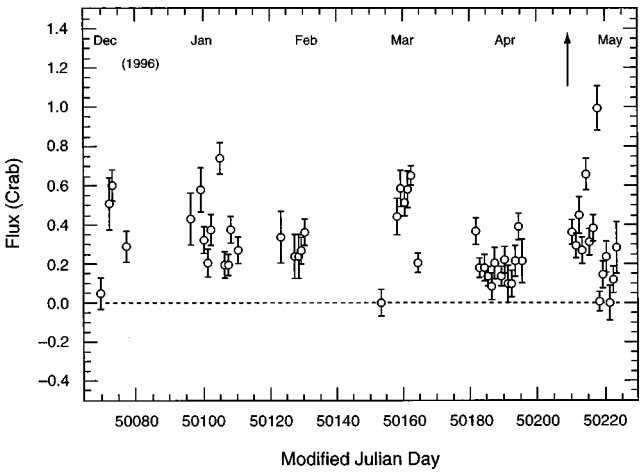

FIG. 20. The daily variations of the flux from Markarian 421 in the 1996 observing season, showing flaring activity. From McEnery *et al.*, 1997.

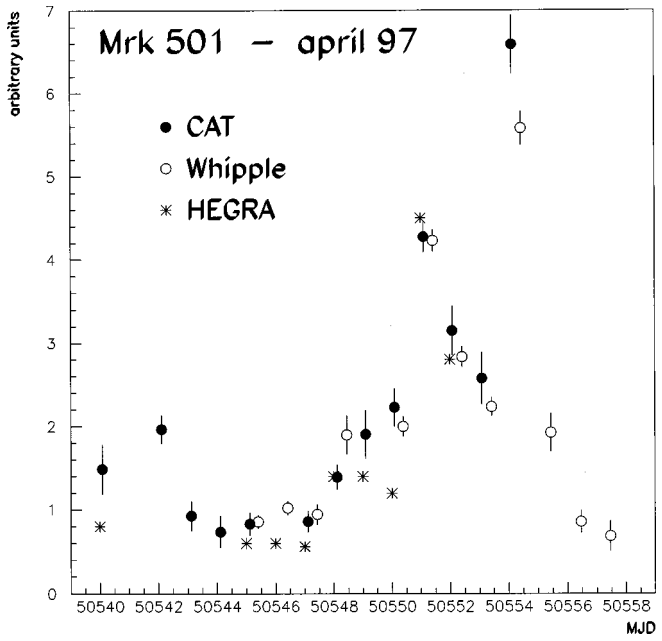

FIG. 21. VHE observations of Mrk 501 taken during April 1997. The three observations were "nearly" simultaneous, due to longitude differences in the observatory positions—Whipple, CAT, and HEGRA.

b. Markarian 501

The second extragalactic source seen by the Whipple group, Mrk 501, is also a nearby BL Lac AGN ($z=0.034$) (Quinn *et al.*, 1996). Between March and July 1995 the flux was measured to be $(8.1\pm1.4)\times10^{-12}$ photons/cm^2/s above 300 GeV, 0.08 that of the Crab (Quinn *et al.*, 1998), with evidence of flaring activity on time scales of days. This source was not seen by EGRET, but an extrapolation of the flux puts it below EGRET's sensitivity. Confirmation of this source was again provided by the HEGRA group in data taken between March and August 1996. They measured an average flux of $(2.3\pm0.4^{+1.5}_{-0.6})\times10^{-12}$ photons/cm^2/s above 1.5 TeV, about 1/3 of the Crab flux (Aharonian *et al.*, 1997).

In 1997, Mrk 501 began a period of intense flaring activity. An intensity several times that of the Crab was definitively observed by three groups: Whipple, CAT, and HEGRA (Aharonian *et al.*, 1997; Breslin *et al.*, 1997; Catanese *et al.*, 1997; Djannati-Ata *et al.*, 1999). This was the first simultaneous detection of variability in the TeV energy regime (Fig. 21). Coincident with the TeV activity, the Rossi X-Ray Timing Explorer satellite observed an increase in the x-ray flux from 1996 to 1997 (Lamer and Wagner, 1998). The x-ray observation has been confirmed by the OSSE detector on board CGRO and the BeppoSAX satellite (Pian, 1998).

Such a strong photon source provides many benefits: it gives a γ-ray-rich database for tests of analysis methods and background rejection techniques. Mrk 501 is the first source to be detected by an EAS-PDA [the Milagrito detector (A. Smith, 1999)]. Mrk 501 should provide sufficient data above 10 TeV to test models of AGNs and the intergalactic infrared absorption (discussed below).

c. 1ES 2344+514

Recently the Whipple group has claimed the detection of VHE emission from a third BL Lac, 1ES 2344+514 (Catanase *et al.*, 1998). This object is the fourth-closest known BL Lac ($z=0.044$). Most of the evidence for emission comes from a flare on December 20, 1995, although observations between October 1995 and January 1996, excluding the night of the flare, also show significant emission. Observations taken between September 1996 and January 1997 do not yield significant evidence for any VHE emission.

d. Implications of the VHE detection of AGNs

As we discussed earlier, there are a number of competing models to explain TeV emission from AGNs. All of the models use the jet as the primary source of high-energy particles. However, they differ in the nature of the accelerated particles (electrons or protons) and the source of the photons (synchrotron photons from accelerated electrons or external photons).

The relevant observations are the correlations between TeV and x-ray emission, the high-energy spectrum, and the time scale of variability. We have explained the importance of these observations in Sec. III.D.1.

Models in which the photons result from synchrotron emission from accelerated electrons (either directly accelerated in the synchrotron self-Compton model or indirectly produced in the S-PIC model) are strongly supported by many of the data. The spectra of these BL Lacs have a characteristic two-hump feature [Figs. 22(a) and 22(b)]. In these models, the low-energy hump is due to synchrotron emission and the high-energy hump is due to inverse Compton scattering of these lower-energy photons. Though the statistics are low, to date the only BL Lacs observed at TeV energies are x-ray-selected BL Lacs (as opposed to radio-selected BL Lacs). This is consistent with self-synchrotron models, as the inverse Compton hump would be at much lower energies in radio-selected BL Lacs. These models are also consistent with the EGRET results for Mrk 501 and 421. The synchrotron cutoff (the high-energy tail of the synchrotron hump) is at 1 keV for Mrk 421 and >100 keV for Mrk 501. Thus, in the case of Mrk 501, the inverse Compton hump begins at energies beyond the sensitive range of EGRET, while in the case of Mrk 421, the inverse Compton hump lies well within EGRET's range of sensitivity. In addition, the observed correlation between the x-ray and γ-ray emission during flares (Fig. 23) is a natural consequence of these models.

Both of the observed AGNs exhibit strong time variability over a large range of time scales. There are long periods of apparent calm and periods of intense activity. In the active phase these objects can become the brightest TeV sources in the sky. To date, the shortest observed time scale of variability was seen by the Whipple experiment on May 15, 1997. During this observing period, the TeV γ-ray intensity from Mrk 421 had a doubling time of ~15 minutes (Gaidos *et al.*, 1996). The

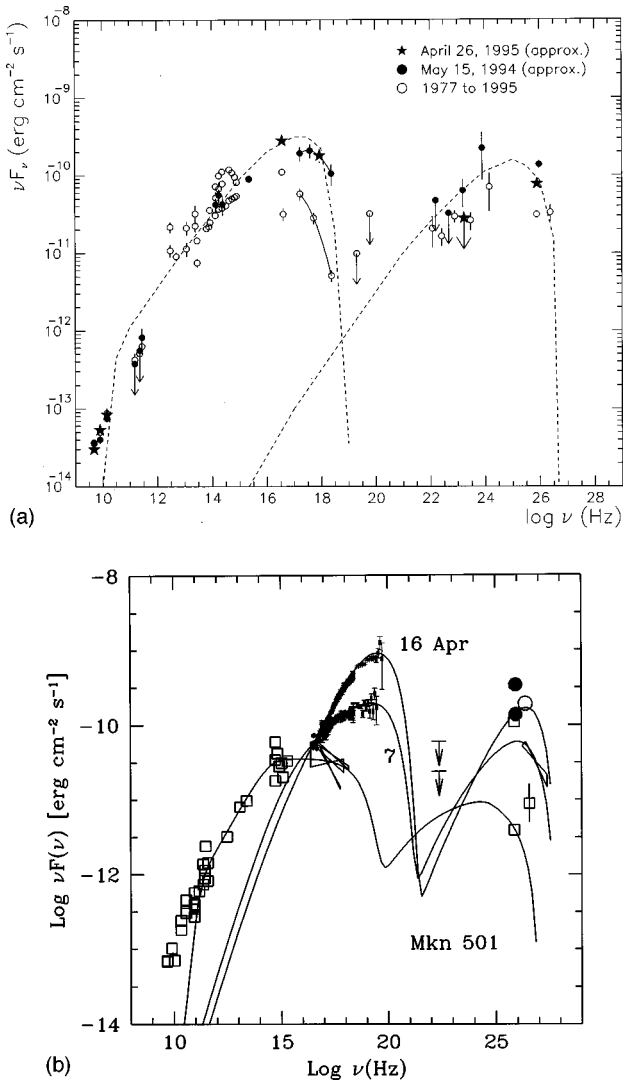

FIG. 22. The observed spectra of VHE blazars: (a) The spectrum of Mrk 421 (Buckley *et al.*, 1997). This paper contains the reference to the data points. The VHE points are from the Whipple telescope, the high-energy points are from EGRET, and the x-ray points are from the ASCA Satellite. The dashed curve shows a scaled synchrotron self-Compton model from Inoue and Takahara (1996). (b) The observed spectrum of Mrk 501 (Pian *et al.*, 1998). This paper contains the reference to the data points. The near-simultaneous VHE data are from Whipple (filled circles) and HEGRA (open circle and the TeV spectral fit), the high-energy upper limits are from EGRET, and the dated x-ray data are from BeppoSAX. Archival data are shown as open squares. The solid lines indicate fits with a synchrotron self-Compton model as described by Pian *et al.* (1998).

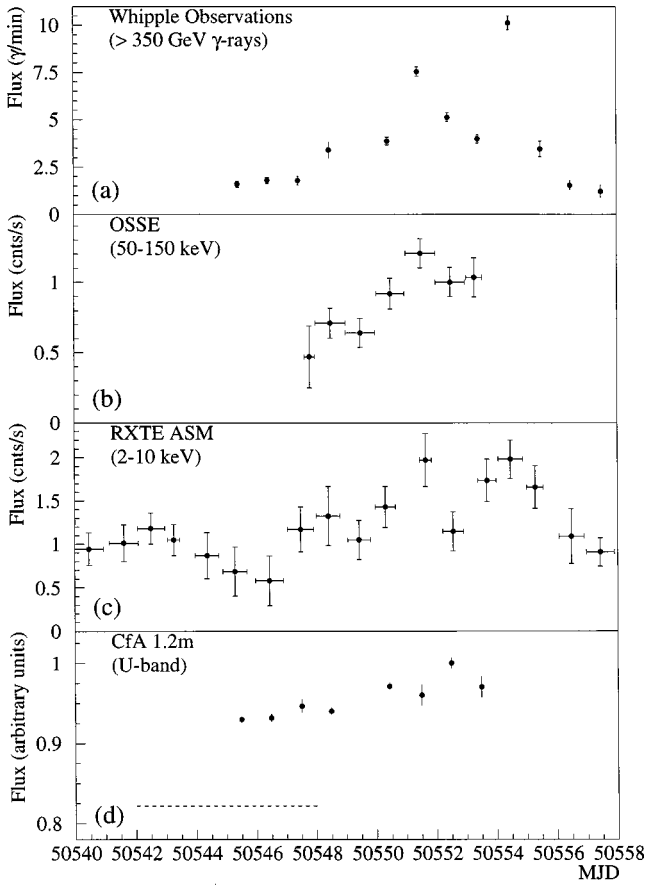

FIG. 23. Multiwavelength observations of Markarian 501, April 1997. From Catanese *et al.*, 1997.

flares from Mrk 501, while more intense, seem to be limited to doubling times on the order of half a day. While the very shortest flaring time can be more naturally explained in leptonic models, a 15-min doubling time is not short enough to rule out the hadronic models.

The energy spectrum of Mrk 501 has been measured beyond 18.5 TeV (Konopelko *et al.*, 1999) (Fig. 24), with no evidence of a spectral break. Such high energies are easily explained in the hadronic models and can be used to determine the ambient magnetic fields in the synchrotron self-Compton model. The synchrotron self-Compton model predicts a relation between the synchrotron cutoff energy $E_{\rm syn}$, the maximum electron energy (in the rest frame of the shock) $E_e(\max)$, the

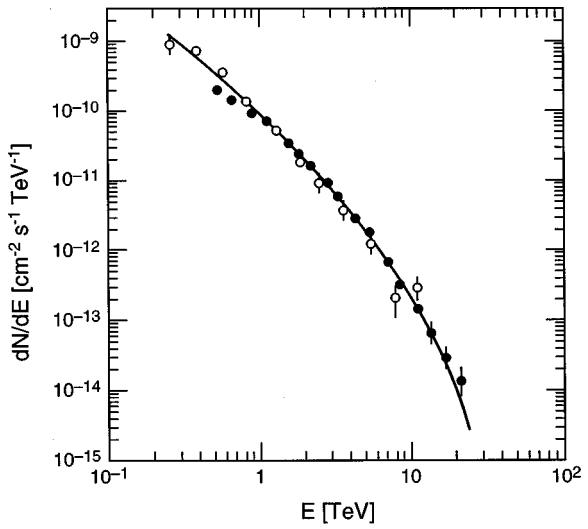

FIG. 24. Markarian 501 VHE spectrum: ●, from the HEGRA detector (Konopelko *et al.*, 1999); ○, from the Whipple telescope (Samuelson *et al.*, 1998).

magnetic field in the blob B (in gauss), and the Doppler factor D,

$$E_e(\max) \approx 5\times 10^9 (E_{\rm syn}/BD)^{1/2}, \tag{11}$$

where all energies are expressed in electron volts. Given that the observed Compton-boosted photon energies E_{IC} must be less than the maximum electron energy ($E_{IC} < E_e D$), the magnetic field is given by $B \approx 2\times 10^{19} D E_{\rm syn}/E_{IC}^2$. In the case of Mrk 501, with $E_{\rm syn} \sim 200$ keV, $D \sim 30$, and 20 TeV photons observed, the magnetic field is of order 0.3 G for electron energies of $E_e \sim 600$ GeV. A systematic study of available data on blazars (Fossati *et al.*, 1997) indicates that, although the peak positions show a large variation (by factors of 10^3 or more), the ratio of energies between the synchrotron and TeV peaks seems to be constant at $\simeq 5\times 10^8$, which in the above expression implies $E_{IC}B \approx 10^{12}$ eV G.

In the synchrotron self-Compton model, $B \approx [4\times 10^{14}/\Delta t_{\rm obs} E_{IC}]^{1/2}$, where $\Delta t_{\rm obs}$ is the fastest possible variation (in seconds) and E_{IC}, as above, is the observed photon energy (in eV). Thus if the observed variability is due to the acceleration and cooling of electrons, then fields of the order of a gauss are needed to account for the observed source variability. The spatial extent of the emission region is constrained by causality to $r \approx 0.5 c D \Delta t_{\rm obs}$, or 27 AU for the 15-min variability of Markarian 421. This distance, of the order of the size of the solar system, is very small compared to the size a galaxy, but large compared to the Schwartzchild radius for a 10^8-solar-mass black hole (2 AU).

e. Intergalactic absorption of γ rays

As we discussed in Sec. III.E, TeV photons from an extragalactic source interact with the IR background. This leads to a steepening in the observed spectrum at photon energies in which the optical depth approaches unity. As a result, there should be a relationship between source distance and maximum observable photon energy. This appears to be confirmed by the fact that only the closest AGNs have been observed in the TeV domain, while in the $\sim$ GeV range, EGRET has observed over 50 AGNs out to redshifts greater than 2. However, given the intrinsic relationship between source distance and required source luminosity for a detection in a magnitude-limited survey, and the strong coupling between intrinsic source luminosity and absorption within the source, it is difficult to draw any firm conclusions.

The energy spectrum of Mrk 501—at about the same redshift as Mrk 421—was measured by three groups, taking advantage of the high state in 1997. The observations imply a steepening spectrum that extends up to at least 18.5 TeV (Fig. 24). A conservative analysis of the Whipple atmospheric Cerenkov telescope data on both Mrk 421 and Mrk 501 (Biller *et al.*, 1998), making no *a priori* assumption on the shape of the infrared spectrum as was done by other authors, yields an upper limit of about 3×10^{-8} eV/cm^3 at 0.1 eV diffuse magnitude, below the best limits derived from the direct observations

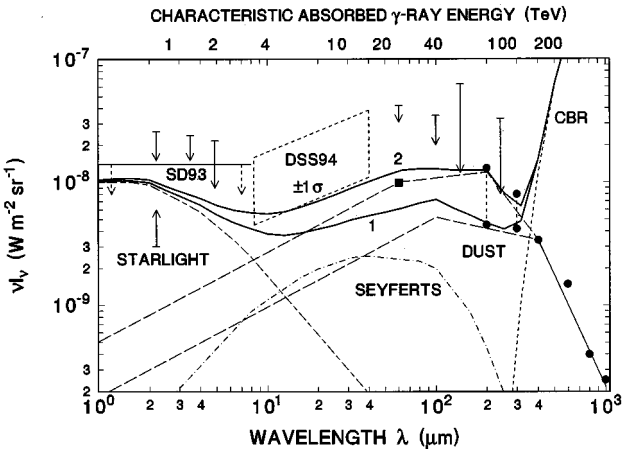

FIG. 25. The low-energy intergalactic photon spectrum from the microwave to the optical. The expected contributions from starlight, Seyfert galaxies, and dust, and the measured cosmic background radiation are shown. The upper horizontal scale shows the characteristic energy for γ-ray absorption by photons of wavelength λ. ●, FIRAS data (Puget *et al.*, 1996); ■, galaxy counts in IRAS data (Gregorich *et al.*, 1995); upper limits from COBE/Dirbe residuals (Hauser, 1996); lower limit at 2 μm based on galaxy counts (Tyson, 1990). The solid line upper limit (SD93) and the dashed parallelogram (DSS94) are based on ACT data (Stecker and deJager, 1993; deJager *et al.*, 1994). From Stecker and deJager, 1997.

of the infrared light at high galactic latitudes made by DIRBE on the COBE satellite. On the other hand, this upper limit lies a decade higher than the recent evaluation of the starlight contribution by Malkan and Stecker (1998), based on a parametrization of the emission spectrum of nearby galaxies convolved with a Z distribution of infrared galaxies. There is still room for speculation, but some phenomena that could have contributed to the diffuse infrared light, such as very massive objects or radiative decays of massive neutrinos, have already been ruled out (Biller *et al.*, 1998).

The as yet unexplored 20–250-GeV energy domain is critical in understanding the nature of the IR radiation, since most of the sources observed by EGRET should be observable in this energy range. In the coming years, experiments sensitive to this energy range will establish the infrared methodology on a sizable statistical sample.

More direct measurements of the infrared background are also being made. Figure 25 (Stecker and deJager, 1997) shows current measurements and upper limits, including those from Mrk 421 (indicated by the dotted parallelogram). The direct measurements are shown as black circles in the figure (derived by Puget *et al.*, 1996). Data from the Infrared Space Observatory, currently undergoing analysis [based on galaxy counts in the near IR region (1–15 μm)] lead to a lower estimate than that given in the figure [which is based on visible starlight (Franceschini *et al.*, 1994)].

It is worth noting that, although they are indirect, the measurements based on the distortion of AGN spectra are one of the only methods available for determining the evolution of the IR background. Because the pho-

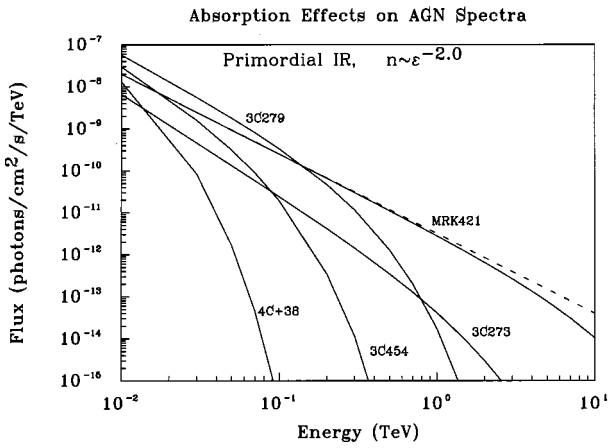

FIG. 26. Expected effect of absorption of VHE photons by primordial IR photons on the energy spectra of several AGNs. From Biller (1995).

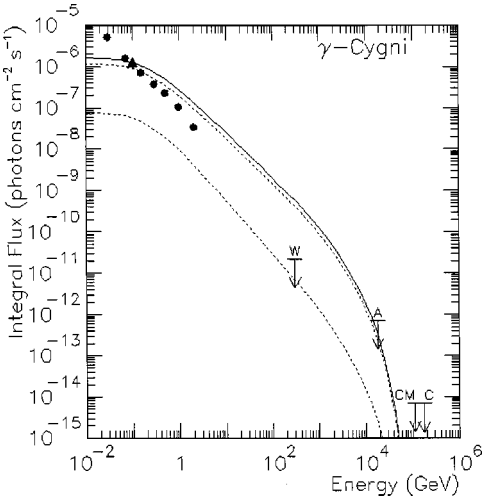

FIG. 27. Upper limits on VHE+UHE emission from γ-Cygni, a supernova remnant, compared to extrapolations from EGRET data (solid curve) and a conservative estimate of the allowable range from Drury (1994). Data points: W, Whipple (Buckley *et al.*, 1997); CM, CASA-MIA (Borione *et al.*, 1995b); C, CYGNUS (Allen *et al.*, 1995a); and AIROBICC (Prosch *et al.*, 1996).

tons from AGNs originate at cosmological distances, they sample the IR background at different epochs in the history of the universe. Thus, by studying the shape of the spectral distortion as a function of redshift, it may be possible to determine the evolution of the IR background radiation. This would be a critical test of theories of galaxy and star formation. The effect of this absorption on several AGNs is shown in Fig. 26 (Biller, 1995).

5. Other objects

In addition to the observed sources, there are objects that should have, but have not, been detected in the TeV regime. The standard theory of cosmic-ray acceleration in supernova shocks (see Sec. III.C) predicts flux levels of TeV γ rays that are comparable to the sensitivity of current instruments. Furthermore, some of the unidentified EGRET sources are near known supernova remnants. The observed fluxes are consistent with expectations for supernova remnants, provided that they transfer most of their kinetic energy to accelerated cosmic rays and that the shock is expanding into interstellar gas clouds with densities of 1 atom/cc (Drury *et al.*, 1994). However, because the error box of EGRET source locations is larger than a degree and some of the supernova remnants have a large angular extent, the identification of these sources remains problematic.

The observation of these sources in the TeV regime may help resolve this difficulty, at least in the cases of supernova remnants with small angular extent. For extended sources, atmospheric Čerenkov telescopes are faced with a higher hadronic background, as the rejection based on the γ-ray directionality is less effective. Nevertheless, upper limits to the γ-ray emission from a number of these sources have been obtained by the Whipple group. These upper limits are well below the predictions of current models and are below the E^{-2} extrapolation of the EGRET fluxes (Buckley *et al.*, 1997; Fig. 27). A century after the discovery of cosmic rays, their acceleration remains an open question.

Recently the CANGAROO group has observed a signal from SNR SN-1006 (Tanimori *et al.*, 1998b). However, this object is a strong x-ray source. The surrounding shock accelerates electrons, which produce x rays by synchrotron radiation. The TeV photons may come from inverse Compton interactions of these electrons. Perhaps the signature of accelerated protons in many supernova remnants, through their subsequent interactions producing neutral pions, will remain hidden under a high flux of inverse-Compton γ rays due to electrons. An unambiguous γ-ray signature of the cosmic-ray acceleration by supernova remnants may be difficult to obtain.

C. Extensive air-shower particle detector arrays

1. Introduction

In the 1990s, several "second-generation" EAS-PDAs began operation (see Table VI in Sec. IV.C.3). The new arrays have lower energy thresholds and much larger areas, and some have much better background rejection through the use of large-area muon detectors. In addition, better timing measurements and the use of lead placed above the counters (to increase the sensitivity to photons in the EAS) give improved angular resolution. These advances led to the observation of the shadows of the moon and the sun (Alexandreas *et al.*, 1991), demonstrating the sensitivity of these arrays. In the absence of a detectable source of γ rays it is extremely difficult to ensure that one understands the response of the detector at the level necessary to search for signals in the presence of high background rates. The shadows of the moon and sun provide calibration "sources" (or, more properly, sinks) from which the angular resolution of the array can be determined. The CASA, CYGNUS, and

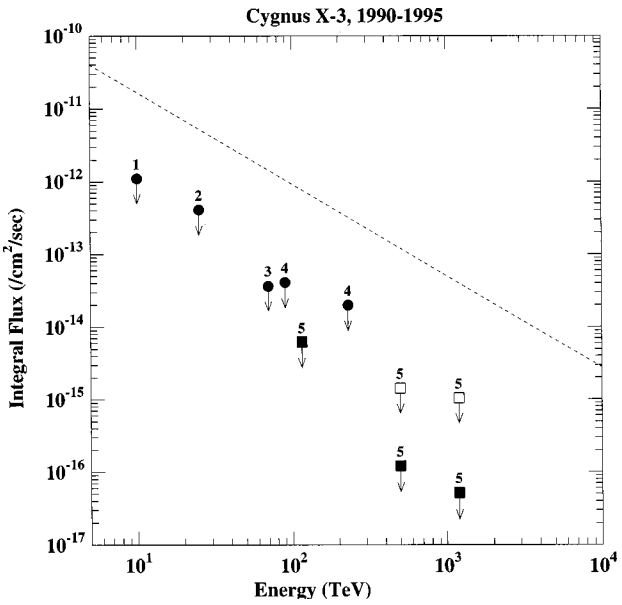

FIG. 28. Recent upper limits on the steady γ-ray flux from Cygnus X-3. The dashed line is a fit to the flux reported in earlier experiments. The results are from (1) Tibet (Amenomori *et al.*, 1992); (2) HEGRA (Karle *et al.*, 1996); (3) CYGNUS (Alexandreas *et al.*, 1993a, 1993e); (4) EAS-TOP (Aglietta *et al.*, 1995); and (5) CASA-MIA (Borione *et al.*, 1997).

Tibet arrays each had the required sensitivity and observation time to observe the shadows of the moon and sun.

The second-generation detectors were built during an era of great promise. The observations of the 1980s indicated that the galaxy contained strong sources of UHE photons. The new arrays, with their greater sensitivity, should have revealed a sky rich with sources. In fact, the ground-based arrays did not observe any sources of UHE γ rays. Even the "established" sources (Cygnus X-3, Hercules X-1, Crab) could not be confirmed. Upper limits to the fluxes from these sources are now over an order of magnitude lower than the detected levels claimed in the 1980s. Figure 28, from Borione *et al.* (1997), shows upper limits on the steady flux from Cygnus X-3 reported between 1990 and 1995 compared with earlier claimed detections.

2. Point-source searches

Many such specific searches have been carried out, none of which has detected a source of UHE photons. The CYGNUS collaboration has searched 50 specific point sources (x-ray binaries, pulsars, cataclysmic variables, and active galaxies) for emission over all time scales from 1 second to 5 years (Biller *et al.*, 1994). They have also looked for emission on the time scales of 1 day, 1 week, and 7 years from 13 AGNs detected by EGRET (Alexandreas *et al.*, 1993c), and for emission from the supernova remnants possibly detected by EGRET (Allen *et al.*, 1995a). The CASA group has searched for emission from Cygnus X-3, Hercules X-1, and the Crab (Borione *et al.*, 1997).

3. All-sky surveys

Several searches have been performed of the entire sky for steady sources of UHE γ rays. All of these searches have yielded null results. The results from the CASA detector are the most stringent published to date. They give upper limits of $\Phi(E \geqslant 140\,\mathrm{TeV}) \leqslant 4.1 \times 10^{-14}\,\gamma\,\mathrm{cm}^{-2}\,\mathrm{sec}^{-1}$ from a steady point source anywhere in the northern sky (McKay *et al.*, 1993).

The CASA group has also looked for emission on a one-day time scale from any point in the northern sky. Again, they saw no evidence of emission from any point in the sky and placed an upper limit of $\Phi(E \geqslant 140\,\mathrm{TeV}) \leqslant 1.0 \times 10^{-12}\,\gamma\,\mathrm{cm}^{-2}\,\mathrm{sec}^{-1}$ for emission from any day during the period between March 1990 and April 1991 (McKay *et al.*, 1993).

4. Searches for UHE emission from gamma-ray bursts

Most gamma-ray bursts observed by BATSE have relatively hard spectra, $dN/dE \propto E^{-2}$. In addition, EGRET has observed six bursts with power-law energy spectra up to the limit of their energy response (18 GeV in one case). A straightforward extrapolation of several of these bursts implies that one would expect to see strong UHE signals. However, a number of EAS-PDAs have shown that gamma-ray burst fluxes do not continue into this energy range. Typical upper limits to the fluence derived with EAS-PDAs are a few $\times 10^{-6}$ ergs $\mathrm{cm}^{-2}\,\mathrm{sec}^{-1}$ (Alexandreas *et al.*, 1994; Borione *et al.*, 1995a). This is similar to the fluence measured by BATSE in the keV regime. The failure to observe UHE photons could be due to either a change in the source spectrum or absorption of the high-energy γ rays in the electromagnetic fields (as discussed in Sec. VI.B.4.d). The latter interpretation is consistent with a cosmological origin of gamma-ray bursts.

5. Searches for primordial black holes

As we saw in Sec. III.D.4, instruments sensitive to TeV γ rays are well suited to search for the final-stage emission from primordial black holes. While air Čerenkov telescopes, with their lower energy thresholds, can see more distant primordial black holes than can particle detector arrays, the much larger observation time and aperture of the EAS-PDAs make them the most sensitive instruments to black-hole evaporation.

Prior to the 1990s many searches had been performed. However, the emission spectrum at TeV energies had not been well calculated, and each experiment assumed a different model for the high-energy emission. This made a direct comparison of the various experimental results difficult. Recent publications (MacGibbon and Webber, 1990; Halzen *et al.*, 1991) have presented realistic calculations of high-energy emission spectra based on quark fragmentation functions. Table VII shows the best current limits on the local rate-density of black-hole evaporation. The best of these limits are over five orders of magnitude larger than that inferred from the 100-MeV diffuse γ-ray flux. However, the limit from the dif-

TABLE VII. Upper limits on the existence of primordial black holes.

Detector	Upper limits 99% C.L. ($pc^{-3}\,yr^{-1}$)
CYGNUS (Alexandreas *et al.*, 1993d)	8.5×10^5
HEGRA (Funk *et al.*, 1995)	4.7×10^6
Tibet (Amenomori *et al.*, 1995)	4.6×10^5

fuse flux is an average over the entire universe, while the TeV limits probe our local environment.

6. Diffuse emission

Diffuse photon emission from the galactic plane is believed to come primarily from the interactions of cosmic rays with material in the galaxy, so searches for diffuse UHE emission from the vicinity of the galactic plane can be used to determine the distribution and energy spectrum of galactic cosmic rays above 100 TeV.

A number of calculations of the expected level of galactic diffuse UHE γ-ray fluxes have been made (Berezinsky and Kudryavtsev, 1990; Aharonian, 1991; Berezinsky *et al.*, 1993). The predicted ratio of the diffuse γ-ray flux to the cosmic-ray flux is typically $\sim 2\times10^{-5}$ above 100 TeV from the direction of the galactic center and somewhat lower at other galactic longitudes. Results on diffuse galactic UHE emission from several EAS-PDAs have been reported (Matthews *et al.*, 1991; Aglietta *et al.*, 1992; Borione *et al.*, 1998). However, none of these detectors has exposure to the galactic center. No significant evidence for diffuse UHE has been observed; the best limits come from the CASA-MIA experiment (Borione *et al.*, 1998) and limit the ratio of the photon flux to the cosmic-ray flux to less than 2.4×10^{-5} at 310 TeV for the region in galactic coordinates ($50°<l<200°$) and ($-5°<b<5°$). This implies that the galactic diffuse emission is probably dominated by cosmic-ray interactions with passive gas molecules. The prospects for the detection of diffuse UHE γ-ray emission are not good because this would require a much larger data set than the 2.2×10^9 events reported by the CASA-MIA experiment. In addition, CASA-MIA has set limits on isotropic diffuse emission (Chantell *et al.*, 1997).

D. Discussion

Because ground-based γ-ray astronomy is an observational science operating in a regime with large backgrounds, it is intrinsically impossible to prove that VHE or UHE emission from a source has been detected; inevitably one must express a result in terms of the probability that the observation is due to a statistical fluctuation of the background. It is relatively straightforward to confirm or refute the existence of steady emission from a source, and it is straightforward to calculate the statistical significance from such an observation. Thus the observation of steady VHE emission from the Crab and from Vela are broadly accepted as genuine.

Episodic emission is much harder to confirm or refute. The existence of episodic emission over one period of time does not imply that there will be episodic emission over any other period of time. Thus the fact that no VHE or UHE emission was observed from Cygnus X-3 or Hercules X-1 in the 1990s does not *prove* that the earlier observations are incorrect. However, it seems highly unlikely that these were prolific sources that turned off just as more sensitive detectors started observing.

It is difficult to assign a statistical significance to an observation of episodic behavior because there is generally no *a posteriori* way to know the correct trials factor for looking at a particular interval of data (both the starting point and the duration). Searches for episodic emission are prone to inadvertent biases in the choice of intervals to be examined. This probably explains why many of the early ''detections'' were not repeated. Bonnet-Bidaud and Chardin (1988) examine the observations of Cygnus X-3 in great detail. A global analysis of the Whipple Hercules X-1 observations in the 1980s (Reynolds *et al.*, 1991) concludes that ''the long-term study of the source does not indicate a signal over the six-year period.''

The VHE and UHE observations of the Crab present a consistent picture. Emission from the pulsar is observed in the high-energy regime. Unpulsed emission is observed above 100 MeV and provides the ''standard candle'' in the VHE regime. The synchrotron self-Compton model appears to explain the steady emission. None of the modern EAS-PDAs has detected UHE emission from the Crab.

To enhance the ''believability'' of a result, we suggest that observers have a plan of how the data will be analyzed *before* looking at the data; this will enable an unbiased assessment of the significance of any result. The plan should include the sources (or regions of the sky) to be examined, the cuts to be made in the analysis (for example, imaging for air Čerenkov detectors or number of muons for air-shower arrays), and the time intervals to be examined. Biller (1996) suggested an *a priori* scheme for choosing time intervals. If a striking observation appears outside the analysis plan, it should then be considered an *a posteriori* observation whose statistical significance cannot be reliably assessed; this might then represent a hypothesis to be tested by future observations (i.e., it might become a new part of a future analysis plan).

VII. FUTURE PROSPECTS

A. Satellite-based detectors

As discussed above, the EGRET detector aboard the CGRO has been remarkably productive. An integral

part of the EGRET instrumentation is a spark chamber that uses consumable gas: EGRET was launched with enough gas for five refills, with no real possibility of replenishment. Each gas fill was expected to last six months (Thompson *et al.*, 1995), although judicious use of the spark chambers has prolonged their lifetime. Clearly EGRET has a limited lifetime and will cease observations in the near future.

There have been several ideas for new satellite-based high-energy γ-ray detectors. There is some consensus that, in addition to the importance of continuing observations after EGRET is no longer operational to observe transient phenomena, it would be desirable for a new telescope to have better angular resolution (to help identify sources in the galactic plane), a larger field of view (to observe more of the sky for a longer period of time), and a larger effective area, especially at high energies (to extend useful observations to higher energies). Below we discuss two proposed future γ-ray detectors, AMS and GLAST.

1. AMS

The Alpha Magnetic Spectrometer (AMS) is designed primarily to detect cosmic anti-nuclei on the International Space Station Alpha (Ahlen *et al.*, 1994). The basic idea is to construct a relatively large ($\sim 1\ m^2\,sr$) spectrometer with a permanent Nd-Fe-B magnet and use silicon-strip detectors and scintillation counters for charged-particle tracking.

AMS can function as a γ-ray detector with the addition of a 0.3-radiation-length tungsten converter plate (Salamon, 1995). The direction and energy of the photon are determined from the measurement of the directions and momenta of the electron and positron in the magnetic field.

The field of view of AMS is roughly 0.6 sr, and it will be sensitive to photons between 300 MeV and 300 GeV. The point-source sensitivity, expressed as the minimum detectable flux from a point source over a year, is expected to be 10^{-5} photons/cm^2/s/GeV, which is comparable to that of EGRET. However, the mass of the space station constitutes a target for cosmic-ray interactions and a source of noise. In addition, AMS cannot be pointed to specific objects as its attitude is fixed to the space station. A shuttle flight took place in June 1998 and a three-year mission is expected early next century, by which time EGRET will have ceased operations.

2. GLAST

The Gamma-ray Large-Area Space Telescope (GLAST) detector is under development by an international collaboration (Michelson, 1994b; Bloom, 1996). In the baseline design, GLAST will use a segmented charged-particle anticoincidence shield, a γ-ray tracker/converter consisting of thin sheets of high-Z converter interspersed with silicon-strip detectors, and a CsI calorimeter. Figure 29 shows a diagram of the GLAST concept. GLAST will have 25 tower modules, each 32 cm×32 cm in cross-sectional area.

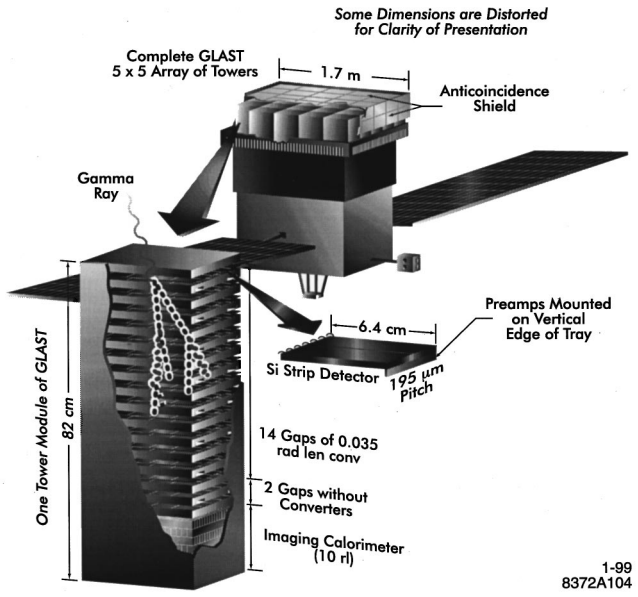

FIG. 29. Conceptual design of the Gamma-ray Large-Area Space Telescope (GLAST).

Figure 30 compares the expected performance of GLAST and EGRET as a function of energy. GLAST will have a larger field-of-view ($\sim 2\pi$ sr), which will enable it to observe a larger part of the sky at once. The point-source sensitivity of GLAST should be nearly 100 times better than that of EGRET.

Improvements with GLAST include the following:

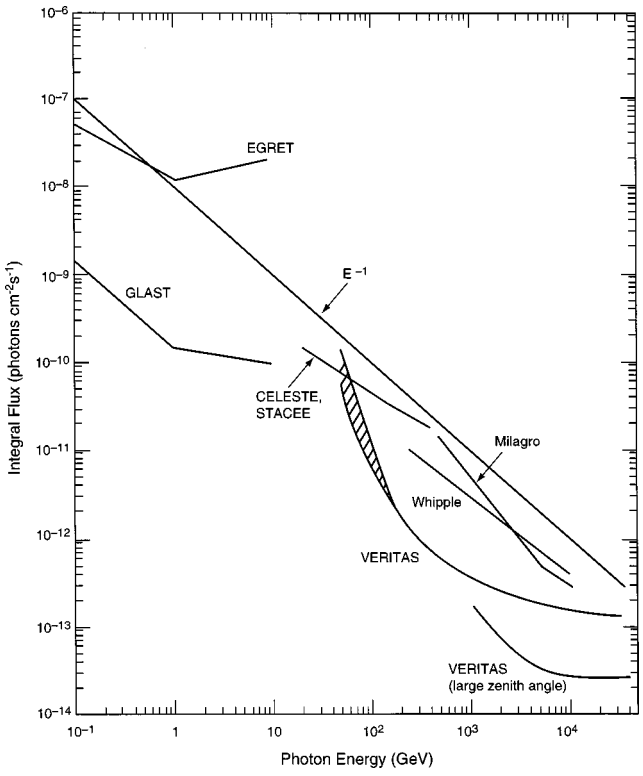

FIG. 30. Performance and sensitivity of existing and planned γ-ray instruments.

(1) A segmented anticoincidence shield, to sharply reduce the loss in effective area at high energies due to shower backsplash from the calorimeter.
(2) The use of silicon strip detectors to track the electron pair. There are 17 tracker/converter layers, each with 0.03-radiation-length converters followed by two planes of (x,y) silicon strip detectors. These layers are followed by two additional tracker layers with no converters. The silicon strip detectors have more than ten times better position resolution than spark chambers, essentially no dead time, and no consumables.
(3) The elimination of the time-of-flight system used to ensure that observed particles enter from the top of the instrument. The fine segmentation of the silicon strip detectors and the use of sophisticated pattern-recognition algorithms determine the direction of the electron-pair momentum. The elimination of the time-of-flight system results in a better aspect ratio and therefore a much larger field of view and an improved response to low-energy photons (as the particles are less apt to scatter out the sides).
(4) The calorimeter will use highly segmented (3 cm×3 cm) CsI(Tl) detectors, 10 radiation-lengths long, read out by solid-state detectors. This design provides better energy resolution and better shower position information for improved background discrimination.

GLAST has been selected by NASA for a Mission Concept Study. The collaboration is considering augmenting the capabilities of the instrument by modifying the calorimeter design so that the incident-photon direction can be determined from the calorimeter alone. The collaboration hopes to form an international partnership so that GLAST can be in orbit by 2005, after considerable prototyping and testing.

B. Improvements in atmospheric Čerenkov telescopes

Improvements in air Čerenkov telescopes are proceeding along two paths: improved flux sensitivity and lower energy threshold. Improved flux sensitivity allows one to detect weaker sources in a shorter amount of time (and thereby study larger regions of the sky) and to study the time variability of the sources. A lower energy threshold allows the study of the energy region between space-based and ground-based instruments. This should allow the measurement of cutoffs in the pulsed-emission energy spectra of many of the pulsars detected by EGRET, the detection of more distant AGNs, and the measurement of the cutoffs in their energy spectra.

Recent progress in imaging air Čerenkov detectors has made possible better angular and time resolution and the use of several imaging telescopes simultaneously observing the same showers. Further progress may come from increasing the number of detected photons (with larger mirrors and/or high-quantum-efficiency detectors). In addition, nonimaging techniques are being pursued, especially in the quest for lower energy thresholds.

1. Better angular and time resolution

The development of the imaging atmospheric Čerenkov telescope was due to the intuition of Weekes and Turver (1997). They believed that recording images of the Čerenkov light pool would improve the angular resolution of an air Cerenkov telescope. The shape of the Čerenkov images could also be used to differentiate between hadronic and electromagnetic showers, leading to additional background rejection. The original Whipple imaging device had 7 pixels; this was increased to 39 pixels, and from 1988–1996 the telescope had 109 pixels (each with a 4-mrad field of view). The field of view has since been increased without change in the pixel resolution. The CANGAROO and CAT telescopes have shown that even smaller pixel sizes (2 mrad) yield further improvements in sensitivity (Lebohec *et al.*, 1998). Since this pixel size is nearly as small as the finest features in a γ shower, smaller pixels will probably not lead to large improvements. With 2-mrad resolution, the longitudinal asymmetry of the image (reflecting the longitudinal development of the air shower) can be resolved and the position of the source located to within 2 mrad along the major axis of the image. In this manner, the direction of the primary cosmic ray can be reconstructed using a single mirror.

The time resolution of the Whipple telescope is ~10 ns and the signal integration time is ~25 ns. However, the Čerenkov photons are synchronous within 2–3 ns. The CAT telescope has achieved 2–3-ns coincidence times by implementing fast comparators (instead of discriminators) on the telescope mount. The integration time for the CAT telescope is 12 ns, which still leaves room for improvement. Such improvement would require the use of GHz flash analog-to-digital convertors.

2. Detecting more Čerenkov photons

The most straightforward improvement of an imaging ACT is to increase the number of Čerenkov photons collected. Usually the mirrors are front plated in order to maintain the reflectivity below 300 nm. Larger dishes collect more photons, but the need for mechanical rigidity implies that the cost increases faster than the area. To keep off-axis imaging precision (up to 3° acceptance) to an acceptable level, the focal length F should be increased as much as the diameter D. The often-used Davis-Cotton mounting, based on identical mirror elements of curvature radius $2F$ mounted on a sphere of radius F, should be avoided for large structures, as it induces a time lag of $\Delta t\ (\mathrm{ns}) = \frac{3}{8}(D/F)D(\mathrm{m})$; this amounts to 3 ns for $F=D=8$ m. For larger dishes, a parabolic shape should be preferable, although it is somewhat more complex (larger off-axis aberrations, nonidentical mirror elements).

The only way to improve significantly the number of collected photons while not compromising performance would be to increase the "quantum efficiency" above the current 20–25% of conventional photomultiplier tubes. Such an improvement would have a major impact in many sectors of professional and research activities.

New photocathodes such as GaAsP might yield twice as many photon conversions, reaching ~50% (Bradbury *et al.*, 1997). Solid-state detectors with ~100% efficiency for visible photons are in a research and development stage; they require a helium cryostat and are limited at present to very small sizes (Wayne, 1997; Ruchti, 1996).

3. Use of several imaging telescopes

The simultaneous use of several imaging telescopes either on the same mount (Chadwick *et al.*, 1998a) or on neighboring mounts at some 50–100 m distance has been investigated rather intensively. The most significant results were obtained by the HEGRA group (Puhlhofer *et al.*, 1997), using an array of five imaging telescopes with 60-m spacing with medium-resolution cameras. They have demonstrated improved hadron rejection with a signal-to-noise ratio of 19 on the Crab Nebula. In addition, the shower axis is determined event by event to within 0.1°, as good as the CAT detector, which has a much finer camera but a single dish.

The low-energy γ-ray events faked by muons falling at a distance of a few mirror radii—producing short circular arcs—are efficiently suppressed by the use of at least two telescopes some 50 m apart. Multiple telescopes may also extend the detection area, thus improving the flux sensitivity.

4. Other strategies: Solar plants

In spite of the overwhelming success of the imaging technique, wave-front detectors are being developed in an attempt to achieve very low energy thresholds (20–40 GeV). Modern wave-front detectors (currently in the prototype stage) make use of the enormous mirror areas available at solar energy plants. These plants consist of a large array of heliostats, large-area mirrors that track the sun and focus the sun's energy onto a heat exchanger located on a central tower. By utilizing a secondary mirror on the central tower, each heliostat can be imaged onto a single photomultiplier tube (Tumer, 1990). Two groups (one operating at Sandia National Laboratory in New Mexico, the other at Thémis, France) have successfully detected Čerenkov pulses from cosmic-ray air showers. While this technique does not allow the shower to be imaged, it can reconstruct the direction of the primary cosmic ray from wave-front timing and sample the lateral distribution of the Čerenkov light pool. A trigger that requires a coincidence over an array of widely spaced mirrors is much more efficient for γ-ray-induced air showers than for proton-induced showers or local muons. Whether this technique can successfully detect 20–40-GeV γ rays above the background of cosmic-ray electrons remains to be proven.

5. Major future projects

a. Projects aiming at a 10–20-GeV threshold: MAGIC, STACEE, CELESTE

Projects aiming at a 10–20-GeV threshold are still in a developmental stage. To date, not a single event has been recorded $\leqslant$20 GeV. Continuous progress has been made with imagers, but the energy threshold has been lowered only by a factor of 2 over the past 10 years. With the strong motivation to overlap with the space observations, major efforts are currently in progress. One approach is that of a super-imaging atmospheric Čerenkov telescope, the second that of the exploitation of solar plants.

At these low energies, the differences in the development of γ-ray and hadron-initiated showers become more pronounced: a greater fraction of the energy of the initial hadron goes to feed the nucleonic component of the shower, while the γ-ray shower remains nearly purely electromagnetic. Therefore the Čerenkov light yield from hadronic showers decreases much faster than that from γ-ray showers as the energy is lowered below 100 GeV, so that the hadronic background becomes less important. However, the background from the cosmic-ray electrons, which is negligible at higher energies due to their steeply falling spectrum (E^{-3}), becomes important at low energies. Showers initiated by electrons are indistinguishable from γ-ray showers. The only way to counter this isotropic background, for point sources of γ rays, is by directional measurement.

The MAGIC project, led by a German collaboration with other European groups (Lorenz, 1998), is based on a large parabolic dish (17 m), using aluminum mirror elements with permanent and automatic alignment control. The quantum efficiency of the photo detection is aimed at 50% with the use of (hybrid) phototubes with GaAsP photocathodes. The project requires progress on many technical matters: mirrors, light mechanical structures, automation, photodetection, massive data flow, and new strategies for event reduction, which will be of benefit to the entire field.

STACEE and CELESTE are projects based on the use of solar plants. STACEE (Williams *et al.*, 1998) will exploit the site of the experimental solar plant at Sandia Laboratory in New Mexico, while the CELESTE experiment (Giebels *et al.*, 1998) is using the decommissioned solar site of Thémis in the French Pyrenees, the same site where the Thémistocle, ASGAT, and CAT experiments are built. The validation of the solar plant scheme has been obtained by the CELESTE group, which has detected the Crab above 80 GeV with an as yet incomplete version of the detector (D. Smith, 1999). In this case the groups may exploit the huge site of Solar-II in California whenever this site becomes accessible.

b. Projects aiming for improved flux sensitivity and extensive observations

Quite a different class of projects is represented by the U.S. project VERITAS (Weekes *et al.*, 1998) and the German project HESS (Hermann, 1997). Both projects take full advantage of the recent progress in the imaging technique, merely extending to arrays of 10 to 15 telescopes of ~10 m diameter, each equipped with cameras of ~500 pixels.

The Japanese group is building a 10-m-diameter telescope with a 500-pixel camera on the CANGAROO site at Woomera, Australia; they plan ultimately to build five such telescopes.

These arrays will permit very flexible observation strategies, either turning each telescope toward a different source or exploiting the enhanced power—in flux sensitivity and noise-rejection efficiency—of several telescopes working together for chosen sources (or a single one). It would be desirable, if these projects were to run contemporaneously, that one be located in the northern hemisphere and the other in the southern, to permit coverage of the whole sky with comparable sensitivity.

C. Improvements in extensive air-shower particle detector arrays

Following the null results from galactic sources reported by the EAS-PDA detectors and the observations of extragalactic objects by air Čerenkov telescopes, much of the motivation for improving the sensitivity of UHE particle detector arrays has disappeared. Earlier detections of galactic sources (Cygnus X-3, Hercules X-1, etc.) have not been confirmed despite an increase of sensitivity of over two orders of magnitude. Given that the universe is opaque to 100-TeV radiation (due to the 3 K radiation) and quite possibly even to 10–30-TeV radiation (due to the infrared background radiation) and there appear to be no strong UHE galactic sources, there is little motivation for continuing the exploration of the UHE universe.

In stark contrast to this bleak picture, recent observations have highlighted the need for a different class of VHE detectors. The observed AGNs are now known to be highly variable; in addition, we now know the level of sensitivity required to observe these sources. The variable and transient nature of the high-energy sky calls for the development of large-aperture, high-duty-cycle VHE γ-ray detectors.

There are two methods by which an EAS-PDA can achieve a lower energy threshold: move to a higher altitude or increase the sampling of the air shower.

1. Higher altitude

The shower development curves show that the energy threshold of a particle detector array decreases rapidly at higher altitudes. For example, approximately the same number of particles from a 30-TeV shower strike a detector located at an altitude of 2100 m as from a 100-TeV shower striking a detector located at sea level.

The Tibet air-shower array was built in 1990 at an altitude of 4300 m above sea level (atmospheric depth $=606\,\mathrm{g/cm^2}$). The array has undergone several improvements since its inception. Currently the Tibet array, Tibet-II (Amenomori *et al.*, 1998), consists of 221 scintillators on a 15-m grid. The trigger rate is 223 Hz with a trigger requirement of four counters. The median energy of triggered events is 17 TeV for γ rays and 30 TeV for protons. In addition, a high-density array, consisting of 109 scintillation counters (some of which are also part of the main Tibet-II array) on a 7.5-m grid, has been constructed. This array operates at a trigger rate of 120 Hz and has a median energy for triggered events of roughly 5 TeV for protons. It is expected that the angular resolution will be about 1° above 3 TeV. Despite this unprecedented low energy threshold (for a particle detector array), the Tibet array has not yet unequivocally observed emission from any source.

2. Increased sampling of the extensive air shower

Conventional particle detector arrays sample 0.5% or less of the electromagnetic component of an EAS. There are two aspects to this relatively poor performance.

- The sparse nature of the particle detector arrays. Particle detector arrays typically cover less than 1% of the physical area with sensitive elements.
- The nature of the sensitive elements. Traditionally a plastic scintillator has been used, which has limited sensitivity to hard photons. Simulations show that, on average, these photons outnumber electrons and positrons four to one in air showers at ground level.

Milagro, a detector currently under construction in northern New Mexico, uses water as the detecting medium to drastically improve the performance of the detector in both of these aspects. The Milagro detector (Allen *et al.*, 1995b) will consist of two layers of photomultiplier tubes placed in a five-million-gallon water reservoir. The reservoir has a surface area of $\sim 5000\,\mathrm{m^2}$ and is 8 m deep; the bottom has an area of $1500\,\mathrm{m^2}$. The top layer of 450 photomultiplier tubes, placed on 3×3 m grid ~ 1.5 meters below the water surface, detects the Cerenkov light generated in the water by the charged shower particles. Since the Čerenkov angle in water is 41°, a relatively sparse array of photomultipliers can detect particles that enter the pond at any point. In addition, the hard photons in the air shower interact in the water, creating electrons and/or positrons, which are also detected by the PMTs. Simulations indicate that $\sim 50\%$ of all electromagnetic particles that reach the detector will be detected.

The second layer of 273 PMTs will be located under 7 m of water. This calorimetric layer will be used to study muons, hadrons, and energy flow in extensive air showers. The total area of this layer is $1500\,\mathrm{m^2}$.

The event rate in Milagro will be ~ 1 kHz, and the median energy for detected γ rays is expected to be about 2 TeV. While the point-source sensitivity will be substantially worse than that of existing air Čerenkov telescopes, Milagro will be capable of detecting all of the known TeV point sources and studying their variability. Milagro will also be the first VHE instrument capable of searching for gamma-ray bursts.

A prototype detector, called Milagrito, was operated from February 1997 to April 1998. This detector consisted of a single layer of 220 PMTs arranged on a $3\,\mathrm{m}\times3\,\mathrm{m}$ grid over the bottom ($1500\,\mathrm{m^2}$) of the Milagro reservoir. Despite the small size of the detector, the trigger rate (with a 100-PMT coincidence) was over 300 Hz. The trigger rate as a function of PMT multiplicity is shown in Fig. 31. Below a multiplicity of ~ 50 PMTs large-angle muons begin to dominate the trigger rate,

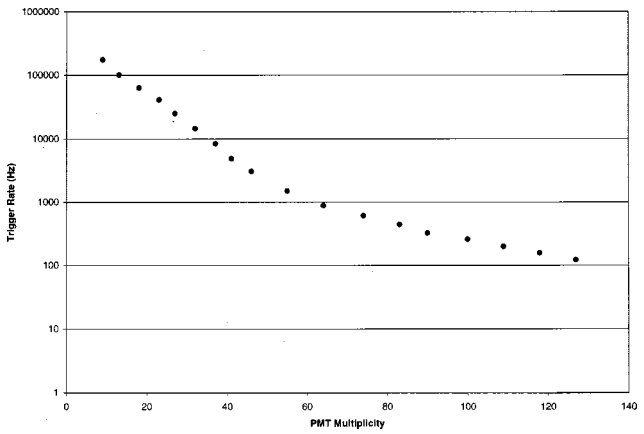

FIG. 31. Trigger rate in the Milagrito detector as a function of required trigger multiplicity. These data were taken with 2 m of water above the photomultiplier tubes. The steep rise in trigger rate near 57 photomultipliers is due to large-zenith-angle muons.

leading to the observed steepening of the trigger rate. For events in which the shower core can be reconstructed (roughly 30% of the triggered events), the angular resolution is ~0.5 degrees. Milagrito was dismantled to allow Milagro to be constructed.

Another approach to lowering the energy threshold of an extensive air-shower counter array is being taken by the ARGO group (Bacci *et al.*, 1998). This group proposes to operate 5000 m^2 of resistive plate chambers at the high-altitude site in Tibet. A resistive plate chamber should have excellent position and time resolution and an appreciable effective area for the detection of photons with energies as low as ~100 GeV.

VIII. OUTLOOK AND CONCLUSIONS

Observations of γ rays in the 1990s have begun to give us a clear and exciting view of the high-energy universe. Observations with CGRO have shown that there are many γ-ray sources, both galactic and extragalactic, as well as a strong component of diffuse emission.

The VHE sky is presently much sparser, although only a small fraction has been studied. However, a few steady galactic sources and several active galaxies have been observed. These AGNs show remarkable variability, which has severely constrained models of VHE emission. The discovery of the AGN Mrk 501 was the first time that a γ-ray source was found by ground-based observations before observations in space. In addition, VHE photons up to 50 TeV have been detected from the Crab. These results came only after ~30 years of refinement of the air Čerenkov technique.

In contrast, observations in the 1990s have shown that there are no bright sources of UHE emission, either steady or episodic. The earlier detections of a number of UHE sources have not been confirmed with more extensive and sensitive observations spanning a decade; it is difficult to escape the conclusion that the earlier detections were erroneous.

Improved VHE detectors are being built or are planned. They will have better sensitivity, lower energy threshold, or much larger angular coverage of the sky. New satellites will be coming on line with better angular resolution and sensitivity extending to 300 GeV. The region between 30 and 300 GeV should finally become accessible. These developments should serve to greatly expand the list of VHE sources and to improve our understanding of the acceleration mechanisms at work.

Most of the major EAS-PDAs have stopped acquiring data, and no new UHE arrays are planned at this time. Renewed interest in this energy regime must probably await new evidence that detectable sources are expected.

The 1990s have seen γ-ray astronomy develop so that it now plays an important role in our understanding of the cosmos. A number of unexpected discoveries have been made and many more are to be expected. High-energy γ-ray astronomy should flower in the next millennium.

ACKNOWLEDGMENTS

We wish to thank our many colleagues who assisted us in the writing of this article. This work was supported by the U.S. Department of Energy, the University of California, and the Institut de Physique Nucléaire et de Physique des Particules.

REFERENCES

Aglietta, M., *et al.*, 1992, Astrophys. J. **397**, 148.
Aglietta, M., *et al.*, 1995, Astropart. Phys. **3**, 1.
Aharonian, F. A., 1991, Astrophys. Space Sci. **180**, 305.
Aharonian, F. A., *et al.*, 1997 Astron. Astrophys. **327**, L5.
Ahlen, S., *et al.*, 1994, Nucl. Instrum. Methods Phys. Res. A **350**, 351.
Aid, S., *et al.*, 1995, Z. Phys. C **69**, 27.
Alexandreas, D. E., *et al.*, 1991, Phys. Rev. D **43**, 1735.
Alexandreas, D. E., *et al.*, 1992, Nucl. Instrum. Methods Phys. Res. A **311**, 350.
Alexandreas, D. E., *et al.*, 1993a, in *23rd International Cosmic Ray Conference*, 1993, Calgary (Department of Physics and Astronomy, University of Calgary, Calgary, Alberta), Vol. 1, p. 353.
Alexandreas, D. E., *et al.*, 1993b, Nucl. Instrum. Methods Phys. Res. A **328**, 570.
Alexandreas, D. E., *et al.*, 1993c, Astrophys. J. **418**, 832.
Alexandreas, D. E., *et al.*, 1993d, Phys. Rev. Lett. **71**, 2524.
Alexandreas, D. E., *et al.*, 1993e, Astrophys. J. **405**, 353.
Alexandreas, D. E., *et al.*, 1994, Astrophys. J. **426**, L1.
Allen, G. E., *et al.*, 1995a, Astrophys. J. **448**, L25.
Allen, G. E., *et al.*, 1995b, in *24th International Cosmic Ray Conference*, 1995, Rome (IUPAP, Urbino), Vol. 1, p. 942.
Amenomori, M., *et al.*, 1992, Phys. Rev. Lett. **69**, 2468.
Amenomori, M., *et al.*, 1995, in *24th International Cosmic Ray Conference*, 1995, Rome (IUPAP, Urbino), Vol. 2, p. 112.
Amenomori, M., *et al.*, 1996, Astrophys. J. **464**, 954.

Amenomori, M., *et al.*, 1998, in *25th International Cosmic Ray Conference*, 1997, Durban (World Scientific, Singapore), Vol. 5, p. 245.
Antonucci, R., and J. Miller, 1985, Astrophys. J. **297**, 621.
Auger, P., 1939, Rev. Mod. Phys. **11**, 288.
Bacci, C., *et al.*, 1998, in *25th International Cosmic Ray Conference*, 1997, Durban (World Scientific, Singapore), Vol. 5, p. 265.
Baillon, P., *et al.*, 1993, Astropart. Phys. **1**, 341; **5**, 79(E) (1996).
Baltrusaitis, R. M., *et al.*, 1985, Nucl. Instrum. Methods Phys. Res. A **240**, 410.
Barrau, A., *et al.*, 1998, Nucl. Instrum. Methods Phys. Res. A **416**, 278.
Becker, W., K. T. S. Brazier, and J. Trümper, 1995, Astron. Astrophys. **298**, 528.
Begelman, M. C., R. D. Blandford, and M. J. Rees, 1984, Rev. Mod. Phys. **56**, 255.
Bell, A. B., 1978, Mon. Not. R. Astron. Soc. **182**, 147.
Berezinsky, V. S., and V. A. Kudryavtsev, 1990, Astrophys. J. **349**, 620.
Berezinsky, V. S., T. K. Gaisser, F. Halzen, and T. Stanev, 1993, Astropart. Phys. **1**, 281.
Bergström, L., P. Ullio, and J. Buckley, 1997, preprint astro-ph/9712318.
Bergström, L., and P. Ullio, 1997, Nucl. Phys. B **504**, 27.
Bertsch, D., K. T. S. Brazier, C. E. Fichtel, R. C. Hartman, S. D. Hunter, G. Kanbach, D. A. Kniffen, P. W. Kwok, Y. C. Lin, and J. R. Mattox, 1992, Nature (London) **357**, 306.
Bignami, G. F., *et al.*, 1975, Space Sci. Instrum. **1**, 245.
Biller, S. D., 1995, Astropart. Phys. **3**, 385.
Biller, S. D., 1996, Astropart. Phys. **4**, 285.
Biller, S. D., *et al.*, 1994, Astrophys. J. **423**, 714.
Biller, S. D., *et al.*, 1998, Phys. Rev. Lett. **80**, 2992.
Bird, D. J., 1994, Astrophys. J. **424**, 491.
Blandford, R. D., and J. P. Ostriker, 1978, Astrophys. J. **221**, L29.
Bloemen, J. B. G. M., 1989, Annu. Rev. Astron. Astrophys. **27**, 469.
Bloom, E. D., 1996, Space Sci. Rev. **75**, 109.
Bonnet-Bidaud, J-M., and G. Chardin, 1988, Phys. Rep. **170**, 325.
Borione, A., *et al.*, 1995a, in *24th International Cosmic Ray Conference*, 1995, Rome (IUPAP, Urbino), Vol. 2, p. 116.
Borione, A., *et al.*, 1995b, in *24th International Cosmic Ray Conference*, 1995, Rome (IUPAP, Urbino), Vol. 2, p. 430.
Borione, A., *et al.*, 1997, Phys. Rev. D **55**, 1714.
Borione, A., *et al.*, 1998, Astrophys. J. **493**, 175.
Bradbury, S. M., R. Mirzoyan, J. Gebauer, E. Feigl, and E. Lorenz, 1997, Nucl. Instrum. Methods Phys. Res. A **387**, 45.
Breslin, A. C., *et al.*, 1997, IAU Circ. 6592 ''Markarian 501.''
Buckley, J., *et al.*, 1997, Adv. Space Res. **21**, 101.
Burnett, T. H., *et al.*, 1990, Astrophys. J. **349**, L25. See also the parametrization of Nagle *et al.*, 1988.
Carter-Lewis, D. A., *et al.*, 1998, in *25th International Cosmic Ray Conference*, 1997, Durban (World Scientific, Singapore), Vol. 3, p. 161.
Catanese, M., *et al.*, 1997, Astrophys. J. **487**, L143.
Catanese, M., *et al.*, 1998, Astrophys. J. **501**, 616.
Cavallo, G., and M. J. Rees, 1978, Mon. Not. R. Astron. Soc. **183**, 359.
Cawley, M. F., D. J. Fegan, K. Gibbs, P. W. Gorham, R. C. Lamb, D. F. Liebing, P. K. McKeown, N. A. Porter, V. J. Stenger, and T. C. Weekes, 1985, in *19th International Cosmic Ray Conference*, 1985, La Jolla (NASA Scientific and Technical Information Service, Springfield, Virginia), Vol. 1, p. 173.
Chadwick, P. M., *et al.*, 1998a, in *25th International Cosmic Ray Conference*, 1997, Durban (World Scientific, Singapore), Vol. 5, p. 101.
Chadwick, P. M., *et al.*, 1998b, Astropart. Phys. **9**, 131.
Chanmugam, G., and K. Brecher, 1985, Nature (London) **313**, 767.
Chantell, M. C., *et al.*, 1997, Phys. Rev. Lett. **79**, 1805.
Cheng, K. S., C. Ho, and M. Ruderman, 1986, Astrophys. J. **300**, 500 (Part I); 1986 **300**, 522 (Part II).
Collins, J., A. Kaidalov, A. Yu. Khodjamirian, and L. McLerran, 1989, Phys. Rev. D **39**, 1318.
Coppi, P. S., and F. A. Aharonian, 1997, Astrophys. J. **487**, L9.
Cronin, J. W., K. G. Gibbs, and T. C. Weekes, 1993, Annu. Rev. Nucl. Part. Sci. **43**, 883.
Daum, A., *et al.*, 1997, Astropart. Phys. **8**, 1.
deJager, O. C., and A. K. Harding, 1992, Astrophys. J. **396**, 161.
deJager, O. C., F. W. Stecker, and M. H. Salamon, 1994, Nature (London) **369**, 294.
Derdeyn, S. M., C. H. Ehrmann, C. E. Fichtel, D. A. Kniffen, and R. W. Ross, 1972, Nucl. Instrum. Methods **98**, 557.
Dermer, C. D., and R. Schlickeiser, 1993, Astrophys. J. **416**, 458.
Dingus, B. L., 1994, in *Proceedings of the 1994 Snowmass Summer Study on Particle and Nuclear Astrophysics and Cosmology in the Next Millennium*, edited by E. W. Kolb and R. D. Peccei (World Scientific, Singapore), p. 99.
Dingus, B. L., *et al.*, 1988, Phys. Rev. Lett. **61**, 1906.
Djannati-Ata, A., *et al.*, 1995, in 24th International Cosmic Ray Conference, Rome, 1995 (IUPAP, Urbino), Vol. 2, p. 315.
Djannati-Ata, A., *et al.*, 1999, Astron. Astrophys. (in press).
Domokos, G., and S. Kovesi-Domokos, 1988, Phys. Rev. D **38**, 2833.
Domokos, G., and S. Nussinov, 1987, Phys. Lett. B **187**, 372.
Drees, M., and F. Halzen, 1988, Phys. Rev. Lett. **61**, 275.
Drury, L. O'C., F. A. Aharonian, and H. J. Volk, 1994, Astron. Astrophys. **287**, 959.
Ellsworth, R. W., 1991, private communication.
Esposito, J. A., S. D. Hunter, G. Kanbach, and P. Sreekumar, 1996, Astrophys. J. **461**, 820.
Fazio, G. G., H. F. Helken, E. Omongain, and T. C. Weekes, 1972, Astrophys. J. **175**, L117.
Fenimore, E. E., *et al.*, 1988, Astrophys. J. **335**, L71.
Fermi, E., 1949, Phys. Rev. **75**, 1169.
Fichtel, C. E., 1996, Astron. Astrophys., Suppl. Ser. **120**, 23.
Fichtel, C. E., R. C. Hartman, D. A. Kniffen, D. J. Thompson, G. F. Bignami, H. Ogelman, M. E. Ozel, and T. Tumer, 1975, Astrophys. J. **198**, 163.
Fichtel, C. E., G. A. Simpson, and D. J. Thompson, 1978, Astrophys. J. **222**, 833.
Fichtel, C. E., and J. I. Trombka, 1997, *Gamma-Ray Astrophysics*, NASA Reference Publication 1386.
Fossati, A., A. Celloti, G. Ghisellini, and L. Maraschi, 1997, Mon. Not. R. Astron. Soc. **289**, 136.
Frail, J., W. M. Goss, and J. Z. B. Whiteoak, 1994, Astrophys. J. **437**, 781.
Franceschini, A., P. Mazzei, P. DeZotti, and L. Danese, 1994, Astrophys. J. **427**, 140.

Frank, J., A. King, and D. Raine, 1992, *Accretion Power in Astrophysics* (Cambridge University Press, Cambridge).
Funk, B., *et al.*, 1995, in *24th International Cosmic Ray Conference*, 1995, Rome (IUPAP, Urbino), Vol. 2, p. 104.
Gaidos, J., *et al.*, 1996, Nature (London) **383**, 319.
Gaisser, T. K., A. M. Hillas, J. C. Perrett, M. A. Pomerantz, R. J. O. Reid, N. J. T. Smith, T. Stanev, and A. A. Watson, 1989, Phys. Rev. Lett. **62**, 1425.
Gaisser, T. K., and G. B. Yodh, 1980, Annu. Rev. Nucl. Part. Sci. **30**, 475.
Giebels, B., *et al.*, 1998, Nucl. Instrum. Methods Phys. Res. A **412**, 329.
Goldreich, P., and W. H. Julian, 1969, Astrophys. J. **157**, 869.
Goret, R. J., T. Palfrey, A. Tabary, G. Vacanti, and R. Bazer-Bachi, 1993, Astron. Astrophys. **270**, 401.
Gould, R. J., 1965, Phys. Rev. Lett. **15**, 511.
Gregorich, D. T., G. Neugebauer, B. T. Soifer, J. E. Gunn, and T. L. Herter, 1995, Astron. J. **110**, 259.
Greisen, K., 1956, Prog. Elem. Part. Cosmic Ray Phys. **3**, 1.
Greisen, K., 1960, Annu. Rev. Nucl. Sci. **10**, 63.
Grenier, I. A., 1995, Adv. Space Res. **15**, 73.
Grenier, I. A., W. Hermsen, and C. Hote, 1991, Adv. Space Res. **11**, 107.
Grenier, I. A., W. Hermsen, and A. M. T. Pollock, 1990, in Proceedings of the Conference on High Energy Gamma-Ray Astronomy, edited by J. Matthews, AIP Conf. Proc. No. 220 (AIP, New York, 1991), p. 3.
Halperin, J., and S. Holt, 1992, Nature (London) **357**, 222.
Halzen, F., E. Zas, J. H. MacGibbon, and T. C. Weekes, 1991, Nature (London) **353**, 807.
Hauser, M. G., 1996, in *Unveiling the Cosmic Infra-red Background*, AIP Conference Proceedings No. 348, edited by E. Dwek (AIP, New York), p. 226.
Hawking, S.W., 1975, Nature (London) **248**, 30.
Heckler, A., 1997, Phys. Rev. D **55**, 480.
Henri, G., G. Pelletier, P. O. Petrucci, and N. Renault, 1999, Astropart. Phys. (in press).
Hermann, G., 1997, in *Very High Energy Phenomena in the Universe*, Proceedings of the XXXII Rencontres de Moriond, edited by Y. Giraud-Heraud and J. Tran Thanh Van (Editions Frontieres, Gif-sur-Yvette, France), p. 141.
Hermsen, W., 1981, Philos. Trans. R. Soc. London, Ser. A **301**, 519.
Hermsen, W., K. Bennett, J. B. G. M. Bloemen, R. Buccheri, F. A. Jansen, A. Mastichiadis, H. A. Mayer-Hasselwander, M. E. Ozel, A. M. T. Pollock, and A. W. Strong, 1987, Astron. Astrophys. **175**, 141.
Hess, V. F., 1913, Phys. Z. **13**, 1084.
C. T. Hill, D. N. Schramm, and T. P. Walker, 1987, Phys. Rev. D **36**, 1007.
Hillas, A. M., 1996, Space Sci. Rev. **75**, 17.
Hillas, A. M., *et al.*, 1998, Astrophys. J. **503**, 744.
Hunter, S. D. *et al.*, 1997, Astrophys. J. **481**, 205.
Hurley, K., 1994, Nature (London) **372**, 652.
Inoue, S., and F. Takahara, 1996, Astrophys. J. **463**, 555.
Karle, A., *et al.*, 1996, Astropart. Phys. **4**, 1.
Kifune, T., *et al.*, 1995, Astrophys. J. **438**, L91.
Kirk, J. G., A. Mastichiadis, and W. Bednarek, 1997, in *Proceedings of the Heidelberg Workshop on Gamma-Ray Emitting AGN*, 1996, edited by J. G. Kirk, M. Camenzind, C. von Montigny, and S. Wagner (Max-Planck Institut für Kernphysik, Heidelberg), p. 13.
Klebesadel, R. W., I. B. Strong, and R. A. Olson, 1973, Astrophys. J. **182**, L85.
Kolb, E. W., and M. S. Turner, 1990, *The Early Universe* (Addison Wesley, New York).
Konopelko, A., *et al.*, 1999, Astropart. Phys., astro-ph/8891983.
Krennrich, F., *et al.*, 1993, in *23rd International Cosmic Ray Conference*, 1993, Calgary (Department of Physics and Astronomy, University of Calgary, Alberta), Vol. 1, p. 251.
Kulkarni, S. R., *et al.*, 1997, IAU Circ. 6732, "GRB 970828 and GRB 970228."
Lamb, R. C., M. F. Cawley, D. J. Fegan, K. G. Gibbs, P. W. Gorham, A. M. Hillas, D. A. Lewis, N. A. Porter, P. T. Reynolds, and T. C. Weekes, 1988, Astrophys. J. **328**, L13.
Lamb, R., C. E. Fichtel, R. C. Hartman, D. A. Kniffen, and D. J. Thompson, 1977, Astrophys. J. **212**, L63.
Lamer, G., and S. J. Wagner, 1998, Astron. Astrophys. **331**, L13.
Lebohec, S., *et al.*, 1998, Nucl. Instrum. Methods Phys. Res. A **416**, 425.
Legage, R. O., and C. J. Cesarsky, 1983, Astron. Astrophys. **125**, 249.
Levinson, A., and R. Blandford, 1991, in *Jets in Extragalactic Radio Sources*, edited by H.-J. Röser and K. Meisenheimer (Springer, New York), p. 534.
Lin, Y. C., *et al.*, 1993, Astrophys. J. **416**, L53.
Linsley, J., 1987, in *20th International Cosmic Ray Conference*, 1987, Moscow, edited by V. A. Kozyarivsky *et al.* (Nauka, Moscow), Vol. 2, p. 442.
Lloyd-Evans, J., R. N. Coy, A. Lampert, J. Lapikens, M. Patel, R. J. O. Reid, and A. Watson, 1983, Nature (London) **305**, 784.
Longair, M. S., 1994a, *High Energy Astrophysics* (Cambridge University, London/New York), Vol. I.
Longair, M. S., 1994b, *High Energy Astrophysics* (Cambridge University, London/New York), Vol. II, p. 348.
Lorenz, E., 1998, in *25th International Cosmic Ray Conference*, 1997, Durban (World Scientific, Singapore), Vol. 5, p. 177.
MacGibbon, J. H., and R. H. Brandenberger, 1993, Phys. Rev. D **47**, 2283.
MacGibbon, J. H. and B. R. Webber, 1990, Phys. Rev. D **41**, 3052.
MacMinn, D., and J. Primack, 1996, Space Sci. Rev. **75**, 413.
Malkan, M. A., and F. W. Stecker, 1998, Astrophys. J. **496**, 13.
Mannheim, K., 1993, Astron. Astrophys. **269**, 67.
Maraschi, L., G. Ghisellini, and A. Celotti, 1992, Astrophys. J. **397**, L5.
Marshak, M. L., *et al.*, 1985, Phys. Rev. Lett. **55**, 1965.
Matthews, J., *et al.*, 1991, Astrophys. J. **375**, 202.
Mayer-Hasselwander, H., *et al.*, 1993, Astrophys. J. **421**, 276.
McAdam, W. B., J. L. Osborne, and M. L. Parkinson, 1993, Nature (London) **361**, 516.
J. E. McEnery, *et al.*, 1998, in *25th International Cosmic Ray Conference*, 1997, Durban (World Scientific, Singapore), Vol. 3, p. 257.
McKay, T. M., *et al.*, 1993, Astrophys. J. **417**, 742.
Merck, M., *et al.*, 1996, Astropart. Phys. **5**, 379.
Meszaros, P., and M. J. Rees, 1993, Astrophys. J. **405**, 278.
Metzger, M. R., *et al.*, 1997, IAU Circ. 6655, "GRB 970508."
Michelson, P. F., 1994a, in *Proceedings of the Workshop on Towards a Major Atmospheric Detector III*, edited by T. Kifune (Universal Academy Press, Tokyo), p. 257.

Michelson, P. F., 1994b, in *Proceedings of the Workshop on Towards a Major Atmospheric Detector III*, edited by T. Kifune (Universal Academy Press, Tokyo), p. 321.
Middleditch, J., R. C. Puetter, and C. R. Pennypacker, 1985, Astrophys. J. **267**, 313.
Mohanty, G., S. Biller, D. A. Carter-Lewis, D. J. Fegan, A. M. Hillas, R. C. Lamb, T. C. Weekes, M. West, and J. Zweerink, 1998, Astropart. Phys. **9**, 15.
Mori, M., 1997, Astrophys. J. **478**, 225.
Mukherjee, R., D. L. Bertsch, B. L. Dingus, G. Kanbach, P. Sreekumar, and D. J. Thompson, 1995, Astrophys. J. **441**, L61.
Murakami, T., M. Fujii, K. Hayashida, M. Itoh, and J. Nishimura, 1988, Nature (London) **335**, 234.
Nagle, D. E., T. K. Gaisser, and R. J. Protheroe, 1988, Annu. Rev. Nucl. Part. Sci. **38**, 609.
Nishimura, J., and K. Kamata, 1952, Prog. Theor. Phys. **7**, 185.
Ong, R., 1998, Phys. Rep. **305**, 93.
Padovani, P., 1997, in *Very High Energy Phenomena in the Universe: Proceedings of the XXXII Rencontres de Moriond*, edited by Y. Giraud-Heraud and J. Tran Thanh Van (Editions Frontieres, Gif-sur-Yvette, France), p. 7.
Petry, D., *et al.*, 1996, Astron. Astrophys. **311**, 13.
Pian, E., *et al.*, 1998, Astrophys. J. **492**, L17.
Prosch, C., *et al.*, 1996, Astron. Astrophys. **314**, 275.
Protheroe, R. J., A. Mastichiadis, and C. D. Dermer, 1992, Astropart. Phys. **1**, 113.
Puget, J-L., A. Abergel, J-P. Bernard, F. Boulanger, W. B. Burton, F.-X. Desert, and D. Hartman, 1996, Astron. Astrophys. **308**, L5.
Puhlhofer, G., A. Daum, G. Hermann, M. Hess, W. Hofmann, C. Kohler, and M. Panter, 1997, Astropart. Phys. **8**, 101.
Punch, M., *et al.*, 1992, Nature (London) **358**, 477.
Quinn, J., *et al.*, 1996, Astrophys. J. **456**, L83.
Quinn, J., *et al.*, 1998, in *25th International Cosmic Ray Conference*, 1997, Durban (World Scientific, Singapore), Vol. 3, p. 249.
Ramanamurthy, P. V., D. L. Bertsch, C. E. Fichtel, G. Kanback, D. A. Kniffen, H. A. Mayer-Hasselwander, P. J. Nolan, P. Sreekumar, and D. J. Thompson, 1995, Astrophys. J. **450**, 791.
Rees, M. J., 1966, Nature (London) **211**, 468.
Reichart, D. E., 1997, Astrophys. J. **485**, L57.
Resvanis, L. K., *et al.*, 1988, Astrophys. J. **328**, L9.
Reynolds, P. T., *et al.*, 1991, Astrophys. J. **382**, 640, and references therein.
Ruchti, R. C., 1996, Annu. Rev. Nucl. Part. Sci. **46**, 281.
Sahu, K. C., M. Livio, L. Petro, F. D. Maccetto, J. vanParadijs, C. Kouveliotou, G. J. Fishman, C. A. Meegan, P. J. Groot, and T. Galama, 1997, Nature (London) **387**, 476.
Salamon, M. H., 1995, in Proceedings of the IV Workshop on Towards a Major Atmospheric Čerenkov Detector, Padova, edited by M. Cresti.
Samorski, M., and W. Stamm, 1983a, in *18th International Conference on Cosmic Rays*, 1983, Bangalore (Tata Institute of Fundamental Research, Bombay), Vol. 11, p. 244.
Samorski, M., and W. Stamm, 1983b, Astrophys. J. **268**, L17.
Samuelson, F. W., *et al.*, 1998, Astrophys. J. **501**, L17.
Scarsi, L., R. Buccheri, G. Gerardi, and B. Sacco, 1981, in *Origin of Cosmic Rays*, IAU Symposium No. 94, edited by G. Setti, G. Spada, and A. W. Wolfendale (Kluwer, Boston), p. 279.
Shapiro, S. L., and S. A. Teukolsky, 1983, *Black Holes, White Dwarfs, and Neutron Stars: The Physics of Compact Objects* (Wiley, New York).
Sikora, M. C., M. C. Begelman, and M. J. Rees, 1994, Astrophys. J. **421**, 153.
Smith, A., 1999, Astropart. Phys. (in press).
Smith, D., 1999, in *Proceedings of the XIX Texas Symposium*, Paris (in press).
Smoot, G. F., 1992, in *Particle Astrophysics*, edited by G. Fontaine and J. Tran Thanh Van (Editions Frontières, Gif-sur-Yvette, France), p. 409.
Sokolosky, P., 1989, *Introduction to Ultrahigh Energy Cosmic Ray Physics* (Addison Wesley, New York).
Sommers, M., *et al.*, 1994, Astrophys. J. **422**, L63.
Sreekumar, P., *et al.*, 1992, Astrophys. J. **400**, L67.
Sreekumar, P., *et al.*, 1993, Phys. Rev. Lett. **70**, 127.
Sreekumar, P., *et al.*, 1998, Astrophys. J. **494**, 523.
Stecker, F. W., and O. C. deJager, 1993, Astrophys. J. **415**, L71.
Stecker, F. W., and O. C. deJager, 1997, Astrophys. J. **476**, 712.
Stecker, F. W., and O. C. deJager, 1998, Astron. Astrophys. **334**, L85.
Stecker, F. W., and M. H. Salamon, 1996, Astrophys. J. **464**, 600.
Sturner, S. J., and C. D. Dermer, 1995, Astron. Astrophys. **293**, L17.
Swanenburg, B. N., *et al.*, 1981, Astrophys. J. **243**, L69.
Tananbaum, H., H. Gursky, E. M. Kellogg, R. Levinson, E. Schreier, and R. Giacconi, 1972, Astrophys. J. **174**, L143.
Tanimori, T., *et al.*, 1994, Astrophys. J. **429**, L61.
Tanimori, T., *et al.*, 1998a, Astrophys. J. **492**, L33.
Tanimori, T., *et al.*, 1998b, Astrophys. J. **497**, L25.
Thompson, D. J., *et al.*, 1976, *The Structure and Content of the Galaxy and Galactic Gamma Rays*, NASA CP-002 (U.S. GPO, Washington, DC), p. 1.
Thompson, D. J., C. E. Fichtel, R. C. Hartman, D. A. Kniffen, and R. C. Lamb, 1977, Astrophys. J. **213**, 252.
Thompson, D. J., *et al.*, 1992, Nature (London) **359**, 615.
Thompson, D. J., *et al.*, 1993, Astrophys. J., Suppl. Ser. **86**, 629.
Thompson, D. J., *et al.*, 1995, Astrophys. J., Suppl. Ser. **101**, 259.
Thorne, K. S., R. H. Price, and D. A. MacDonald, 1986, *Black Holes*, The Membrane Paradigm (Yale University, New Haven).
Tumer, O. T., 1990, Nucl. Phys. B (Proc. Suppl.) **14A**, 351.
Tyson, J. A., 1990, in *The Galactic and Extragalactic Background Radiation*, edited by S. Bowyer and C. Leniert (Kluwer, Dordrecht), p. 245.
Urban, M., A. Bouquet, B. Degrange, P. Fleury, J. Kaplan, A. L. Melchior, and E. Pare, 1992, Phys. Lett. B **293**, 149.
Urry, C. M., and P. Padovani, 1995, Publ. Astron. Soc. Pac. **107**, 803.
Vacanti, G., *et al.*, 1991, Astrophys. J. **377**, 467.
Vacanti, G., P. Fleury, Y. Jiang, E. Pare, A. C. Rovero, X. Sarazin, M. Urban, and T. C. Weekes, 1994, Astropart. Phys. **2**, 1.
van Paradijs, J., *et al.*, 1997, Nature (London) **386**, 686.
Vestrand, W. T., P. Sreekumar, and M. Mori, 1997, Astrophys. J. **483**, L49.
von Montigny, C., *et al.*, 1995, Astrophys. J. **440**, 525.
Wayne, M. R., 1997, Nucl. Instrum. Methods Phys. Res. A **387**, 278.
Weekes, T. C., 1988, Phys. Rep. **160**, 1, and references therein.
Weekes, T. C., *et al.*, 1989, Astrophys. J. **342**, 379.

Weekes, T. C., *et al.*, 1998, in *25th International Cosmic Ray Conference*, 1997, Durban (World Scientific, Singapore), Vol. 5, p. 173.
Weekes, T. C., and K. E. Turver, 1997, in *Proceedings of the 12th ESLAB Symposium*, Frascati, ESA, SP-124, p. 279.
Williams, D. A., *et al.*, 1998, in *25th International Cosmic Ray Conference*, 1997, Durban (World Scientific, Singapore), Vol. 5, p. 157.
Yoshikoshi, T., *et al.*, 1997, Astrophys. J. **487**, L65.